CAPACITY FADE OF VALVE REGULATED LEAD ACID & LITHIUM IRON PHOSPHATE BATTERIES THROUGH HIGH RATE, PULSED LOADS

by

CHRISTOPHER LEE WILLIAMS

Presented to the Faculty of the Graduate School of

The University of Texas at Arlington in Partial Fulfillment

of the Requirements

for the Degree of

MASTER OF SCIENCE IN ELECTRICAL ENGINEERING

THE UNIVERSITY OF TEXAS AT ARLINGTON

APRIL 2016

Acknowledgements

Dr. David Wetz - Thank you for being a dedicated leader, a friend, and a mentor in my life. You are the single hardest working individual I have ever met. May you and your family be blessed in the years to come.

Dr. Wei-Jen Lee – From a teacher, to a mentor, and now a friend. The guidance through every class you have provided has shaped and molded me into an engineer I am today.

Matt Martin – The option that was always right. Thank you Matt, for guiding me and letting me learn under you. You always did great work and should be proud of all your accomplishments.

Clint Gnegy-Davidson – The only persons beard in the lab that had more hair than what was on my head. Thank you for all the help you provided throughout my work in the Pulsed Power and Energy Lab.

Isaac Cohen – Thank you Isaac for your help thought my time at the Lab. Congratulations on your PhD. I know with all the knowledge you have gained you will prosper in life ahead.

Derek Wong – Thank you for all the expertise you provided me on the materials aspects of my research. I hope you and your wife are happy for the years to come. Remember Derek, she’s a keeper. So don't mess it up.

David Dodson – Through every joke and adventure we had in the lab I hope your time there will let you grow as much as I did.

Kendal Mckinzie – I cannot thank you enough for helping me on every project in the lab, you are truly a hard worker and great friend.

Mom & Dad – Thank you for help putting me through college and providing all of the loving support throughout my life.

Kristin McCreery – Thank you for being the love of my life and putting up with me throughout college. I love you with all of my heart.

April 25, 2016

Abstract

CAPACITY FADE OF VALVE REGULATED LEAD ACID & LITHIUM IRON PHOSPHATE BATTERIES THROUGH HIGH RATE, PULSED LOAD

CHRISTOPHER LEE WILLIAMS, MS

The University of Texas at Arlington, 2016

Supervising Professor: David A. Wetz

Electrochemical energy storage has become more power and energy dense in recent years. Many applications demanding energy storage operate in a pulsed manner. The most common chemistries considered for use in these applications include valve regulated lead acid (VRLA) and lithium-ion (LI). In the work presented here, one of each of these types of batteries has been assembled with ~60 V open circuit potentials (OCPs) and is in the process of experimentally characterizing their capacity fade and impedance growth when they are used to drive a high current pulsed load in a 5 seconds on / 5 seconds off pulsed profile. All of the batteries are being discharged and recharged at rates much higher than their 1C rating. Using standard voltage, current, and thermal diagnostics as well as periodic electrochemical impedance spectroscopy (EIS) measurements, the capacity fade and impedance growth of each chemistry is being studied to understand how the high rate pulsed profile ages the cells. Empirical and lumped element models of the impedance rise will be developed to understand what is aging internally and how it affects the usable life of the batteries compared with manufacturers rated life predictions. The experimental and modeling efforts will be summarized and conclusions will be drawn to provide the audience with a better understanding of how each of these technologies ages when used in high rate, pulsed applications.

Table of Contents

List of Illustrations

List of Tables

Chapter 1

Introduction

Low loss energy storage is a critical component needed for stability and reliability in electrical systems. The types of electrical systems that depend upon energy storage are expanding every day and range everywhere from a simple handheld flashlight to multi-MW electrical power distribution networks (Huibin & Wei-Jen, 2011) (Turner, Kelly, Storm, Wetz, & Wei-Jen, 2015). The US military is currently evaluating batteries for use in a host of forward operating base power systems (Wetz, Shrestha, & Novak, Back to Results Elevated Rate Cycling of High-Power Electrochemical Energy Storage Devices for Use as the Prime Power Source of an EM Launcher, 2013), shipboard power systems (Cohen, Westenhover, Wetz, Heinzel, & Dong, 2015), soldier power supplies (Wilhelm, Surgenor, & Pharoah, 2006) , and even complex weapon systems (Wetz, Shrestha, & Novak, Back to Results Elevated Rate Cycling of High-Power Electrochemical Energy Storage Devices for Use as the Prime Power Source of an EM Launcher, 2013). In any of these applications, choosing the right form of energy storage to use depends on constraints allowed by the system. A few of the possible constraint categories include safety, cost, lifetime, reliability, efficiency, thermal management, voltage, current, power, weight, and volume. There are many different types of energy storage available and the flexibility of the constraints drives the decision of which advantages and disadvantages of each type of energy storage are allowable. In any application, safety is always the first constraint that must be solved; but beyond that, power and energy density are often the most critical when being considered for mobile applications. The power and energy density constraints combine those of voltage, current, power, capacity, weight, and volume into two comparable metrics that can be used to evaluate various energy storage options.

Presently, the US Navy is considering the use of electrochemical energy storage devices for use in shipboard power systems, both as a power buffer as well as a prime power supply for a host of directed energy applications. Even if the type of energy storage is narrowed down to electrochemical, there are still several different types of electrochemical energy storage to be considered and many manufacturers of each. In power buffering and directed energy applications, the load profile seen by the energy storage is transient in nature and often very high power. These types of profiles have not been typically supplied by electrochemical batteries, therefore research into how these types of load profiles will impact battery performance and aging is needed. Though some research into how energy storage ages at high rate is present in the literature (Williams, Martin, Wetz, & Gnegy-Davidson, 2015) (Wetz D. A., 2011) , is minimal and warrants further study. Older chemistries such as lead acid, molten salt, and nickel based batteries have been used for the past century and are still being considered for use in Navy

applications, however, these types have a tendency to de-rate quickly, especially when operated at higher rates (Wetz, Shrestha, Novak, & Donahue, Capacity fade of a high power battery when evaluated for use within a prime power supply, 2014). Lithium-Ion technology has become more mature in recent years and has already shown a great deal of potential for use at high rates with measurable, but not always catastrophic, degradation of their usable capacity and lifetime (Wetz, Shrestha, Novak, & Donahue, Capacity fade of a high power battery when evaluated for use within a prime power supply, 2014).

In the research study presented here, valve regulated lead acid (VRLA) and lithium-iron phosphate lithium-ion (LI-LFP) batteries have been sized and studied at the roughly 60 VDC level at powers as high as 43 kW under transient profiles. The profiles being studied are generally representative of those the US Navy is interested in though they are not directly tied to any single application. To better understand the effect of high rate operation on the aging of VRLA and LI-LFP, multiple experiments have been performed using a few different cooling methods. The aim of the work is to validate the sizing study performed, evaluate the electrical and thermal performance of the two respective chemistries, and to measure the capacity fade and impedance growth of each one when loaded under similar conditions. The sizing study will be presented along with a rational for the chemistries chosen. The design of experiments and experimental results obtained from each chemistry will also be presented and finally some conclusions will be made.

Chapter 2

Background

New types of electronic technology emerge every year and in turn new types of energy storage methods are needed to fuel modern society's thrust for portable energy. Batteries are a part of so many everyday lives. Whether they are used in simple consumer electronics or in lifesaving equipment, the user depends on them. As everyone who has used a battery for a prolonged period has likely found, they age quickly as a function of cycle life meaning that over time, they are not able to power their load for as long as they did at the beginning of their life. Though this is a nuisance for consumers, it could mean life or death in many applications and therefore being able to understand and predict battery aging and capacity fade is critical. In most applications, batteries are operated at low rates. For example, a digital camera typically only draws tens of milliamps from its battery at any given time. Figure 2-1 lists the typical power consumption of a few consumer cameras available in the market today.

Camera	Average Power (Watts)	Rated Voltage (V)	Battery Voltage (V)	Ampere draw per hour (mAh)	Power consumed for 4 hours (Wh)
Sony FS700	6.7	7.2/8.4*	7.2	931	27
Blackmagic Pocket Camera	7.4	12-20	12	617	30
Canon 70D	9	7.2	7.2	1250	36
Canon 5D Mark III	10	7.2	7.2	1389	40
Canon C300	11.7	7.4/8.4*	7.4	1581	47
Blackmagic Cinema Camera	18	12-30	12	1500	72
Sony F5	24	11-17	12	2000	96
Canon C500	24	7.4/8.4*	7.4	3243	96
Sony F55	25	11-17	12	2083	100
Red Epic/Scarlet	60	11.5-17	12	5000	240
Sony F65	65	10.5-17	12	5417	260
Arri Alexa	85	11-34	12	7083	340

Figure 2-1. This figure shows the average power consumption of some consumer electronics (Sudhakaran, 2014)

The battery manufacturer will often specify a usable lifetime of hundreds to even thousands of cycles so long as the battery is used within its datasheet ratings. They are able to quote a high number of cycles because they have rated the battery, both electrically and thermally, within constraints that make material degradation predictable. Within their typical operational level, both manufacturers and independent researchers have published a great deal of research fundamentally explaining how electrochemical batteries age and fade in capacity over their lifetime (Wetz, Shrestha, Novak, & Donahue, Capacity fade of a high power battery when evaluated for use within a prime power supply, 2014) (Bazant & Pinson, 2010) (Wetz D. A., 2011) (Williams, Martin, Wetz, & Gnegy-

Davidson, 2015). The research to date has provided invaluable insight into what happens to electrochemical materials as they age and fail however, not all loads are the same, and many demand that a battery be capable of supplying very high power – some in the form of very short transients to meet dynamic load demands. Transient loads often only use a small portion of the batteries usable capacity, but well exceed the typical rated power levels of a single cell. Stacking additional cells in parallel increases size and weight only to achieve the power demand while leaving a great deal of excess capacity that will not be utilized. For this reason, there are advantages to push the limits of batteries and achieve the required power without adding an excess number of cells in parallel. Though the impact of high rate operation has been studied (Wetz, Shrestha, Novak, & Donahue, Capacity fade of a high power battery when evaluated for use within a prime power supply, 2014) (M. Dubarry, 2010) (Li, 2001) (Wang, 2009), the amount of research in the literature is limited and the C rates evaluated are typically no higher than 2C. The research performed here aims to expand upon this research topic and fill the knowledge gap.

Fundamental Operation of Electrochemical Storage

The Ragone plot in Figure 2-2 graphically presents the energy density and power density of different energy storage types and chemistries. The two properties are plotted against each other to demonstrate how an increase in power density often comes with a decrease in energy density and vice versa. Some of the technologies are operated through chemical processes while others are operated mechanically. The chart shows lithium-ion to be a dominating electrochemical storage device, but also shows that it is still low in energy density and power density when compared with fossil fuels. Despite this advantage, fossil fuels are not always the way to go and are often not always possible aboard the intended application. Given the push to be mobile and the push to be more environmentally friendly, technologies such as electrochemical batteries have found a new place in the demands for electrical power.

A battery novice may ask, ‘what is a battery?’ A battery is an electrical power source that converts stored chemical energy into electrical power through a process of electrochemical reactions. Batteries use chemical compounds to store energy and then releases its energy into electricity (North Western University , 2015). Figure 2-3 illustrates, on an atomic level, how a lithium-Ion battery converts its chemical storage into an electrical current by releasing an electron in the lithium element. Ideally, there is no path to block the lithium-ions migration in and out of the host electrode structures, but as a cell ages, blockades are formed that prevent the efficient transfer of lithium. More about this will be explained throughout this text.

Batteries come in an indefinite number of shapes and sizes, but the most economical and commonly used rechargeable battery form factor is the 18650 package. This is the form utilized in most electric vehicles today. The term 18650 refers to the size of the cell. The diameter is 18 mm and the height of the cell is 65 mm. The major drawback to using batteries as a source is the voltage sag under conduction, due to the inherent voltage drop under load, which dictates that the load must operate within a range defined by the chemistry. The lithium-ion chemistry typically offers a conduction voltage ranging between 3.3 V and 3.8 V at low conduction rates. At higher rates, the conduction voltage drops lower. The drop in potential is proportional the cell's internal equivalent series resistance (ESR) as defined by Ohm's Law. In small devices like cell phones for example, the low DC voltage is not often a major issue. However, when manufacturing an electric vehicle, where the motors often require several hundred Volts, large packs of batteries are required. The interconnection and management of many different cells in modules and batteries is not a trivial task and therefore understanding of how the cells behave, perform, and age is critical.

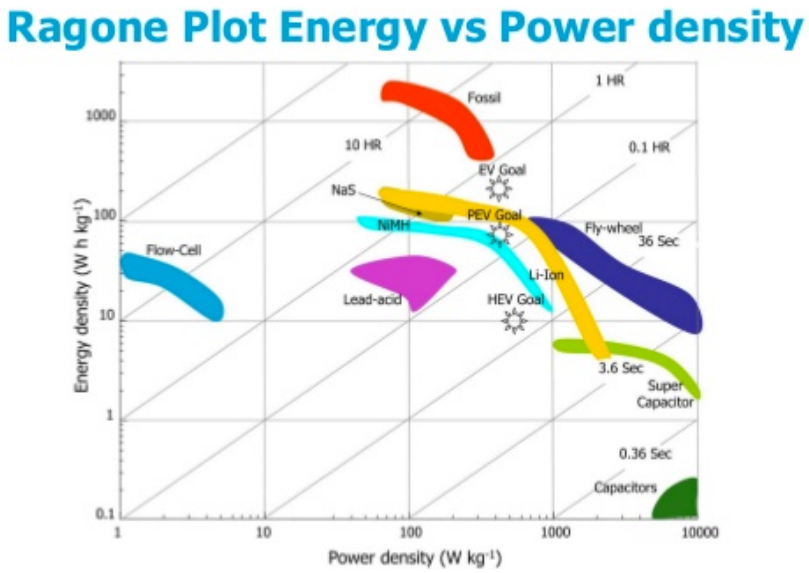

Figure 2-2 Ragone Plot for currently available electro chemical storage devices. (TU Delft OpenCourseWare, 2013)

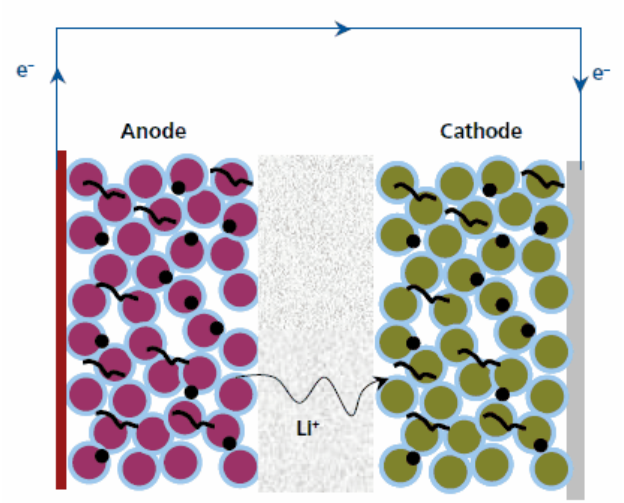

Figure 2-3 Lithium transfers from the anode to cathode during discharge. (Sigma Aldrich, 2008)

Battery Terminology

The reader should be familiar with the terminology used to describe the operation of lithium-ion cells. Since lead acid was the first type of chemistry regularly available, the terminology that describes them is the foundation upon which different chemistries are described today. A number of these terms are described below.

Float Voltage

The term 'float voltage' describes the termination voltage when charging a battery. Often times, the chargers voltage will be held at the float voltage as current drops to maintain the batteries 'state of charge' (SOC).

State of Charge

'State of charge' (SOC) is often given as a percentage and defines the percent of storage energy still available for use. When the battery is fully charged, it is at 100% SOC and when it is empty, it is 0% SOC. This is analogous to filling up a gas tank in a car and using it as the car drives

Open Circuit Potential (OCP)

Chemical over potentials define the electrical potential that is developed between the cathode and the anode of a battery. As briefly discussed earlier, when a battery is loaded, the voltage drops proportional to the IR drop across the ESR. When the battery is unloaded, the cell's potential is restored to near the chemical over potential. This potential is defined as the 'open circuit potential' (OCP) and should not be confused with the conduction voltage, which will be described next.

Conduction voltage

The 'conduction voltage' defines the voltage of the cell when it is under any load. The conduction voltage will change depending on the power demanded by the load, decreasing as the power increases. The voltage drop is a

result of the IR drop across the cell's ESR. While it will not be discussed in detail here, a cell's ESR changes significantly as a function of SOC and especially temperature. Ohm's Law states that there will be a voltage drop across resistive elements when current flows through the element. Naturally this means, that as the power demanded of the cell increases, the increased current results in a voltage drop across the cell's ESR that can almost make it unusable. In order to measure a cell's ESR at DC, the cell must be discharged at two rates, one that is very low, C/20 to C/2 for example, and then again at the rate of interest. Then, using Equation 1 and the conduction voltages measured from the two discharge curves, the ESR can be estimated.

$$DC_{ESR} = \frac{\Delta V}{\Delta I} \qquad \text{Equation 1}$$

Equalization

The 'equalization voltage', also known as the 'over-voltage potential', is the voltage at which the electrochemistry is stressed beyond the float voltage to re-obtain chemical stability. Even under normal discharge conditions, the cells that make up a lead acid battery age differently and this causes the various cells within a module to have different usable capacities and DC ESR's within a single module. By slightly overcharging the cells within a module, the cells with higher capacities will dissipate the extra energy into heat while those with lower capacities will be equalized to have the same or close to the same capacity at the higher ones. This type of equalization is not used on all types of chemistries.

Capacity

'Capacity' is measurement of how long a battery is able to supply charge to its load or accept charge from a power supply at a certain rate. Capacity is defined in units of Ampere-Hours (Ah). For example, a 1 Ah battery is able to supply roughly 1 A to a load for 1 hr. Similarly, it takes 1 hr to recharge the cell when a charge current of 1 A is applied. To understand how much energy is stored in a cell, the unit of Watt-hours (Wh) is used and this is solved by multiplying the time integrated current by the conduction voltage. Ah can also be used to describe the amount of charge in units of Coulombs as described in Equation 2.

$$1Ah = 3600\ Coulombs \qquad \text{Equation 2}$$

C-Rate

The term 'C-Rate' is used to normalize the rate of charge and discharge to the amount of capacity stored in the cell, module, or battery. The term is directly related to the capacity terminology. A 1C discharge of a 1 Ah battery means that the battery is being discharged at 1 A. A 2C discharge means it is being discharged at 2C, etc. As the discharge C rate increases, the conduction voltage decreases as described earlier.

Anode

The ‘anode’ is the negative electrode of the battery during a discharge only. When the cell charges however, the anode becomes positive. During a discharge, the anode gives up electrons but during a recharge, the anode accepts electrons.

Cathode

The ‘cathode’ is positive terminal of the battery during a discharge and the negative terminal during a recharge. The cathode oxidizes from the anode meaning that it is the element absorbing the electrons.

Deep Cycle

A ‘deep cycle’ refers to a cycle in which more than 20% of the usable capacity is removed and then restored. Another term often used to define the discharge portion of a ‘deep cycle’ is known as ‘high depth of discharge.’ In a ‘deep cycle,’ the electrode chemistry is stressed heavily and repeated cycling to high depth of discharge can cause premature aging of electrochemical devices.

Shallow Cycle

A ‘shallow cycle’ is opposite of a deep cycle and refers to a cycle where less than 20% of the usable capacity is utilized. Repeated shallow cycles do not have as much of an impact on cell aging as repeated deep cycles do.

Power Density

The term ‘power density’ refers to the power a cell is able to deliver with respect to either its mass or its volume. The term ‘gravimetric power density’ or ‘specific power density’ normalize the power to the mass while the term ‘volumetric power density’ is used to normalize the power to the cells volume. Since power is related to both the voltage and current, these terms are useful in comparing various types of energy storage to each other.

Energy Density

The term ‘energy density’ is very similar to that of ‘power density’ with the difference being that energy stored is being normalized to the mass or volume of the cell. The terms ‘gravimetric energy density’ and ‘specific power density’ are used to normalize the energy stored with respect to mass while ‘volumetric power density’ is used to normalize the energy density to the cell volume. Like the ‘power density’ the ‘energy density’ term encompasses properties such as the voltage and current so it is again useful for comparing different technologies.

Lead Acid Chemistry

Lead Acid batteries have been used for centuries. The first documented lead acid rechargeable battery was built by a French physicist named Gaston Planté in 1859 (Magnet Academy, 2010). His breakthrough changed the world. A representative model of Planté's rechargeable battery is shown in Figure 2-4.

Figure 2-4 Gaston Planté's design of the first rechargeable battery which utilized the chemical storage capabilities of Lead and sulfuric acid an electrolyte.

Figure 2-5 demonstrates the basics construction of a lead acid cell. Inside, there are two plates, one made of lead and the other made of lead-oxide. In between them, sulfuric acid is used as an electrolyte. During a discharge, electrical current flows from the lead-oxide cathode to the lead anode since the lead gives up electrons that the lead-oxide accepts. Electrons flow through an external circuit from the cathode to the anode while ions flow in the electrolyte. The exchange of electrons and ions results in both plates becoming solid lead-sulfate. As byproducts of the reactions, hydrogen gas, water (H2O), also oxygen gas are created. The chemical equations defining a discharge are listed in Equation 3-4 below.

When recharging a lead acid battery, the lead-sulfate electrodes are returned back to the states of lead and lead-oxide respectively. Normally, not all of the lead-sulfate is completely transformed back to its original state. The percentage that remains unconverted can be accelerated by environmental conditions including heat. The inefficient re-transformation of the anode and cathode is what commonly ages the cell and decreases its chemical stability. The hydrogen gases that are produced are normally dissipated out of the cell and into the environment. This creates an unbalanced chemical equation that will not allow the anode to transform back into its pure lead form. However, there are modern advances in lead acid battery constructions to combat this chemical aging.

$$\mathrm{Pb} + \mathrm{HSO_4^-} \rightarrow \mathrm{PbSO_4} + \mathrm{H^+} + 2\mathrm{e^-} \quad \text{Anode (Negative Plate)} \qquad \text{Equation 3}$$

$$\mathrm{PbO_2} + \mathrm{HSO_4^-} + 3\mathrm{H^+} + 2\mathrm{e^-} \rightarrow \mathrm{PbSO_4} + 2\mathrm{H_2\,O} \quad \text{Cathode (Positive Pate)} \qquad \text{Equation 4}$$

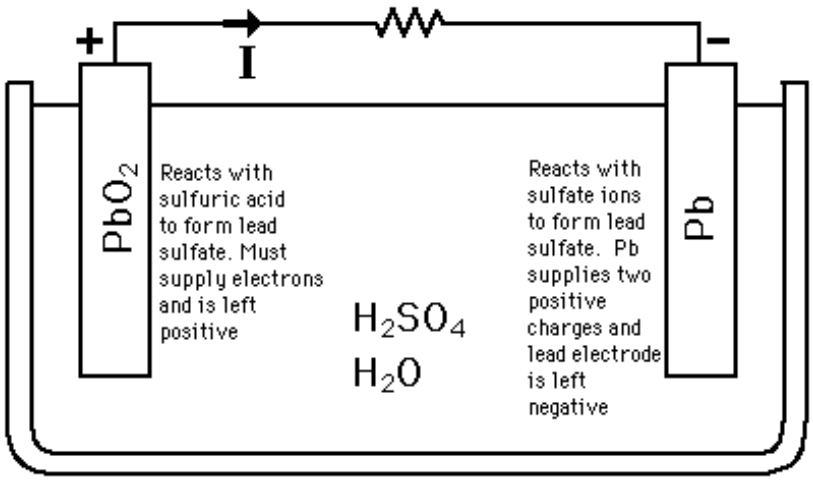

Figure 2-5. Typical Construction of Lead Acid battery (Georga Sate University , 2000)

Today, lead acid batteries are used in countless applications. These include ignition starters, various consumer electronics and even as backup power in the form of large uninterruptable power supplies (UPSs). UPSs that range anywhere from small household size to incredibly large utility grid backups have been developed and are in use around the world (Turner, Kelly, Storm, Wetz, & Wei-Jen, 2015) Renewable energy supplies, both solar and wind, use lead acid batteries both to store the energy they generate and as backup power sources when the renewables drop off. All of these applications are plagued by the capacity fade discussed earlier. The valve regulated lead acid (VRLA) form of construction is used to decrease the creation of the hydrogen gas and extend the lifetime of the cell. A VRLA module utilizes the internal pressure of the battery and a one-way pressure release valves to decrease the aging effects. The valves ensure that the oxygen produced by the positive plate is contained within the cell so that it can be reabsorbed by the negative plate. This causes the production of hydrogen by the negative plate to cease, prolonging the life of the battery and keeping harmful gases from escaping into the storage area. (East Penn Manufacturing, 2015) As a standard, these batteries utilize soaked fiberglass mats to contain the sulfuric acid electrolyte between the anode and cathode electrodes. This ensures that this type of module can survive in harsh environments. The glass mat is referred to as absorbent glass mat (AGM). This technology operates best between its temperature is maintained within 20^{o}C and 30^{o}C and it is electrically operated at what manufactures define as the 10-hour rating. The 10-hour rating is the rate at which the battery can be run continuously at for roughly 10 hours. In terms of the C rate discussed earlier, it could be thought of as 0.1C. These types of lead acid batteries are often referred to as maintenance-free since their electrolyte never has to be refilled during the warranty lifetime, which can be up to five years. This however, does not mean that there is still not necessary maintenance that is needed on the cells. Procedures such as charging

to the ‘equalization voltage’ are often considered forms of maintenance that should be periodically performed to preserve lifetime.

Lithium Ion

Over the past several decades, lithium-ion batteries have grown technology to levels previously considered impossible. As shown earlier, they offer power and energy densities considerably higher than other electrochemical batteries. They are now routinely replacing lead acid and nickel metal hydride batteries in many applications and have become the normal supply of most consumer electronics including cellular phones, electric cars, and laptops just to name a few. Without this type of battery chemistry, the battery life of the applications just listed would be considerably less than they are today and would not have as widespread use as they do. The first lithium ion battery first appeared commercially in 1991. Goodenough, Yazami, and their teams were the first to publish and help create the lithium ion battery with a graphene anode (Nagaura & Tozawa, 1998). This type of anode is what helps dendrites from being created inside the cell. A dendrite is a crystalline mass that grows and causes the anode and cathode to connect electrically. Prior to this research, lithium-ion batteries suffered from dendrite formation that eventually lead to many fires and the release of hazardous material (Lithium Battery Saftey and Handling Guildline, 2006).

To charge a lithium-ion battery, an external power supply creates a potential difference that pushes electrons out of the cathode and into the anode. A chemical reaction occurs that liberates lithium-ions from the cathode. The ions migrate through the electrolyte and are captured by the anode electrode as is shown in Figure 2-6. When the power supply is removed, the ions are stored in the anode setting up an electrical potential difference that allows the cell to do electrical work when connected to a load. When connected to the load, the opposite reaction occurs as electrons are pushed from the anode to the cathode through the load and lithium ions are released by the anode to flow back into the cathode. The release and capture of ions within the anode and cathode host materials is known as intercalation and de-intercalation. It can be thought of as the parking of cars in a parking lot. There are so many cars and so many spaces and filling them all efficiently is desirable. The equation below is an example of a charge and discharge reaction of a Lithium Manganese battery with a graphene electrode.

$$Li_xC_6 + Li_{-x}MO_2 \leftrightarrow C_6 + LiMO_2 \qquad \text{Equation 5}$$

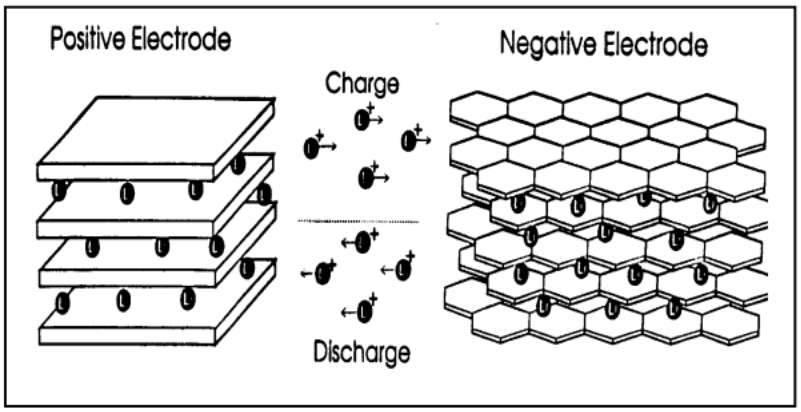

Figure 2-6. This figure shows the exchange of ions being pased from the postive and negative elctrode

Construction of the 18650 cells is shown in Figure 2-7. (Sigma Aldrich, 2008)

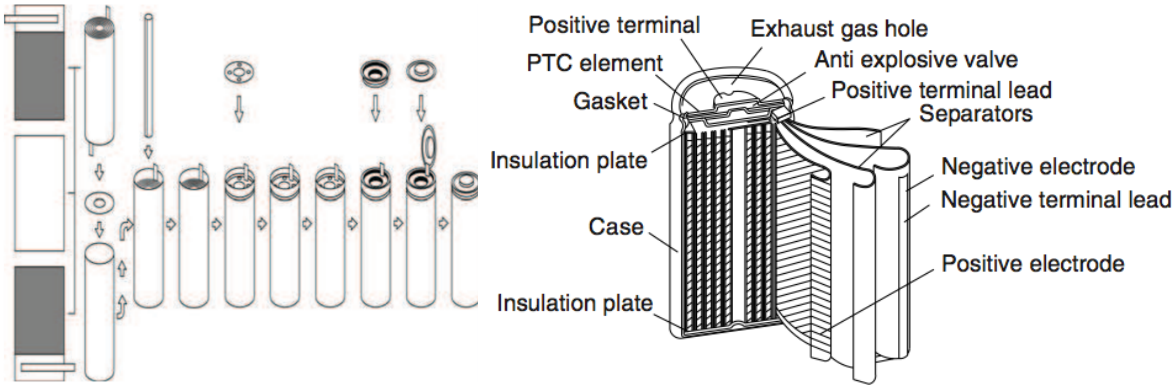

Figure 2-7. Assembly and construction of a 18650 cell (Brodd, 2009).

In Figure 2-7 the assembly and broken down construction is shown. The first step, on the left of the figure, is where the coated the anode and cathode on a conductive metal. Normally aluminum and copper are used as the anode and cathode materials and then separated by a porous sheet that holds the electrolyte. All three of these items (anode, pours sheet, and cathode) are rolled around each other and then placed into the aluminum casing. Another name when the anode and cathode are wrapped around each other is jelly roll. After the jelly roll is inserted into the case, a rubber cap placed over top of the jelly roll with the cathode tab exposed. The cathode tab is then welded to a metal cap that is placed and then crimped to the metal case. During aging the anode and cathode degradation is due to increased cycling life and surrounding conditions, such as temperature. Throughout this paper it will be described on how this occurs.

Degradation of a Lithium-ion cell does not always happen uniformly and can be caused by different factors. When there is capacity loss of a cell, the major contributing factors are electrode disintegration, material deterioration, and loss of free lithium. (Bazant & Pinson, 2010) (Li, 2001) Typically, these effects are from high

temperatures generated from high rate which fatigue the cell. This type of fatigue causes the SEI (solid-electrolyte interphase) layer to grow on the negative electrode. The SEI layer is the fundamental source of capacity fade, which is formed during recharging of the battery. Initially, the SEI layer protects the electrode from solvent decomposition but as cycling life of the cell increases, the SEI layer grows and prevents the majorly of the lithium from being transferred from electrodes. Normally, the SEI layer forms uniformly across the negative electrode, but due to high rates the layer forms sometime erratically which causes advanced aging in the cell. (Wetz D. A., 2011) (Wetz, Shrestha, Novak, & Donahue, Capacity fade of a high power battery when evaluated for use within a prime power supply, 2014) (Wetz, Shrestha, & Novak, Back to Results Elevated Rate Cycling of High-Power Electrochemical Energy Storage Devices for Use as the Prime Power Source of an EM Launcher, 2013) As the SEI layer increases in thickness the internal impedance increases, causing more I^2R losses inside the cell, this can be seen in Figure 2-9. (Bazant & Pinson, 2010)

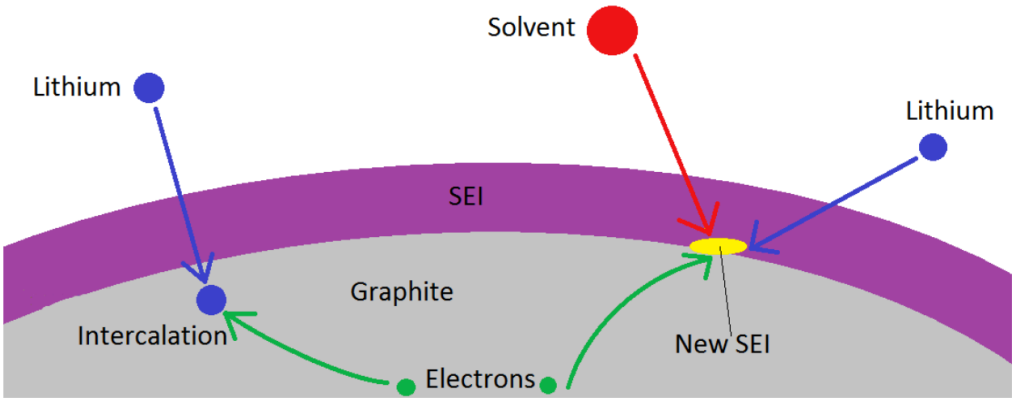

Figure 2-8. Example of how a SEI layer grows due to the solvent, electrolyte, and lithium combine to create a growth on the crystalline structure. Which occurs regularly during cycle life.

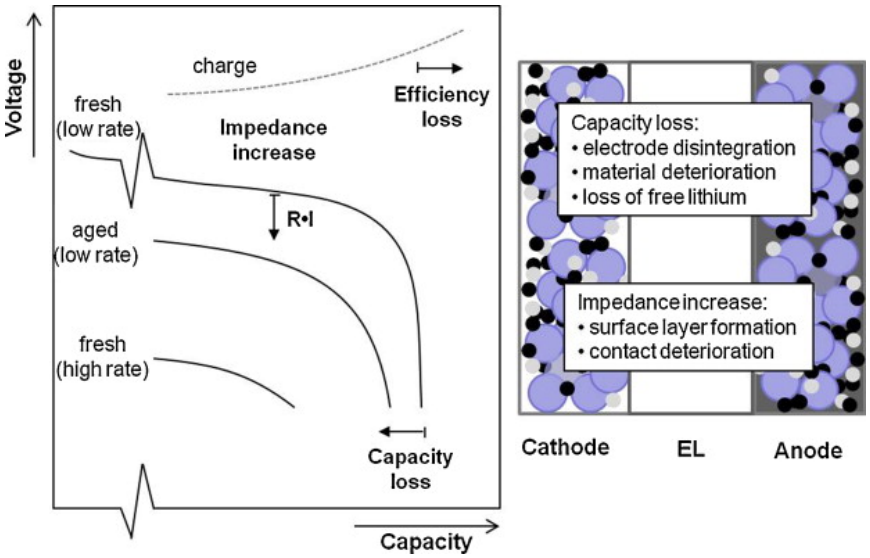

Figure 2-9. This figure explains how capacity loss happens during cycle life on the left. As well how the impedance growth effects the output voltage and efficiency losses.

In the years to come, there is going to be a global change in automotive industry. We will soon see that combustion engines will become less available and electric power trains will take over. With this, batteries will become a dominate storage device in all vehicles; not just to start them, but power them as well. With this new era of vehicles, there has to be some way to understand the health of the batteries. Traditionally a mechanic could take apart anything on a car and repair the section that is failing. Soon the mechanics will not be allowed to disassemble a battery pack due to the complexity and its sensitivity. This requires a method that can show how a battery is changing due to its cycle life. This is where electrochemical impedance spectroscopy, otherwise known as EIS, become essential. The way EIS works is by sending a pure sinusoidal wave of either voltage or current and measuring the output to gain an impedance measurement, simply ohms' law. Traditionally, this is known as a frequency response analysis, FRA. Normally FRA's return a bode plot which is magnitude vs. frequency and phase vs. frequency. However, EIS returns imaginary impedance vs. real impedance which can help explain how a cell deteriorating over time. A traditional EIS plot is shown in Figure 2-10. To simply understand each section, it is broken down into high and low frequency response. The first section represents the high frequency induction in the system. The next section, Section 2, gives the resistance of the cell, otherwise known as the ESR. Section 3 describes the SEI layer and how it is growing or decaying during cycle life. This is a very important section to know when a cell is beginning to fail because this section will become very large and start to show a reflection with capacity. The second semi-circle, in section two, represents the double layer capacity and charge transfer. Basically, how hard is it to get charge from one electrode to the other. The last section, section 5, represents the

active material of the electrodes, which explains how much lithium is recombining with electrodes to make a complete reaction. (D. Andrea, 2011)

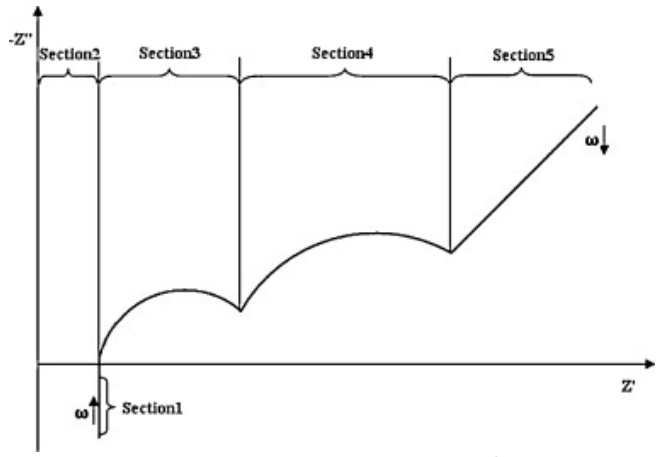

Figure 2-10. Impedance spectrum in a Nyquist plot for a Lithium-ion battery.

In Figure 2-10 there are five sections that the example EIS plot are broken into. Section 1 relates to the inductance in the system at high frequency's. Section 2 is the ESR of the cell which lays on the real axis. Section 3 is the first semi-circle which is related to the SEI layer. Section 4 represents the double layer capacity and charge transfer resistance. Finally, Section 5 is the diffusion processes in the active material of the electrodes. With all of these sections a circuit model can be generated to understand how particular sections are growing. These circuit models will be explained later in the paper.

With all of the sections combined, from the figure above, a circuit model can be created to help understand how the battery is being effected over its cycle life. With a circuit model like Figure 2-11, each section can be put into either an inductor, capacitor, or resistor. Traditionally, lithium-ion batteries always have two capacitors to build both humps in the EIS curve. Without EIS, the battery would have to be cut open and then examined under a microscope. This would prove costly in industry, but with this method of health detection an in depth model and understanding can be discovered with having to destroy a battery pack.

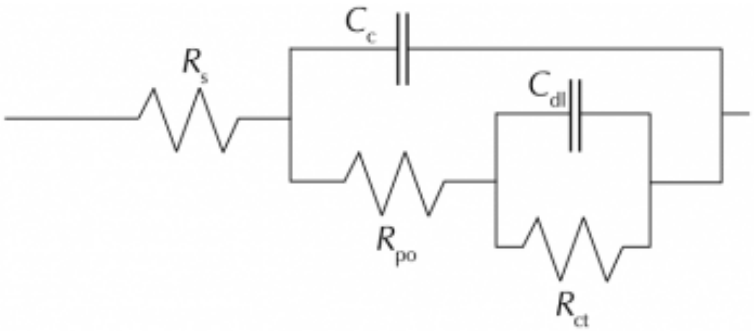

Figure 2-11. Typical EIS circuit model for a Lithium-ion battery using a two electrode measurement.

Simulated Load and Energy Storage Sizing

In the design of experiments performed here, the program sponsor asked that we assume that eventually a prime power supply would be needed to supply power to a pulsed or continuously operated load at the 600 kW to 800 kW level. It is further assumed that power from the battery prime power will be conditioned through a DC/DC converter before being fed into the pulsed load itself as seen in Figure 2-12. Two possible operational scenarios include continuous operation over a 2 minute period or pulsed operation over a 4 minute period with a 50% duty cycle. In the latter, it is assumed that the load will draw power from the prime power in increments of 5 seconds with 5 seconds of down time in between each pulse. A representative power architecture is shown in Figure 3 – 1 below.

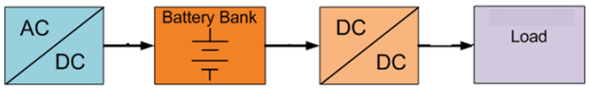

Figure 2-12. Simple schematic of the electrical architecture being considered for study here.

The test plan was heavily influenced by the constraints of the project sponsor. These constraints are listed below

1. Scaled experiments should be performed assuming that in the final application, the battery must be capable of 600 to 800 kW of operation for 2 minutes continuously or 4 minutes with a 50% duty cycle.
2. A lead acid and a lithium-iron phosphate lithium-ion (LFP-LI) chemistry must be evaluated under similar profiles
3. The scaled batteries experimentally evaluated must include multiple modules connected in series/parallel so that interconnection can be studied
4. Practical cooling options should be explored for each type
5. The capacity fade and impedance growth should be studied using both experimental and analytical methods

It is hypothesized that the tests conducted in this paper will show that the lead acid chemistry would age rapidly due to the high temperatures associated with high rate operation and the Lithium-ion chemistry would have minimal capacity loss and would uniformly age throughout its cycle life. The results section and conclusion will go in to more debt on how these findings will be true.

Electrochemical Sizing Study

Given the constraints listed in the previous section, it was decided that batteries with open circuit potentials (OCPs) near the 60 VDC level would be experimentally evaluated. The 60V potential was chosen since it is high

enough that it requires multiple modules to be placed in series, but low enough to be safely touched without concern. As discussed earlier, there are several different manufacturers of VRLA and LFP-LI chemistries. Therefore, a sizing study was performed to identify which type and manufacturer of cells should be studied experimentally. The sponsor asked that the assumption be made that while operational at the 600 kW to 800 kW level, the battery would discharge roughly 800 ADC to the power electronic converter. This assumption equates to the need for a usable capacity of roughly 27 Ah from the battery, with some variation depending on battery conduction voltage. Given these constraints, many different COTS (commercially off the shelf) batteries could be used. These include, but are certainly not limited to, the K2 26650P LFP, GAIA 20Ah LFP, GAIA 38Ah LFP, Saft VL30AFe, Saft VL20PFe, EnerSys XE60 VLRA, EnerSys XE40 VLRA, C&D UPS12-400MR VRLA, C&D UPS12-300MR VRLA, and the C&D UPS12-210MR VRLA.

Lithium-ion

When discharging an electrochemical cell, two primary conditions are used to cutoff the discharge. The first is a cutoff when the minimum voltage is reached meaning that all of the usable capacity at the rate under test has been exhausted. Keep in mind that the usable capacity varies strongly as a function of rate. The second condition is a thermal cutoff when the cell's body or terminal exceeds a certain safety threshold. If a thermal cutoff is reached, that does not necessarily mean that all of the usable capacity has been exhausted. The K2 Energy 26650P LFP datasheet lists a maximum current capability of 42 A (K2 Energy Solutions, 2015). From experimentation in the lab, the manufacturer's rating was confirmed but without cooling, the cell's peak temperature nearly always reached the recommended maximum temperature making cooling critical at this rate. In the laboratory, it was found that liquid cooling is able to cool the cells at this rate; but as just mentioned, this will become more of a requirement for performance and lifetime improvement. Without cooling, the cells should be operated at lower rates and more cells have to be connected in parallel to decrease the discharge current per cell. Since the capacity of the smaller form factor cells is so much lower than that of larger form factor cells, the parallel count can become quite high and as a result, the complexity of the battery management system (BMS) and cooling hardware. Also the likelihood of having a weak link within the system increases when higher quantities of cells are required. Even if 100% of the 1C capacity could be utilized at higher rates, which it can't, a minimum of eleven parallel cells would be required to meet the capacity requirement alone since the cells store roughly 2.6 Ah each. Even at 42 A of discharge current, eleven cells couldn't meet the roughly 800 A of current that the sponsor requested meaning that considerably more than 27 Ah must be stored to meet the power requirement. Since the full 1C capacity cannot be used at higher rates, a minimum of twenty to thirty cells must be connected in parallel

to achieve the load requirements. Sharing of current in multi-parallel batteries has also been brought up as a concern among energy storage researchers (Wong, Taufik, Anwari, & Ldris, 2011). With this in mind, it was likely that cells of smaller form factors would not be studied here. These include the A123 Nanophosphate™ cells which have similar capacity as the K2 Energy cells but a marginally higher peak current rate (A123, 2015).

The 20 Ah and 38 Ah LFP large format cells, respectively, manufactured by GAIA were also considered for the load profile here. Under the conditions being studied here, a connection of three parallel strings of the 20 Ah cells or two parallel strings of the 38 Ah cells would likely suffice, reducing the overall cell count to much less than that of a K2 Energy or A123 26650 battery respectively. The GAIA 20 Ah and 38 Ah cells, respectively, have performed well when evaluated by in the laboratory at current rates as high as 500 A however at the time this work was started, these cells were not readily available for purchase so they were taken off the table of consideration.

The Saft VL20VFe and the Saft VL30AFe cells were also considered. While the VL20VFe would be exceptional for this set of experiments, Saft was not readily manufacturing the cells at the time and could not sell us low quantities for taking them off the table. The VL30AFe is one of Saft's more commercially available cells and was readily available for sale at the time. UTA had previously tested the VL30PFe cells, which was an earlier version, and was comparable in operational performance up to 400 A. Given the previous work with this cell, cost, and low parallel count required to meet the 800 ADC load requirement, this cell was chosen. Given its high usable capacity at 400 ADC, the usable capacity is slightly higher than is needed but it was decided to evaluate this cell in a 20S/2P configuration for the study here.

Valve Regulated Lead Acid

When selecting the VRLA to be tested, it was understood that the Navy had already developed an energy storage module (ESM) made up of C&D UPS12-400MR VRLA modules. It was mentioned by the sponsor that the Navy ESM is configured in a 74S/4P manner and is designed for roughly 600 kW of continuous load. Assuming 600 kW and 800 kW loads, this 74S/4P configuration of modules would require each module to supply 2.03 kW and 2.7 kW, respectively, to the pulsed load. Given the cold cranking amp rating of these modules,1200 CCA, each of these power ratings is relatively low for these modules, however VRLAs are rarely operated at high rates to full depth of discharge (DoD). Given the interest in understanding how the ESM's size could be reduced for low DoD applications, the C&D UPS12-400MR VRLA was first evaluated under several different power profiles to understand how they perform and age at higher rates. If it were able to operate at higher rates, this could lead to making the existing ESM smaller, for example with two parallel strings instead of four. The results obtained from

that effort are presented later in the report. From that work, it was found that the C&D UPS12-400MR should be more than capable at rates up to 5.4 kW per module when evaluated under the pulsed load profile for up to 5 minutes. For that reason, it was decided that a 5S/2P battery of C&D UPS12-400MR modules would be studied here.

Sizing Study

Considering the discussion above, the sizing study presented in Tables 1 through 4 was performed. In Table 1, the values are presented on a per unit basis where a single lithium-ion cell is considered a unit and a single 6-cell lead acid module is considered a unit. In Table 2, the modular metrics are presented where a module consists of one or more units of each respective type of cell/module. Table 3 presents the load characteristics being considered. In Table 3 it should be seen that a load assumes a battery voltage of 56 V, a load power of 800 A, and a conduction time of 2.5 minutes. The profile will be pulsed on and off under the 5 second on/ 5 second off profile. This is 0.5 seconds longer than asked for by the sponsor in order to demonstrate capability 20% in excess of the sponsor's needs. A constant power (CP) load condition of 43 kW is utilized since that is roughly equivalent to cycling a 50 V battery at 800 A of conduction current. Most loads require a CP rather than a constant current (CC) so a constant power load is more representative of the end application. The recharge current is dictated by a recharge time of 15 minutes and the required battery capacity is sized 120% greater than required by the load so that there is enough capacity even when operating only between 0% and 80% SOC. Finally, the battery is oversized by an additional 120% so that there is enough capacity to meet the load requirements even when the battery's capacity has faded to 80% of its initial capacity Table 4 presents the overall parameters of a ~60V battery made up of each type of module which will discharge enough capacity to meet the requirements of Table 3. The study was performed using data collected from each technology at UTA as well as information from each cells' manufacturer datasheet.

It should be noted that the sizing tables have been modified and improved upon considerably as the evaluation of each technology has been performed. The data shown in Tables 1 through 4 highlight the vast differences in size, weight, power density, energy density, and cell/module count amongst the different technologies. The lithium-ion is clearly more power and energy dense than the lead acid. It is critical that the reader understand that the cooling technologies considered in the case of the K2 Energy, Saft VL30AFe, and GAIA 20 Ah cells, are not optimized. The values used are representative of aluminum cold plates developed and evaluated at UTA for each respective technology. There are advanced cooling options being designed by other performers funded by the Navy that should be considered for further improvement in the size and weight values presented here.

Table 1 Lithium-ion, Lead Acid and G4 Per Unit Comparison.

These parameters take into consideration the smallest available form of each option, hereby referred to as a unit. For Lithium, units represent single cells. For lead acid, units represent one 6-cell 12V battery. A unit represent one complete 10-Cell 15V battery.							
	Saft VL30AFe Li-Ion	**UPS12-400MR VRLA**	**K2 26650 LFP Li-Ion**	**K226650UP02 LFP Li-Ion**	**GAIA 20 Ah LFP Li-Ion**	**A123 26650**	**Notes**
Capacity @ 1hr Rate (Ah)	30	92	2.4	2.85	20	2.5	Datasheet values
Maximum Discharge (A)	400	400	35	50	500	60	Datasheet values
Max. Recharge Current (A)	120	200	5	5.7	100	10	Datasheet values
Capacity at Max Current (Ah)	29	32	2	2.75	17.5	2.5	Measured in UTA testing
1 kHz ESR (mOhm)	1.1	3	9	6	0.8	6	Datasheet values
DC ESR (mOhm) (1C - 0.5C)	1.47	4.5	33.1	22.1	1.5	15.4	Measured in UTA testing
DC ESR (mOhm) (15C - 0.5C)	0.82	2.5	15.2	10.1	0.85	10.9	Measured in UTA testing
1C Nominal Voltage	3.25	12	3.2	3.2	3.25	3.3	Estimated
Rated Charge Voltage (V)	3.8	13.2	3.65	3.65	3.65	3.6	Datasheet values
Unit Conduction Voltage at Max Rated Current (V)	2.92	11.00	2.67	2.75	2.83	2.65	Datasheet values
Mass (kg)	1.048	35	0.085	0.084	0.93	0.076	Datasheet values
Length (cm)	N/A	34	N/A	N/A	N/A	N/A	Datasheet values
Width / Diameter (cm)	5.4	16.6	2.54	2.54	6	2.54	Datasheet values
Height (cm)	22.2	21.6	6.5	6.5	15.7	6.5	Datasheet values
Volume (L)	0.51	12.20	0.03	0.03	0.44	0.03	Datasheet values

Table 2. Lithium-ion and Lead Acid Module Comparison.

These parameters take into consideration the constructed module parameters for a given option. For instance, a GAIA 20 Ah module consists of 10-Cells in series, as will the Saft module. A previously tested K2 module consisted of 16-Cells in series, which is what will be used. A G4 module is synonymous with a Unit in this case, since the 10-Cell module is the smallest available. The lead acids assume a normal bought package of 6 cells. These units account for estimated measured/estimated module size including busswork and cooling.							
	Saft VL30AFe Li-Ion	**UPS12-400MR VRLA**	**K2 26650 LF Li-Ion**	**K226650UP02 LFP Li-Ion**	**GAIA 20 Ah LFP Li-Ion**	**A123 26650**	**Notes**
Number of Series Units Per Module	10	1	10	10	10	10	INPUT PARAMETER
Number of Parallel Units per Module	1	1	1	1	1	1	INPUT PARAMETER
Per Module Capacity @ 1hr Rate (Ah)	30	92	2.4	2.85	20	2.5	Per Unit Capacity * Number of Per Units in Parallel
Max. Per Module Discharge Current (A)	400	400	35	50	500	60	Max Per Unit Discharge Current * Number of Per Units in Parallel
Max. Per Module Recharge Current (A)	120	200	5	5.7	100	10	Max Per Unit Recharge Current * Number of Per Units in Parallel
Per Module Capacity at Max Current (Ah)	29	32	2	2.75	17.5	2.5	Max high current capacity * Number of Per Units in Parallel
Per Module 1 kHz ESR (mOhm)	11	3	90	60	8	60	Per Unit ESR * Number of Per Units in Series / Number of Per Units in Parallel
DC ESR (mOhm) (1C - 0.5C)	14.7	4.5	330.8	220.53	15	154	(Empirical Value * Number in Series) / Number in Parallel
DC ESR (mOhm) (15C - 0.5C)	8.2	2.5	151.7	101.13	8.5	109	(Empirical Value * Number in Series) / Number in Parallel
ESR Scale Factor	0.75	0.83	1.69	1.69	1.06	1.82	Empirical ESR at Max C / Datasheet 1 kHz
Estimated Module 1C Nominal Potential (V)	32.5	12	32	32	32.5	33	Max Per Unit Rest V * Number of Per Units in Series

Per Module Rated Charge Voltage (V)	38	13.2	36.5	36.5	36.5	36	Max Per Unit OCP * Number of Per Units in Series
Per Module Conduction Voltage at Max Rated Current (V)	29.2	11.0	26.7	27.5	28.3	26.5	Per Unit Conduction Voltage * Number of Per Units in Series
Module volume (Units Only) (L)	5.08	12.20	0.33	0.33	4.44	0.33	Number of Per Units in Series * Number of Per Units in Parallel * Per Unit Volume
Module Mass (Units Only) (kg)	10.48	35	0.85	0.84	9.3	0.76	Number of Per Units in Series * Number of Per Units in Parallel * Per Unit Mass
Cold plate Mass Estimate (kg)	14.00	0	0.78	0.78	9.90	0.78	Saft, GAIA, and K2 are based off of the ThermAvant cold plates made for each type already either at UTA or NRL
Bus Work Mass Estimate (kg)	1.408	0.5	0.08	0.04	1.408	0.11	
BMS Mass (kg)	1.25	0	1.25	1.25	1.25	1.25	
Total Per Module Mass (kg)	27.1	35.5	3.0	2.9	21.9	2.9	
Length Scale Factor	1.4						
Width Scale Factor	1.25						
Height Scale Factor	1.15						
Per Module Length (cm)	37.8	34.0	17.8	17.8	42.0	17.8	
Per Module Width (cm)	13.5	16.6	6.4	6.4	15.0	6.4	
Per Module Height (cm)	25.5	21.6	7.5	7.5	18.1	7.5	
Total Per Module Volume (L)	13	12.2	0.9	0.9	11.4	0.9	
Cooling / Bus Work / BMS Mass Ratio	61%	1%	71%	71%	57%	74%	

Table 3. Load Parameters.

Battery Potential (V)	56	INPUT PARAMETER
Load Power Required (kW)	42.5	INPUT PARAMETER
Operational Discharge Time (min)	2.5	INPUT PARAMETER
Recharge Time (min)	15.0	INPUT PARAMETER
Capacity Aging Overhead Included	120%	Amount of Fade and it Still work (Greater than 100%)
Capacity SOC Overhead Included	120%	On average, a given cell can supply 79% of its nominal capacity at max rate. Estimate of useable capacity depending on planned rate (Greater than 100C%)

Table 4. ~60V Battery Specifications.

These calculations leverage the single unit parameters listed above to calculate module requirements for any given brand / chemistry. Requirements are derived based on the load specifications input above.							
	Saft VL30AF Li-Ion	**UPS12-400MR VRLA**	**K2 26650 LF Li-Ion**	**K226650UP02 LFP Li-Ion**	**GAIA 20 Ah LFP Li-Ion**	**A123 26650 ANR26650M1-B**	**Notes**
Consider Power Only	**0**						**1 = yes, 0 = no**
Consider Capacity Only	**0**						**1 = yes, 0 = no**
Consider Power and Capacity	**1**						**1 = yes, 0 = no**
Useable Capacity at Max or Estimated Discharge Current	**0**						**1 = Max Current, 0 = Est Current**
Use Max or Avg. Recharge Current Rate	**0**						**1 = Max Current, 0 = Est Current**
Base Voltage off of Max Charge, Min Conduction, or 1C Nominal	**3**						**1 = Max Charge, 2 = Min Conduction, 3 = 1C Nominal**
Percentage of Max Current Allowed	100%	100%	100%	100%	100%	100%	INPUT PARAMETER
Number of Modules and Cells In Series							
# of Modules in Series Req. for Input Potential	2	5	2	2	2	2	Ceiling of (Desired OCP / Module OCP)
# of per Units in Series per Parallel String	20	5	20	20	20	20	Number of Per Units in Module * Number of Modules
Estimated Voltage and Current during Discharge							
Max Discharge Current Allowable Per Parallel String (A)	400	400	35	50	500	60.0	Percentage of Max Current Allowed * Max Current Per String
Estimated Minimum DC Conduction Voltage at Max Current (V)	58.4	55	53.4	53.9	56.5	52.9	(Module 1C Potential - (1kHz ESR * ESR Scale Factor)) * Number of Modules
Estimated Battery Current Assumed Using Min Conduction Voltage (A)	728	773	796	788	752	803	Load Power / Estimated Min Cond Voltage
ESR Voltage Drop (V)	6.6	5	10.6	10.1	8.5	13.1	(Number of Modules * Module 1C Voltage) - Conduction Voltage
Load Capacity Required							
Load Capacity Required Assuming Min Conduction Voltage, Load Power, and Operational Time (Ah)	30.3	32.2	33.2	32.9	31.3	33.5	Power * Time / Cond Voltage

Power Sourced and Dissipated during Discharge							
Max Power Available from each Series String of Modules (kW)	23	22	2	3	28	3	Discharge Current * Conduction Voltage
Estimated Discharge Heat Loss (kW)	4.8	3.9	8.4	8.0	6.4	10.5	ESR Voltage Drop * Estimated Current
Energy Stored and Dissipated as Heat and to the Load during Discharge							
Energy Consumed by the Load (MJ)	6.4	6.4	6.4	6.4	6.4	6.4	Input Load Power * Input Load Time * 60
Heat Energy Lost During Discharge in ESR (MJ)	0.7	0.6	1.3	1.2	1.0	1.6	Heat Power * Input Time * 60
Total Stored Energy Needed (MJ)	7.1	7.0	7.6	7.6	7.3	8.0	heat Energy + Load Energy
Verification of Load Capacity using Energy (Ah)	30.3	32.2	33.2	32.9	31.3	33.5	Total Energy / 1C Nominal Voltage
Stored Capacity Required to meet Discharge Demands							
Final Battery Capacity Needed with Overheads Included (Ah)	43.6	46.4	47.8	47.4	45.1	46.2	(Load Capacity + Heat Loss Capacity) * Overhead Factors
Usable Capacity per Parallel String of Modules Assuming Max Current (Ah)	29	32	2	2.75	17.5	2.4	Module Capacity at Max Rate
Usable Capacity per Series String of Modules Assuming Estimated Current (Ah)	29.4	33.1	2.2	2.1	18.1	2.4	Capacity estimated from equation derived as a function of current
Calculation of Worst Case Current Per Parallel Module during Discharge							
Min # of Required Parallel Modules Assuming Current Alone	2	2	23	16	2	14	Celing of (Current / Max Current)
Worst Case Estimate of Current Per Parallel Module (A)	364	386	35	49	376	57	Current per Module
Number of Modules Required to meet Discharge Demands							
Min # of Required Parallel Modules to meet Capacity Requirement assuming Max or Est Current with Overhead Factors Entered	2	2	23	23	3	21	Ceiling of (Required Capacity with Overhead Factors / Module Capacity)
Min # of Required Parallel Modules to Meet Load Power Requirement Alone	2	2	23	16	2	14	Desired Power / Power Per String

Final Number of Parallel Modules Considered Here	2	2	23	23	3	21	Compares input requests and Decides either C22 or C26
Final Number of Actual Cells in Parallel	2	2	23	23	3	21	Number of Per Units in a Module * Modules in Parallel
Calculation of Module Usage during Discharge (Indication of how Over or Under Sized it is)							
Percentage of Usable Capacity Used	51%	49%	67%	67%	58%	66%	Load Capacity / (Number of Parallel Modules * Capacity in Each)
State of Usable Capacity at End of Discharge	49%	51%	33%	33%	42%	34%	100% - Percentage Used
Final Values Based on Discharge Demands and Calculations Above							
Final Estimated Conduction Voltage (V)	59.0	55.2	53.5	57.1	60.7	57.7	Module 1C nominal - (Module Current * DC ESR)
Final Current Required Per Parallel Module (A)	364	386	35	34	251	38	Estimated Battery Current / Final Number of Parallel Modules
Final Discharge C Rate	12	4	14	12	13	15	Current per Module / 1C Rate
Total 1C Module Stored Capacity (Ah)	60	184	55.2	65.55	60	52.5	Number of Parallel Modules Considered * Module 1C Capacity
Total Usable Capacity At Rate (Ah)	58.9	66.2	49.6	49.6	55.3	50.4	Capacity estimated from equation derived as a function of current * # of Parallel Modules
Energy Stored assuming 1C Nominal Potential (MJ)	14.0	39.7	12.7	15.1	14.0	12.5	1C Capacity * Number of Series Modules * Module 1C Nominal Potential * 3600
Power Delivered Per Parallel String (kW)	21.3	21.3	1.8	1.8	14.2	2.0	Total Power / Final Number of Modules
Total Battery Power inc. Heat (kW)	47.3	46.4	50.9	50.5	48.9	53.0	(Number of Parallel Strings * Power Per String) + Battery Heat
Estimated Voltage and Current during Recharge							
Max Possible Battery Recharge Current (A)	240	400	115	131.1	300	210	Number of Modules in Parallel * Max Recharge Current
Max Battery Charge Potential (V)	76	66	73	73	73	72	Number of Modules in Series * Module OCP
Average Recharge Current at Desired Recharge Time (A)	121	129	133	132	125	134	Capacity including Overhead / (Desired Recharge Time * 60)
Average Recharge Current Per String at Desired Recharge Time (A)	60.6	64.4	5.8	5.7	41.7	6.4	Avg. Current / # of Parallel Strings
Recharge Current Value used Here (A)	121	129	133	132	125	134	If the user enters max, it uses max and if the user enters estimated it uses the estimated value

Voltage Over potential at Recharge Current (V)	0.8	7.7	0.8	0.8	0.8	1.97	Low Current DC ESR * Recharge Current
Recharge Time to Reach 80% SOC (min)	9.2	8.8	10.5	10.5	9.8	10.5	((80% - End SOC) * 1C Capacity * 60 for min conversion) / Recharge Current
Remaining time for CV Recharge (min)	5.8	6.2	4.5	4.5	5.2	4.5	Input recharge time - 80% Recharge time
Power Sourced and Dissipated during Recharge							
Peak Recharge Power (kW)	9	9	10	10	9	10	Avg. Current * Charge Voltage
Estimated Recharge Heat Loss at Peak Current (kW)	0.22	0.19	0.51	0.33	0.16	0.35	Recharge current^2 * Low Current ESR
Capacity Required to meet Recharge Demands							
Capacity Added during CC High Rate Recharge (Ah)	18.5	19.0	23.3	23.1	20.4	23.4	Recharge time * Recharge current / 60
Capacity Added during CV Recharge (Ah)	25.1	27.4	24.5	24.3	24.6	24.8	Capacity Extracted - Capacity Added during CC recharge
Energy Stored in the Battery During Recharge							
Energy Added during CC High Rate Recharge (MJ)	5	5	6	6	5	6	Capacity Added * Charge Voltage * 3600
Energy Added during CV Recharge (MJ)	7	7	6	6	6	6	Capacity Added * Charge Voltage * 3600
Total Energy Added (MJ)	12	11	13	12	12	13	Sum of two energy values just above
Estimated Battery Weight and Volume							
Estimated Total Weight of Per Units Alone (kg)	42	350	39	39	56	32	Number of Series Modules * Number of Parallel Modules * Module Cell Mass
Estimated Total Volume of Per Units Alone (L)	20	122	15	15	27	258	Number of Series Modules * Number of Parallel Modules * Module Cell Volume
Est Total Weight of Battery (kg)	109	355	136	134	131	122	Number of Series Modules * Number of Parallel Modules * Module Mass
Est Total Volume of Battery (L)	52	122	41	41	68	38	Number of Series Modules * Number of Parallel Modules * Module Volume
Estimated Power and Energy Densities							
Power Density of Cells Alone (kW/kg)	1.11	0.13	1.10	1.60	1.52	2.09	Power per String * Number of Parallel Strings / Per Unit Mass
Total Capable Power Density (kW/kg)	0.43	0.12	0.32	0.46	0.65	0.55	Power per String * Number of Parallel Strings / Battery Mass
Energy Density of Cells Alone (Whr/kg)	82	10	68	68	55	84	High Rate Module Capacity * Number in Parallel * Voltage / Per Unit Mass
Total Capable Energy Density (Whr/kg)	32	10	19	20	23	22	High Rate Module Capacity * Number in Parallel * Voltage / Battery Mass

Chapter 3

Experimental Setup and Equipment

The experimental set up constructed and utilized in the work discussed here is shown graphically in Figure 3-1. The block diagram illustrates how the batteries are cycled electrically, how data acquisition is made, and how the batteries are cooled when forced air-cooling is studied.

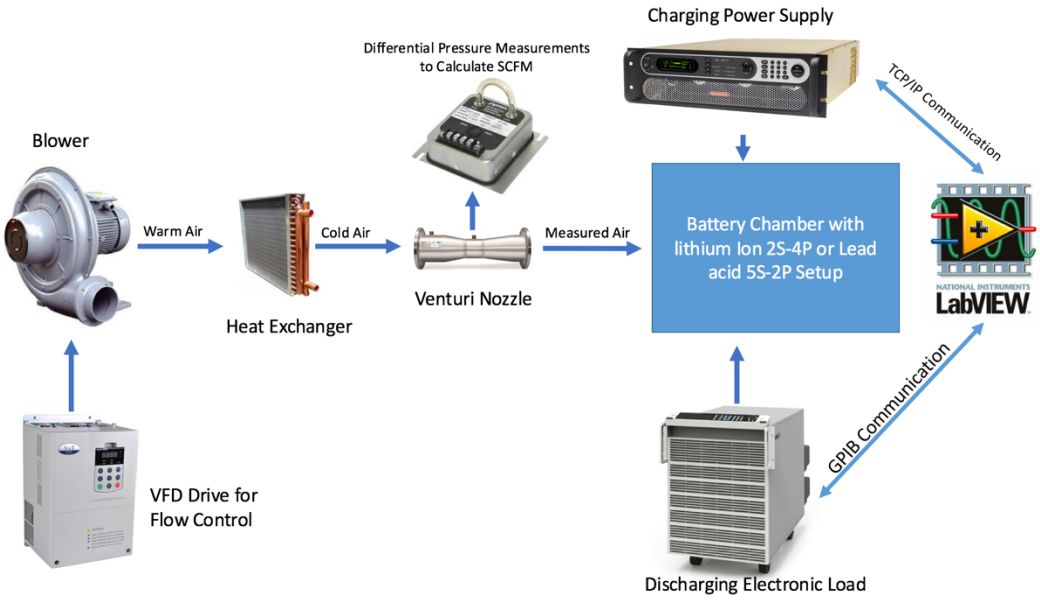

Figure 3-1. Block diagram of experimental setup. This is a high level overview of the equipment and communication used to cool and cycle the batteries.

Forced Air Cooling

One form of cooling that was of interest to the sponsor is forced air-cooling. The cooling system constructed here consists of a large 20 HP blower that is used to maintain a controllable rate of air-flow, a liquid cooled heat exchanger that is used to cool the incoming air, and a Venturi nozzle that is used to make air flow measurements.

When designing the air-flow cooling system, the first requirement was to roughly calculate what air-flow rate was required to cool the batteries. To start, an estimate of the heat dissipated by each cell was used by approximating the expected I^2R losses. From the sizing study presented earlier, it is estimated that the VRLA battery will dissipate roughly 4 kW of heat and the LFP-LI battery will dissipate roughly 5 kW of heat. It was estimated that between 600 and 800 CFM of air would be needed to dissipate those levels of heat. Next an estimate of the pressure drop between the blower and the battery chamber was calculated to be equal to roughly 40 in of water. Given the air-flow rate of 800 CFM and pressure drop of 40 in of water, a Model 6E blower from Cincinnati Fan was chosen, seen in Figure 3-2.

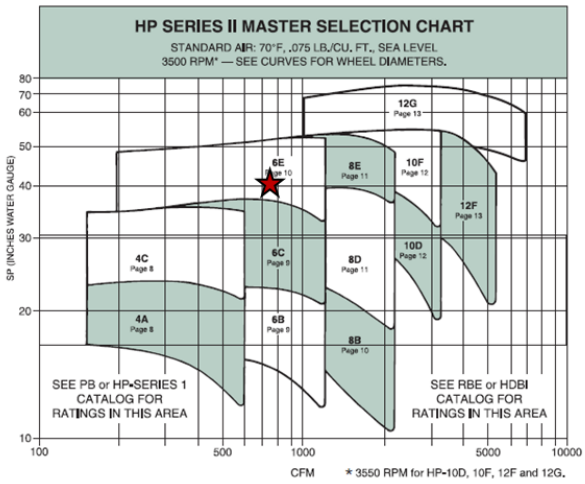

Figure 3-2. Sizing chart used to select the air-cooling fan.

To cool the incoming air, a liquid cooled heat exchanger with a surface area of 61 cm x 61 cm. Three closed-loop circulating chillers, each with a cooling rate of 2.9 kW, are connected in parallel and used to flow 30 GPM of a 50/50 mix of distilled water and polyethylene glycol through the heat exchanger. Finally, a Venturi nozzle is used to measure the flow rate of the air between the heat exchanger and the chamber which houses the battery under test. The Venturi nozzle works by the Venturi effect in which the

pressure drop across an air-choke point is used to measure the air-flow rate (Gilson Engineering, 2012). A more schematic of the air-cooling system is shown in Figure 3-3 and a photograph of the blower, heat exchanger, and Venturi nozzle are shown in Figure 3-4.

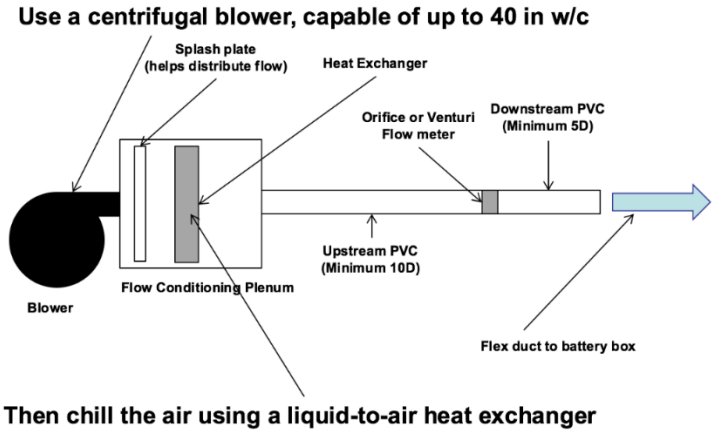

Figure 3-3. This is a diagram of the air flow set up, notice how the upstream and downstream pipes are different lengths to make the air flow measurements more accurate.

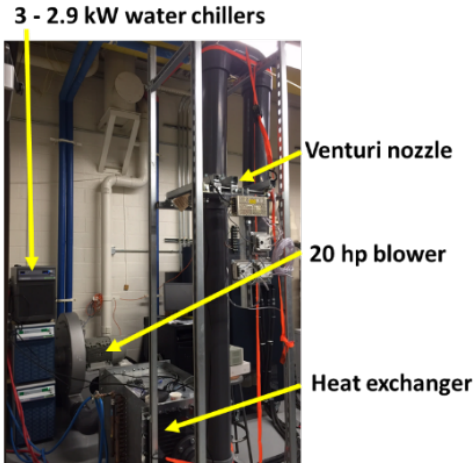

Figure 3-4. Photograph of the 20 hp centrifugal blower, heat exchanger, Venturi flowmeter, and airflow distribution line out to a battery chamber. National Instruments data acquisition was used to read in the data from the Venturi nozzle.

Each battery is housed in its own 122 cm x 91 cm x 92 cm steel chamber that was designed and constructed by the UT Arlington Physics Machine Shop using 0.32 cm thick steel plate and tube steel to fit this experiments needs. A PVC pipe is inserted into a 10 cm hole in the chamber's side through which the forced air is passed. Holes are drilled down the length of the PVC pipe to flow air into the chamber and seven additional 10 cm holes are in the side of the chamber to allow the air to return out to the lab space. A photograph of one of the chambers is shown in Figure 3-5.

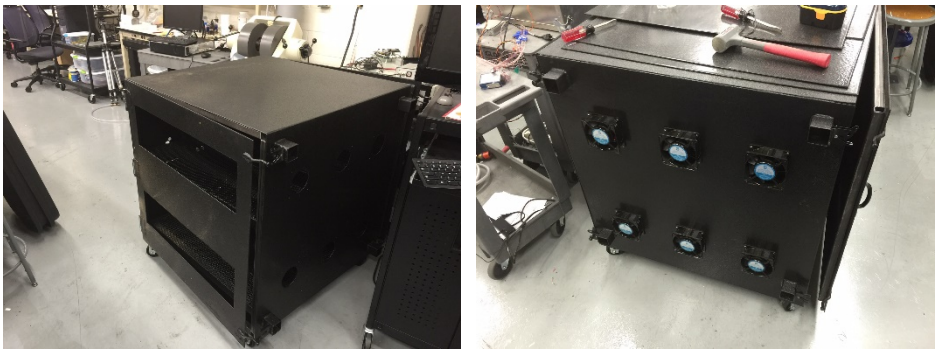

Figure 3-5. Photograph of the battery test chambers designed and constructed. In the left figure, the front of a chamber is shown and in the right figure, the side of the chamber is shown where exhaust fans are located

To cycle the batteries electrically, programmable loads and power supplies are used. The programmable loads utilized are manufactured by Chroma and have electrical ratings of 80V/1000A/15kW. Since the load requires 43 kW, three loads must be utilized in parallel. Programmable power supplies manufactured by Ametek are utilized with ratings of 80V/188A/15kW. Recharge currents of roughly 125 A are required to achieve the 15-minute recharge time, so only one power supply is required for each experiment. A photograph of the programmable loads and power supplies is shown in Figure 3-6.

Figure 3-6. Photograph of eight of nine 15 kW programmable loads and eight 15 kW power supplies used in this research. In the left most figure, a zoomed in view of the loads and supplies is shown. In the right most figure, the full setup is shown.

The voltage of each module is monitored in real time using custom designed differential voltage monitoring cards. Due to the higher common mode potentials associated with a differential measurement across individual cells, traditional data acquisition devices that have maximum common mode voltages of 5 V – 100 V cannot be used. To allow the use of these acquisition devices, the voltage monitor boards were designed such that the differential cell voltages were level shifted down to a 0 V – 10 V common mode range, buffered to prevent impedance issues with the acquisition devices, and low-pass filtered to remove noise. The voltage monitor's output is tied directly to the input of a National Instruments (NI) 9205 differential voltage monitoring CDAQ card, which is set to 0 V – 10 V range with a theoretical resolution of approximately 15mV, 16-bit ADC and 11:1 attenuation [9]. The actual resolution in practice is on the order of 50 mV, with 100 mV being the target initially. A 8 slot, USB NI CDAQ chassis is used to transfer the data recorded by the 9205 card to the NI LabVIEW Visual Instrument (VI) panel. A photograph of the differential voltage monitoring card is shown in Figure 3-7.

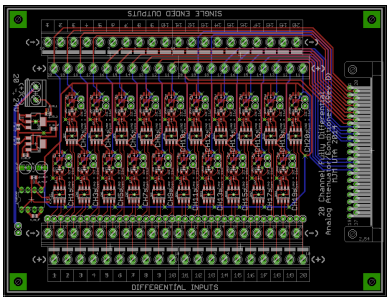

Figure 3-7. Custom designed and fabricated differential voltage monitoring boards used to monitor individual VRLA module voltages.

Since VLRA modules have a modestly decent ability at self-regulating cells, no other form of battery management system (BMS) is used on the VRLA battery. In the case of the LFP-LI battery, a BMS is utilized to properly balance the 20S/2P battery. An ACTIA i+Me BMS, shown in Figure 3-8, is utilized. The BMS is able to balance the cells at 0.4 A which is significantly higher than most commercial off the shelf (COTS) systems enabling the battery to balanced faster. Using RS-232 communication, the BMS is able to transfer each cell's voltage to the data acquisition system for measurement and control, which will be discussed soon.

Figure 3-8. Photograph of one ACTIA i+Me BMS master (above) and slave (below) module.

The operational temperature of a battery is a critical indicator of its condition and prolonged heat can significantly degrade their capacity. Therefore, it is critical that cell/module temperature is measured at all times so a history is maintained and also as a

safety cutoff in the event the temperature gets too hot. The temperature of each cell/module is monitored using Type T thermocouples, which have an accuracy of roughly 1^{o}C, that are fed into a number of NI 9213 thermal data acquisition cards. The 9213 cards offer sixteen channels of thermal data acquisition with cold junction temperature compensation and acquisition rates as high as 75 S/s per channel. A separate set of 9213 cards is used for each battery and like the 9205 cards, an eight slot NI CDAQ chassis is used to transfer the recorded data to the host VI. A photograph of the thermal acquisition setup is seen in Figure 3-9.

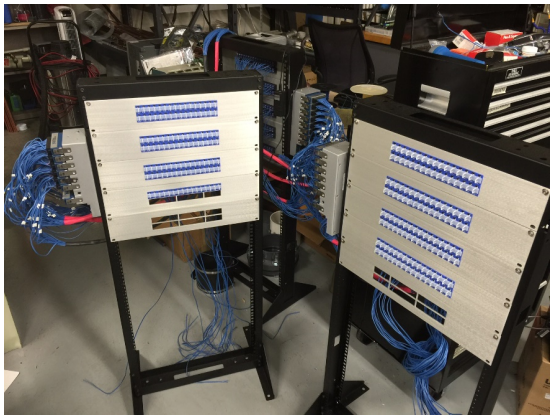

Figure 3-9. Thermal and voltage data acquisition. Seen are the thermocouple distribution blocks with National Instruments (NI) data acquisition modules mounted on the left side.

As already stated, the data acquisition is all made using a host VI written using the NI LabVIEW programming interface. The NI VI is also used to control the operation of the programmable loads, via a GPIB protocol, and programmable power supplies, via a TCP/IP protocol. While each battery is being cycled, the VI transmit control signals to the loads and power supplies to set their charge/discharge power and current respectively. During any cycle, if the voltage of any individual cell or module exceeds the rated maximum or minimum value, the NI VI will shut down the load and power supply to prevent the battery from being damaged. In addition to the voltage, the VI monitors the

temperature of all cells and modules in real time and shuts down the system if any one of them exceeds the maximum rating of the device. As it is a large graphically programmed interface, it is difficult to provide much more detail here. A photograph of the VI front panel is shown in Figure 3-10.

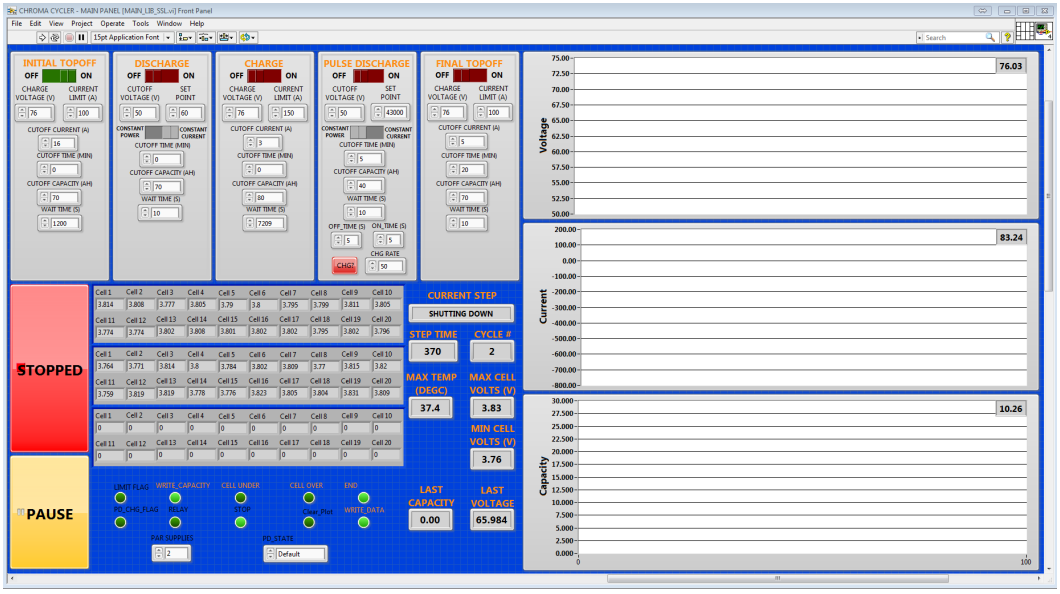

Figure 3-10. Control system used to cycle and control the battery.

Finally, the batteries themselves will be discussed. A photograph of the VRLA battery as it is housed in its chamber is shown in Figure 3-11 and a similar photograph of the LFP-LI battery is shown in Figure 3-12. Both batteries utilize 0.64 cm thick bus work with rounded edges manufactured from Copper 11000. The cross sectional area of this sized bus work is able to carry roughly 600 Amps of current without significant voltage drop.

Figure 3-11. 5S/2P C&D UPS12-400MR battery assembled in a test chamber. Two sets of 3/0 wire is connected to each series set of cells.

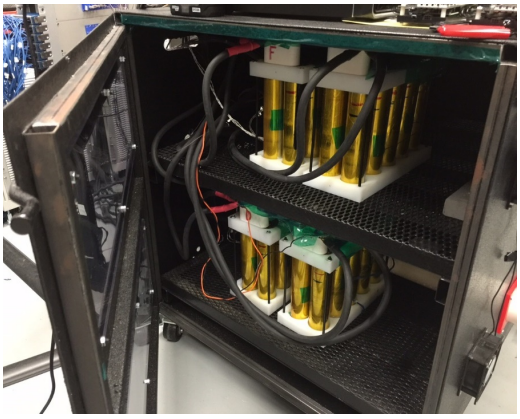

Figure 3-12. Photograph of the 20S/2P Saft LFP-LI battery assembled in a test chamber. As they are shown, they are housed in plastic housings used for evaluation with forced-air cooling.

The last portion of the experimental setup that requires discussion are the liquid cooled cold blocks utilized as an alternative cooling method for the LFP-LI battery. The VRLA battery is too large for liquid cooling to really be practical, but the LI on the other hand is well conformed for liquid cooling. The cold blocks utilized here are manufactured by ThermAvant LLC. They are manufactured from Aluminum 6061 alloy and have a cooled water loop inside as shown in Figure 3-13. Water is supplied through the cold plates using the same three - 2.9 kW water chillers used to pass water through the heat

exchanger. The coolant used is the same 50/50 mix of water and glycol and it is passed through the blocks at a flow rate of 5 L/minute. The flow rate was specified by the sponsor and water temperatures of 20°C and 30°C were evaluated. A photograph comparing the air cooled and liquid cooled LI batteries are shown in Figure 3-14.

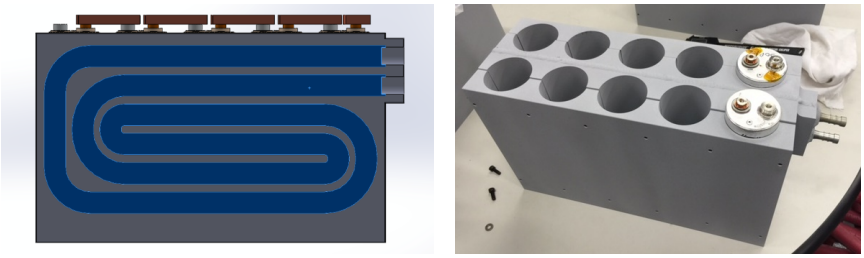

Figure 3-13. ThermAvant aluminum cooling plates. A solid model (left) showing the internal water loop is presented along with a photo (right) of an assembled block respectively.

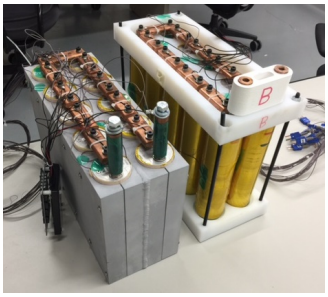

Figure 3-14. Photographic comparison of a 10S/1P liquid cooled (left) and air-cooled (right) LFP-LI module respectively.

Chapter 4

Experimental Data

Lead Acid

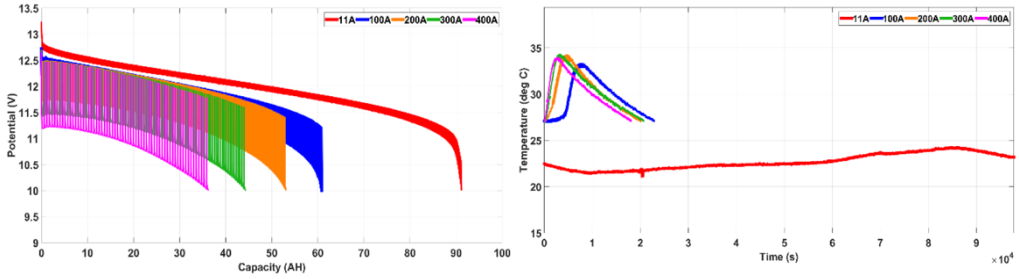

Figure 4-1. Pulsed Power and Energy Laboratory baseline 5on/5off plots. The left plot shows the discharge curves at various current ratings and the right give the temperature curves with respect to testing time.

Early in the design of the VRLA battery, preliminary research was performed to understand how the C&D modules perform when they are operated at 2.7 kW, 3.6 kW, and 5.4 kW respectively, as well an independent analyses of different rates was tested by UT Arlington shown in Figure 4-1 . These are the power levels required for the C&D module to operate in 74S/4P, 74S/3P, and 74S/2P configurations and source 800 kW to the load. Though it depends heavily upon the conduction voltage of the battery, the pulsed load requires roughly 27 Ah from its battery over a 2 or 4-minute period respectively depending upon whether the operation is continuous or pulsed at 50% duty cycle. The C&D UPS12-400MR VLRA is nominally a 100 Ah battery when cycled at its 10 hr rate. When this metric is considered alone, a single series string of C&D UPS12-400MR VLRA stores over 3.5 times the energy required by the load for a single pulsed discharge. However, when a VLRA module is operated at higher rates, its usable capacity decreases considerably. Most VLRA datasheets will list the modules usable

capacity at various rates however; it has been previously found at UTA that the values listed by manufacturers in their datasheets can be considerably greater than what is observed in practice, with variations especially high at lower operational temperatures. Table 5 lists the capacity and operational power required from each parallel string/module in each of the configurations considered. Evaluations in these configurations is of interest as the ability to operate the modules at higher rates reduces the number of parallel strings and therefore the full battery's size, weight and complexity. Table 5 summarizes the experiments performed.

Table 5. Test Matrix performed on the C&D UPS12-400MR VLRA.

	C&D UPS12-400MR [1]							
# of parallel strings in the ESM	**Mass of Modules Alone (kg)**	**Volume of Modules Alone (L)**	**Power required per parallel string (kW)**	**Power required per individual module within each string (kW)**	**2 minute capacity per parallel string for a single shot[2] (Ah)**	**2.5 minute capacity obtained during lab testing[5] (Ah)**	**Peak capacity extracted during high depth of discharge (DoD) experiments[7] (Ah)**	**Useable Capacity remaining after 100 continuous, high DoD, cycles (Ah)**
4	10,182	1,753	200	2.7	8.57	8.99	54.92	Not Tested
3	7,636	1,314	267	3.6	11.43	Not Tested	45.82	30.90
2	5,091	877	400	5.4	17.14	18.4	38.48	21.97
1[3]	2,545	438	800	10.8	34.29	Not Tested	Not Tested	Not Tested
C&D 400MR Max	N/A	N/A	548	7.4[4]	23.49	Not Tested	26.21	15.41

1. Table assumes the load of 800kW (worst case scenario)
2. Assumes conduction voltage of 1.75V / Cell
3. Beyond the capability of the C&D UPS12-400MR
4. Absolute maximum discharge power from C&D UPS12-400MR Datasheet
5. To slightly exceed requirements, pulsed experiments in the lab were performed for 5 minutes with a 50% duty cycle
6. Modules were discharged using a continuous power profile from full charge until the module voltage reached its minimum voltage of 10V
7. As will be seen, the capacity extracted starts out low and as the module heats up the useable capacity increases. It peaks and then begins to decline as a result of aging

During the initial round of evaluations, two scenarios were experimentally tested. The first scenario experimentally evaluated was aimed at measuring the performance and lifetime of the modules when they are experimentally evaluated under a continuous constant power (CP) profile from their full charge voltage to their minimum discharge voltage. This method of testing results in a high depth of discharge (DoD) and is a worst

case scenario study that defines the modules usable capacity at high rate. High DoD greatly accelerates the aging and capacity fade of batteries. At high DoD, the battery chemistry is stressed harder as the end of the discharge is reached. It has been previously shown by Okada, et.Al, that a high depth of discharge results in increased corrosion layer formation and increasing impedance growth. This results in higher stresses on the electrodes and electrolytes when electrochemical reactions are forced to occur despite there being an abundance of species left to react. When fully recharged, the electrolytes are stressed to near their maximum ratings resulting in faster decomposition. Also when fully recharged, the rate of side reactions, which occur when the batteries are resting, increases resulting in increased breakdown of the electrolyte and increase interphase layers being formed on the electrode/electrolyte interface. It is for this reason that manufactures typically recommend that batteries be cycled between 80% and 20% of their listed capacity ratings to increase cycle life.

As seen in Table 5, the power required from the C&D battery in a 1P configuration is beyond its maximum rates and for that reason, this scenario was not evaluated in any way. Two identical batteries were cycled one hundred times at power levels of 3.6kW and 5.4 kW, which are roughly the operational power requirements for operation in 3P and 2P configurations respectively. A third battery was cycled one hundred times at 7.4 kW, which is the maximum power rating of the C&D module. After each discharge, the module was immediately recharged using a constant voltage (CV) procedure with a peak current limit of 200 A. That was the highest recharge current possible in the PPEL at the time. At these rates, the modules were able to supply capacities of 45.82 Ah (3P – 3.6 kW), 38.48 Ah (2P – 5.4 kW), and 26.21 Ah (Max – 7.4 kW), respectively. It should be noted that these measurements were the peak capacities obtained after each respective battery had heated up to near the max temperature recorded. Figure 4-2 through Figure 4-5 show the

capacity extracted and mean temperature over the one hundred cycles performed at each of the rates listed. It should be mentioned that the batteries were sitting out in a large open-air environment allowing a significant exposure to circulating air around them.

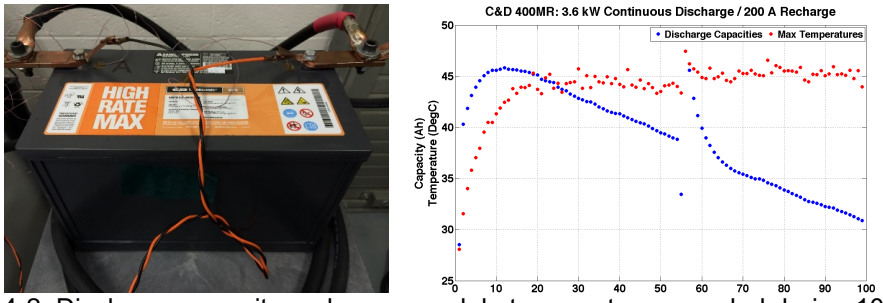

Figure 4-2. Discharge capacity and mean module temperature recorded during 100 - 3.6 kW CP discharge cycles.

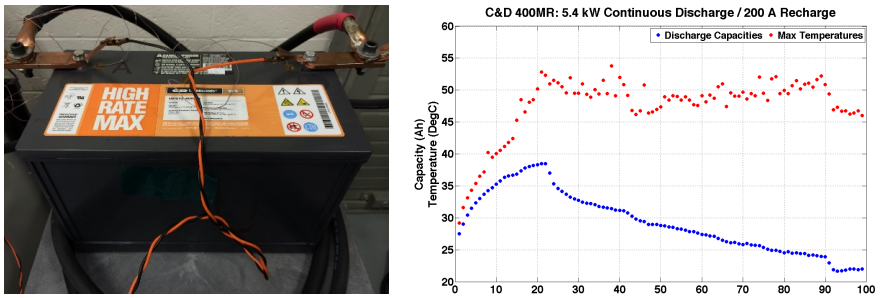

Figure 4-3. Discharge capacity and mean module temperature recorded during 100 - 5.6 kW CP discharge cycles.

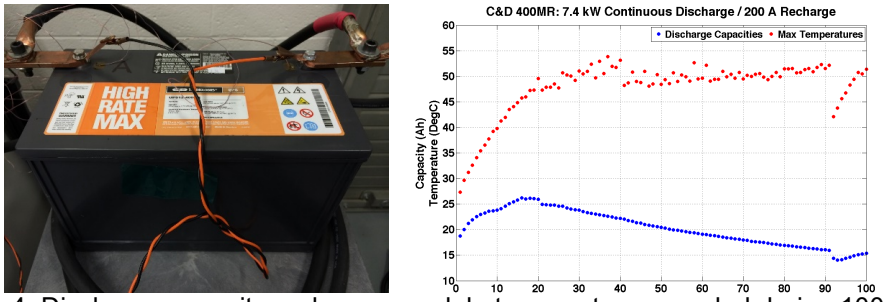

Figure 4-4. Discharge capacity and mean module temperature recorded during 100 – 7.4 kW CP discharge cycles.

As seen in Figure 4-2 through Figure 4-4, the capacities extracted from each of the modules initially starts out low and increases as the module heats up. After roughly 10

cycles at 3.6 kW, and 20 cycles at both 5.6 kW and 7.4 kW respectively, the usable capacity of the battery begins to decrease sharply following a roughly linear decrease. It should be noticed in Figure 4-2 that there is an increase in the capacity around cycle 60. At that stage in the testing, the cycling was paused for a short time while modifications were made to the data collection equipment. When cycling was resumed, a sharp increase in the usable capacity is measured for one cycle that quickly decreased as cycling continued, eventually continuing to follow the trend leading up to cycle 60. The increase at cycle 60 occurred because the modules were given short time to electrochemically stabilize during the down time; however as mentioned, it is not a long-term gain. What should be taken away from the plots is that if the modules are stressed to their limits in terms of depth of discharge and recharge rate, their usable capacity will quickly fade. This data shows that if the batteries are fully drained at high rates under the pulsed profile, they will only be good for a short time before they need to be replaced.

In the second scenario evaluated, C&D modules were cycled to a lower DoD and where it is assumed they will only be used for one 2-minute or 4-minute discharge prior to being recharged. This scenario is most common and provides a good representation of what would be expected upon fielding of these modules in the application of interest to the Navy. It is important to remember the capacity required for a single shot from each parallel string that is listed in the tables above. Table 5 indicates that the C&D UPS12-400 MR stores more than enough capacity for a single shot in 4P, 3P, and 2P configurations. In this scenario of testing, the shallow DoD means that only a small fraction of the module's usable energy is utilized in each of the 4P, 3P, and 2P configurations. This shallow DoD operation is much easier on the battery, since it is never pushed to its operational voltage limits, and therefore a higher cycle life is expected. In the evaluations performed, pulsed discharges were extracted in a 5s on/ 5s off manner

for 5 minutes. This is one minute longer than that required of the pulsed profile and the additional minute was performed to ensure that the operational requirements were met and just slightly exceeded. The results that will be shown here, Figure 4-5, are those in which the module was discharged at 5.4 kW (2P) as this seems like the solution that is the most feasible for the pulsed profile to implement. After 5 minutes of pulsed discharge at 5.4 kW, the module is recharged at the 76-minute recharge rate, which is lower than that used earlier in the high DoD experiments, but representative of what the pulsed profile was considering for execution at the time this work began. In Figure 4-5, there are three sub-figures plotting the capacity extracted, module case temperature, and end conduction voltage. Because the 5-minute time limits the discharge, every cycle should take out the same capacity so long as the battery is healthy. However, as impedance grows, the conduction voltage will decrease and push the current and capacity higher. Eventually, the battery will age to a point where its conduction voltage drops below the modules minimum operational voltage, 10.0 VDC, before the desired capacity is extracted. It is at that point that the module will be considered to be at the end of its life.

In Figure 4-5, it is seen that over 1,100 cycles were performed with what appears to be good performance. In the upper sub-figure, it should be noticed that the capacity extracted from the module is nearly consistent at around 18 Ah; however, it is slightly increasing as the battery ages and the conduction voltage decreases, as expected. In the middle sub-figure, the mean case temperatures are shown exceed 35^{o}C. It should be pointed out that the exposure to open-air allows the module to dissipate its heat and maintain the modest temperature rise. It will be seen later that higher temperatures are recorded under similar test conditions in a more confined environment, which could reduce this usable lifetime considerably. Many of the variations measured in temperature are primarily due to variations in the ambient room temperature. In the lower sub-figure, it

should be noticed that the last conduction voltage measured is decreasing, meaning that the battery is aging, roughly linearly as a function of cycle life. It is currently unknown if that linear trend would continue or if there will be a sharp knee at some point. Further testing will confirm that, but that has not been performed to date. The bottom line is that if this data holds when these types of modules are assembled into a battery with two parallel strings, then these modules are sufficient for supplying the 800 kW to the lad in either 4P, 3P, or 2P configurations so long as the DoD is kept low and the recharge current is kept moderate. Further evaluation of this battery at the pulsed 5.4 kW rate should continue later when time allows however at the time of this writing, emphasis was placed on evaluation at the 60 VDC level.

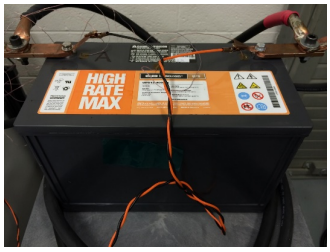

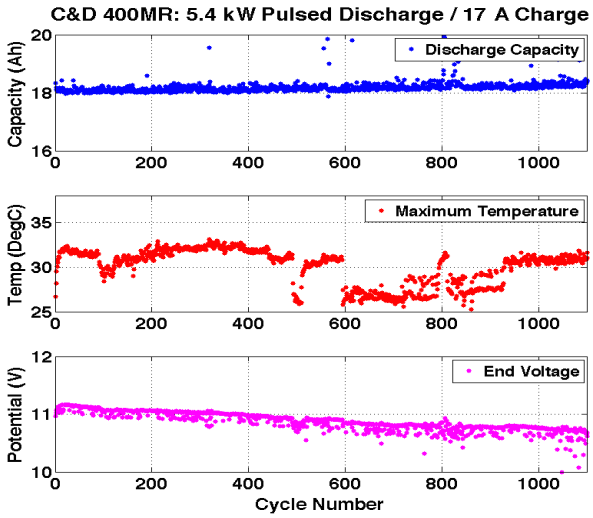

Figure 4-5. Discharge capacity, mean module temperature, and end of discharge conduction voltage recorded during 600 – 5.4 kW pulsed discharge cycles.

Upon completion of the 1,100 cycles, the module was characterized at the 10 hr rate to measure the level of capacity fade induced. Though not plotted, the battery initially had roughly 100 Ah of usable capacity at the 10 hr rate. After the 1,100 cycles of high rate discharge, the module had just under 65 Ah of usable capacity. Therefore, while the module still has a fair amount of life left in it for this application, the capacity is fading and this is most likely due to high internal temperatures at the core from I^2R losses. This data implies that the 800 kW load could be supplied by two parallel strings of UPS12-400 MR VRLA modules and that they will have a modestly long lifetime. Therefore, the results of the sizing study were confirmed at this point and it was decided that the 5S/2P battery would be constructed and cycled at that time.

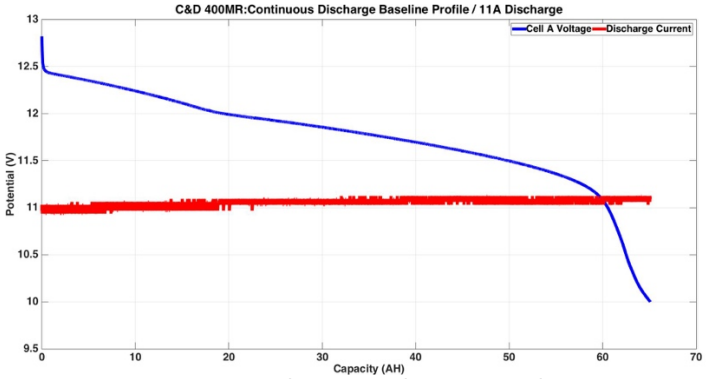

Figure 4-6. Voltage measured as a function of capacity after 1100, 5.4 kW pulsed discharge cycles had been completed. The initial capacity was roughly 100 Ah and after 1100 cycles, the capacity has decreased to roughly 65 Ah.

Prior to beginning the experiments at the 60 VDC level, all ten VRLA modules were characterized at their 10 hr rate and impedance (EIS) scans were made. For those unfamiliar with EIS measurements, an EIS measurement applies a small sinusoidal potential, typically a few mV, on top of an electrochemical cell's OCP. The applied potential is known and the sinusoidal current induced is measured. Division of the two

measurements using Ohm's law reveals a complex impedance that represents the impedance of the cell. Changes in the complex impedance as cycle life evolves can be used to understand how the impedance of the cell evolves over time.

The 10 hr discharge capacities recorded from each of the ten modules are shown in Figure 4-7. Each of the 11 A CC discharges occurred after the modules had been topped off to their full state of charge (SoC) potential. Though there is variation in the 10 hr capacities, this is common for VRLA modules and it is not cause for concern. The initial EIS curves are shown in Figure 4-8. There is great consistency among all of them and this serves as a great basis for where the modules begin impedance wise.

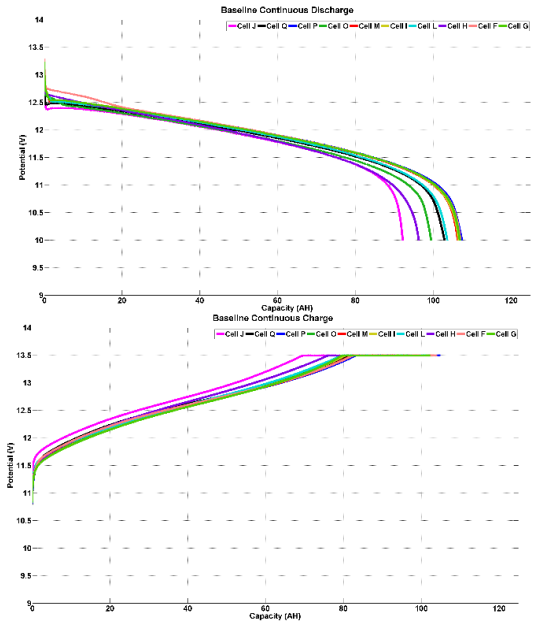

Figure 4-7. Ten hr (11 A CC) discharge (left) and recharge (right) capacities of all 10 VRLA modules used to make up the 60 VDC VRLA battery.

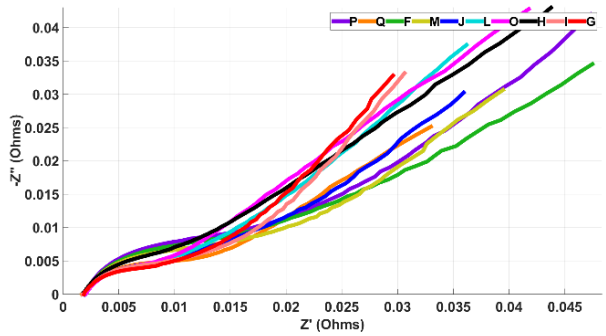

Figure 4-8. EIS measurements collected from all ten VRLA batteries at cycle 0.

Using the EIS data, it is possible to formulate an equivalent circuit model for the battery as discussed earlier in the background section. An equivalent circuit model representing the C&D UPS12-400MR, can be seen in Figure 4-9. In the circuit, R1 makes up the real resistance introduced by the materials within the battery and the connection grid structure holding the lead. C1 represents the electro capacity of the cell's anode and cathode. The electro capacity represents the physical amount of charge each host material can store. The constant phase element, CPE, represents the impedance introduced as charged particles migrate in and out of the electrode host structures. The R2 and C2 elements are used to understand the growth and decay of the SEI layer. Towards the end of this section, more will be presented to show how these parameters change as the lead acid batteries are cycled at high rates.

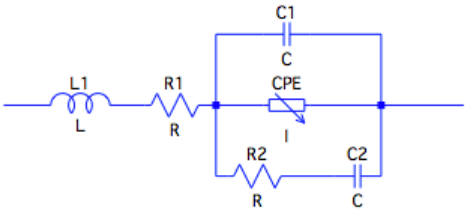

Figure 4-9. Circuit model to simulate the internal impedance of the lead acid batteries.

A digital automotive battery analyzer, manufactured by Cen-Tech, was used as an alternative measurement of module impedance growth and capacity fade. A large sample space of new UPS12-400MR modules were used to estimate the equivalent series

resistance (ESR) and cold cranking amps (CCA) of new VRLA modules. . SAE defines the CCA test through the J537 code, which states that a battery must be cooled to -18°C (0°F) for 24 hours before beginning the CCA test. Once 24 hours have passed, the battery must be discharged at the rated CCA and will have been considered to have passed if the battery voltage remains above 7.2 V i.e. 1.2 V/cell for 30 seconds. A commercial battery analyzer, Model 66892, was used to test the CCA of the selected batteries. The test consisted of connecting the battery analyzer to the battery and then selecting the CCA to be tested. After the test had concluded, the analyzer would display the ESR, CCA, and the current open circuit voltage. Batteries of different states including those subjected to the 43 kW profile mentioned before and fresh batteries were analyzed, respectively. Each test on the battery included testing at two different CCA rates.

The UPS400MR datasheet lists two different CCA ratings, 1000 A and 1200 A respectively. The datasheet suggests that 1000 A be measured when evaluating the modules for traditional usage and 1200 A when considering them for marine applications. The reason for having two ratings is not entirely clear however since they were both listed on the datasheet, both were evaluated using the Cen-Tech analyzer (East Penn Manufacturing, 2015). When measuring data from the modules, the user inputs the manufacturer's datasheet CCA value and the measurement device uses that as a starting point from which to calculate what it thinks the CCA rate is. Figure 4-10 and Figure 4-11 plot histograms of the CCA measurements made at the 1000A and 1200A rate, respectively from twelve new modules. It is interesting to note from the histogram plots that the device measures the modules CCA rating to be a few hundred amperes higher than either of the two datasheet values.

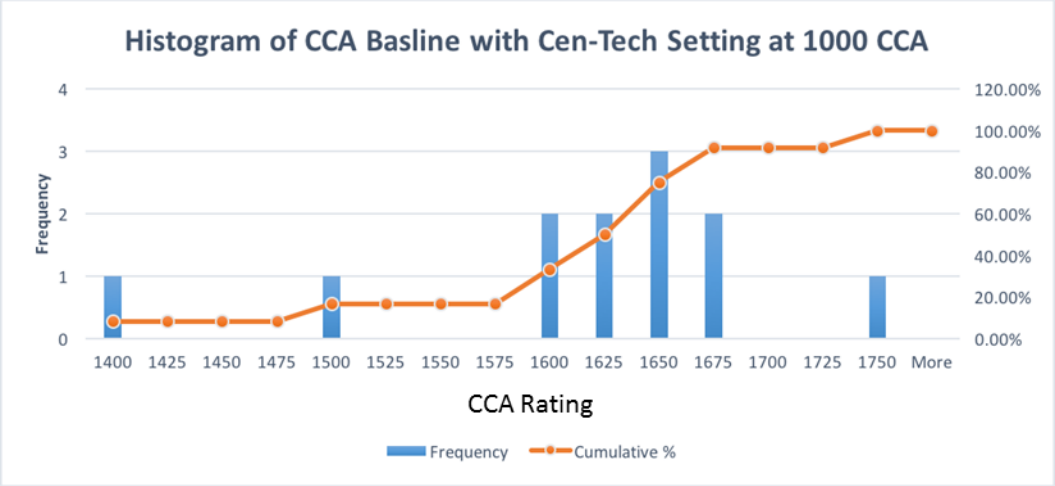

Figure 4-10. The histogram along with a cumulative plot shows the CCA of the battery should be 1600-1675 at the beginning of the battery's life.

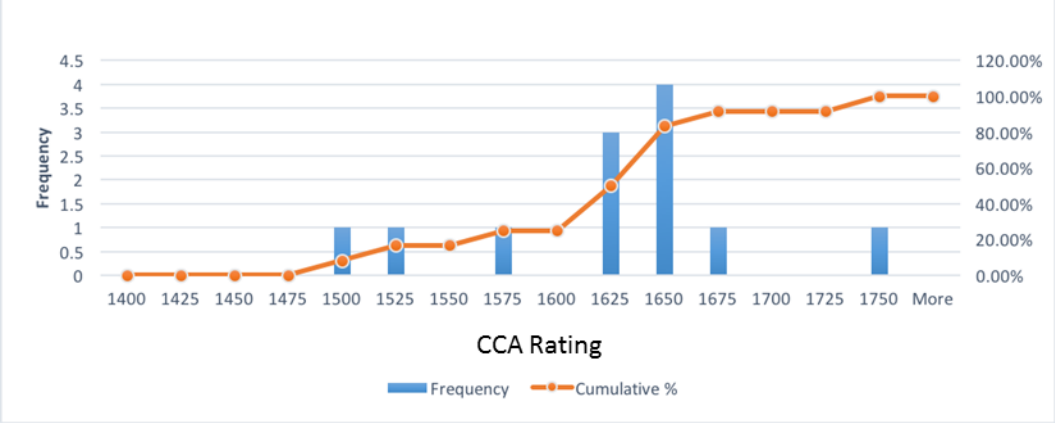

Figure 4-11. This histogram is nearly the same as Figure 4-10, which helps confirm that the CCA rating at the beginning of the batteries life should be between 1600-1675 CCA.

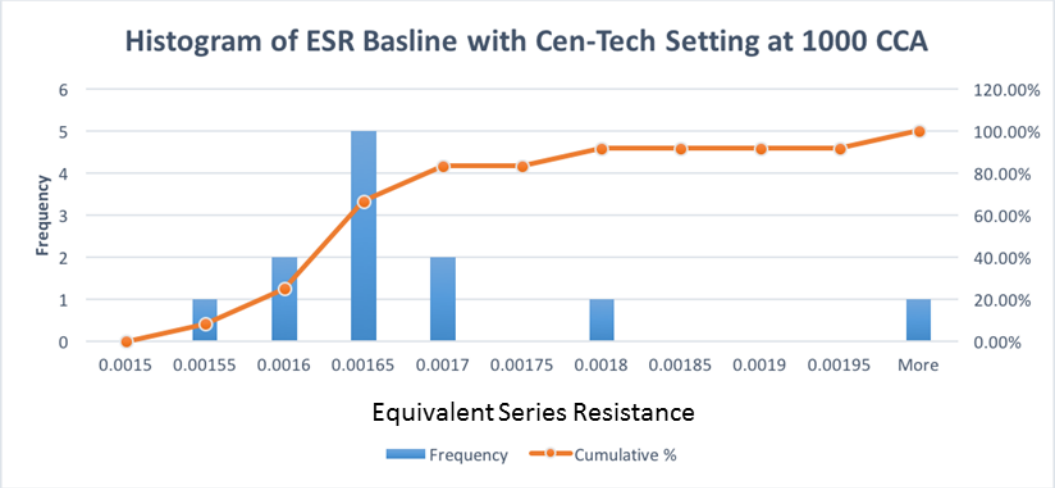

Figure 4-12. With the CCA setting at 1000 A on the Cen-Tech analyzer, the most common baseline ESR is measured between 1.5 mOhms to 1.7 mOhms.

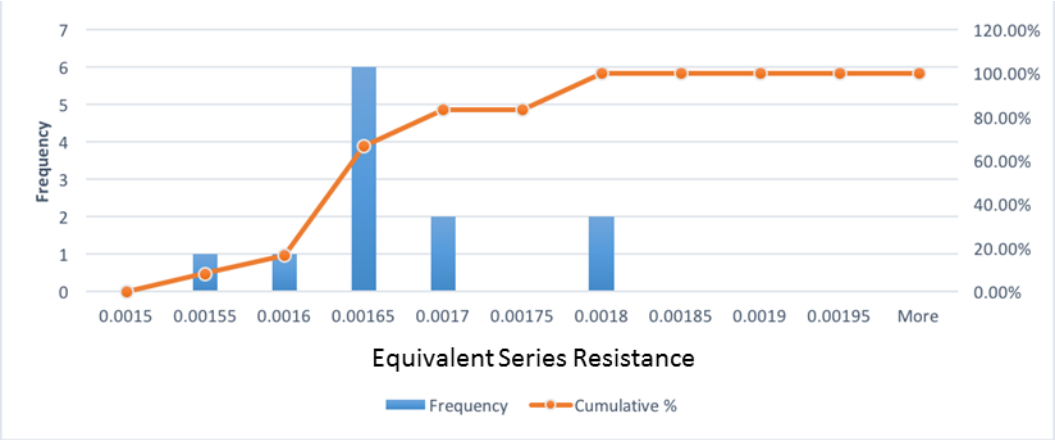

Figure 4-13. With the CCA setting at 1200 A on the Cen-Tech analyzer, the most common baseline ESR is measured between 1.6 mOhms to 1.7 mOhms which is within the expected range identified at 1000 A.

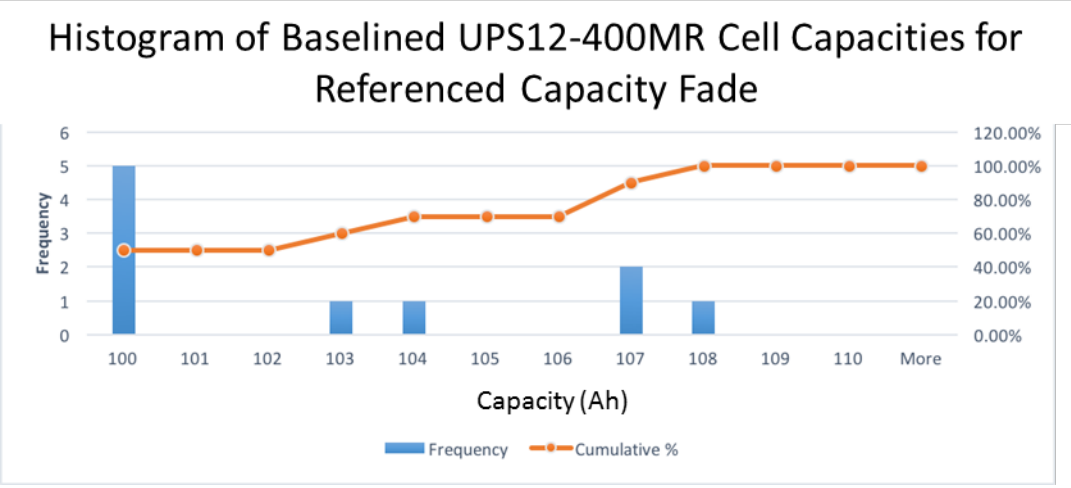

Figure 4-14. This plot is a histogram of the sampled VRLA batteries capacity results from the non-cycled UPS12-400MR, the densest area in the figure gives incite to what baseline capacity should be.

Table 6. Datasheet and measured capacity, ESR, and CCA values of the UPS12-400MR module.

Investigated Parameters	**Datasheet Value**	**Measured Value**
Capacity (Ah) Tested with UTA Chroma equipment	103	100-103
ESR (mOhm) (@60Hz) Tested with AutoLab	2.5	2.1-2.25
CCA (Ampere) Tested with Automotive Battery Analyzer	1000 & 1200	1600-1675

A total of 256 high rate pulsed cycles were completed on the ~60 V VRLA battery studied here. At the conclusion of 256 cycles, it was found when baselining the modules that the usable capacity across the ten modules was highly variable and significantly less then they initially had. The manufacturer datasheet recommends using an equalization technique where the cells within the module are each slightly overcharged to regain chemical stability. In an attempt to regain some of the capacity fade induced by high rate

cycling, all ten modules were equalized using a 14.2 V applied potential. This voltage is less than the maximum recommended by the manufacturer, however because the cells had been heavily stressed during cycling, it was decided that applying too high a potential may do more damage than good so 14.2 V was applied. In short, it was the equalization procedure did not help in regaining usable capacity and in fact; it may have actually done more harm to the cells thought the reason for that is still very unclear.

It was immediately found on cycle 257, that there was not enough usable capacity remaining to meet the high power load demand. The discharge procedure was halted early by the control system due to module undervoltage. Despite reaching an early termination, an additional 60 cycles were attempted anyway to try to regain some of the capacity losses. It will be shown later that while some of the capacity was recovered, it was not significant enough to ever meet the load requirement during those cycles. 256 cycles are obviously far fewer cycles than the 1100 performed at the single module level. The hypothesized reason for the reduction in usable life will be discussed later. The 256 cycles were performed over a series of six different test series'. A summary of the manner in which the 256 cycles were performed is presented in

Table 7

Table 7. Summary of 316 cycles performed to date on the UPS400MR VRLA battery (5S/2P).

Date	File Name	CP	CC	Pulsed Discharge	Baseline?	Charge Rate	Discharge Rate	Chiller Temp	Air Speed	# of Cycles	Comments
3/16/15	EIS on all 10 Cells										First EIS of Cells
5/4/15	10Hr Baseline		X		Yes	22A	22A			1	156 Ah
5/4/15	20Min 5on 5 off		X	X		20min (110A)	800A			3	Commissioning
5/5/15	20Min 5on 5 off		X	X		75min (28 A)	800A			10	Commissioning
5/8/15	20Min 5on 5 off		X	X		20min (110A)	800A			10	Commissioning
5/14/15	20Min 5on 5 off		X	X		20min (110A)	800A			15	Test Series 1
6/15/15	20Min 5on 5 off	X		X		20min (110A)	43kW			46	Test Series 2
6/18/15	10Hr Baseline		X		Yes	22A	22A			1	154 Ah
6/22/15	EIS on all 10 Cells										
8/7/15	20Min 5on 5 off	X		X		20min (110A)	43kW	20C	~650 SCFM	24	Test Series 3 (blower shutdown overnight due to drive error)
8/7/15	20Min 5on 5 off	X		X		20min (110A)	43kW	20C	~650 SCFM	75	Test Series 4
8/21/15	20Min 5on 5 off	X		X		20min (110A)	43kW	40C	~650 SCFM	75	Test Series 5
9/21/15	Cell F Individual Baseline		X		Yes	10 Hr Rate (11A)	11A			1	Capacity Recorded ~41 Ah
9/23/15	Cell P Individual Baseline		X		Yes	10 Hr Rate (11A)	11A			1	Capacity Recorded ~80 Ah
9/23/15	Cell Q Individual Baseline		X		Yes	10 Hr Rate (11A)	11A			1	Capacity Recorded ~48 Ah
9/25/15	Cell M Individual Baseline		X		Yes	10 Hr Rate (11A)	11A			1	Capacity Recorded ~58 Ah
9/30/15	Cell I Individual Baseline		X		Yes	10 Hr Rate (11A)	11A			1	Capacity Recorded ~72 Ah
10/5/15	Cell L Individual Baseline		X		Yes	10 Hr Rate (11A)	11A			1	Capacity Recorded ~72Ah
11/21/15	20Min 5on 5 off	X		X		20min (110A)	43kW	40C	~650 SCFM	61	Test Series 6
1-15-2016	EIS & Baseline of All Cells		X		Yes	10 Hr Rate (11A)	11A			N/A	Capacity Recorded in Figure 4-31

A sample 43kW discharge is shown in

Figure 4-15 and the temperature rise measured during the 15 cycles of Test Series 1, discharged at 800 CC (Constant Current), without forced air-cooling is presented in Figure 4-16. It is worth noting from

Figure 4-15 that the 43 kW test profile is nearly identical to the 800A CC profile with the exception being mild fluctuation in the current around 800 A as conduction voltage varies.

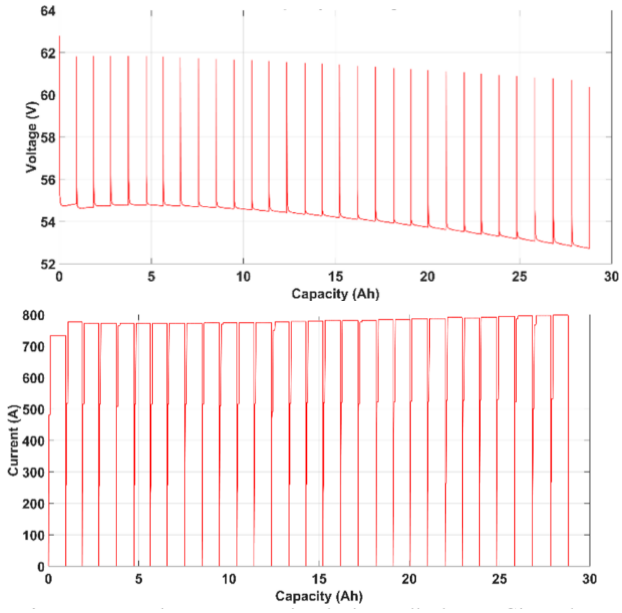

Figure 4-15. Voltage vs. capacity (left) and current vs. capacity (right) measured when the C&D UPS12-400MR battery, cycled under the 43 kW, 5 s on/ 5 s off profile for 5 minutes.

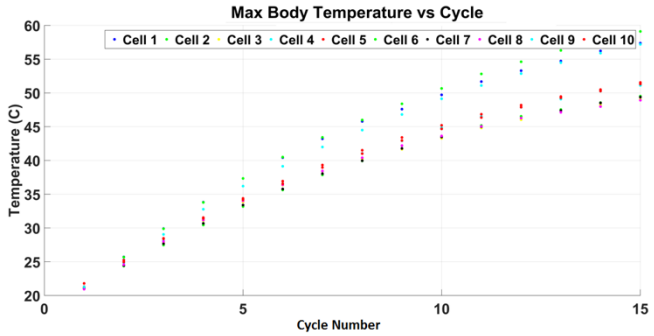

Figure 4-16. Peak temperature measured from each of the 10 VRLA modules during Test Series 1.

From Figure 4-16 it should be noticed that after 15 cycles, the maximum temperature of the VRLA's had reached 55^{o}C but it had not yet stabilized. Therefore, the next test series, Test Series 2, was performed to cycle the VRLA for as many cycles as needed for the maximum temperature to stabilize. The temperature profile for that series of 46 cycles, performed without any form of assisted cooling, is shown on the left side of Figure 4-17 where it should be noticed that the peak temperature measured begins to stabilize just above 70^{o}C. As mentioned earlier, the conduction voltage of VRLA modules is strongly temperature dependent. This is seen in the plot presented on the right side of Figure 4-17, where the conduction voltage starts out around 52 V and gradually increases to around 56 V after 16 cycles. While 70^{o}C is not far outside the maximum rated operating temperature of many VRLA modules, it is much hotter than manufacturers recommend. C&D Technologies lists in their datasheet that cycle life will be reduced by a factor of two for every 6^{o}C the modules are run at above 21^{o}C. This means that while operation in a 2P configuration is more than possible, the cycle life of the batteries will be hit hard. It is also noticed that the 71^{o}C measured is much hotter than the 35^{o}C peak temperature measured when a single cell was cycled under similar conditions in an open air environment. With all of this in mind, it is not out of the realm of possibility that a VRLA battery could be run at these rates without forced air cooling; however, it would depend upon the size of the room in which the batteries are placed and its ability to absorb the heat generated by the batteries. In these tests, the ten VRLA modules are assembled in a roughly 891 L box with the modules taking up roughly 122 L of that space.

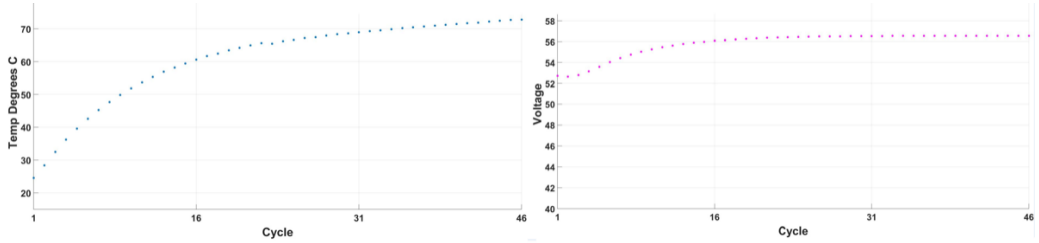

Figure 4-17. Peak temperature (left) and minimum conduction voltage (right) measured from each of the 10 VRLA modules during Test Series 2.

Figure 4-18 shows the EIS measurements made from a few select modules after the cooling experiments were completed. When comparing the EIS results here to those presented earlier in Figure 4-8, there is not considerable variation noticed from the data presented earlier in Figure 4-8. There does appear to be some variation in the charge transfer impedance hump, more on the change in impedance will be discussed further into the paper.

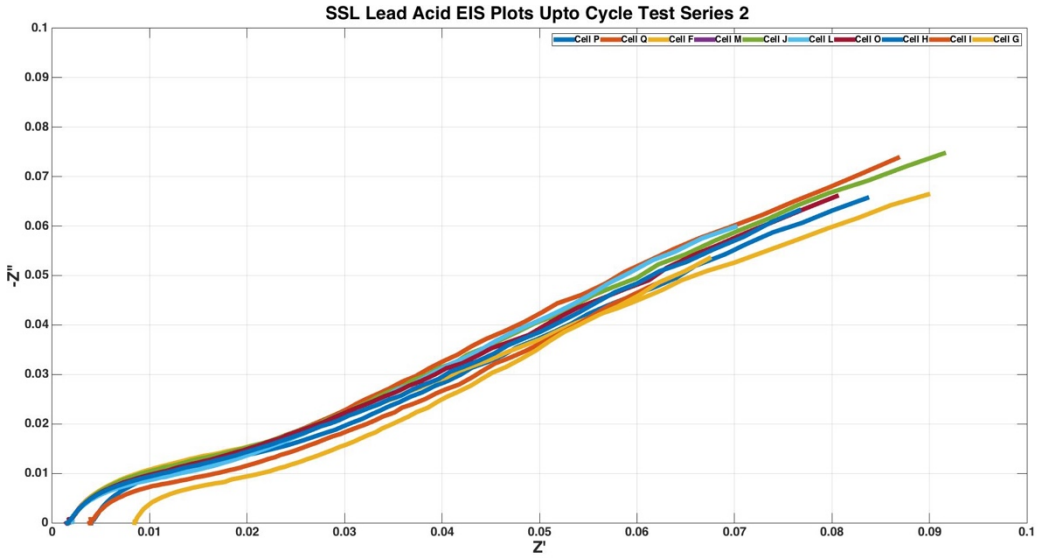

Figure 4-18. EIS measurements made from select VRLA modules after the cooling experiments had been completed, up to Test Series 2.

In the next test series performed, Test Series 3, air-cooling was utilized to measure how this would affect temperature stabilization. Working with researchers at NSWC Philadelphia, it was estimated that between 500 and 800 SCFM of airflow would be needed to reject the roughly 4 kW of heat generated during a roughly 800 A discharge. During this test series, the airflow rate was set to 650 SCFM and the three 3 kW water chillers were set to regulate the heat exchanger water temperature to 20^{o}C. A test series of 75 cycles was planned; however while running overnight, vibration in the fan's motor caused the variable frequency drive to shutdown prematurely after 10 cycles. By the next morning, when the problem was discovered, 24 cycles had been completed, 14 of which were performed without any air-cooling allowing a peak temperature of just over 55^{o}C to be reached before the test series was halted. This prompted the next test series, Test Series 4, to repeat these experiments without the blower shutting down. The thermal and end conduction voltage measurements made during Test Series 4 are shown in the left and right side, respectively, of Figure 4-19. A stable peak temperature of roughly 47^{o}C was recorded after 16 cycles. This is 30^{o}C cooler than the peak temperature recorded earlier without air-cooling. As expected the end conduction voltage increases slightly as thermal equilibrium is reached after which it remains relatively stable at just under 56 V. Plots of the airflow rate and air temperature as it enters the chamber, respectively is shown in Figure 4-21.

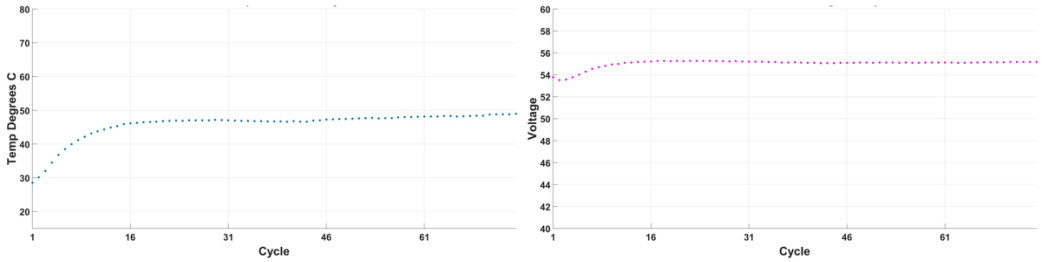

Figure 4-19. Peak temperature (left) and minimum conduction voltage (right) measured from each of the 10 VRLA modules during Test Series 3 when cycled 75 times under the 43 kW, 5 s on/ 5 s off profile for 5 minutes. In these experiments, air-cooling was used. The chiller temperature was set to 20°C and the air speed was set to 650 SCFM.

Test Series 5, is a repeat of Test Series 4 with the only difference being the regulation temperature of the water chillers being set to 40°C rather than 20°C. The thermal and conduction voltage results from that test series are shown in Figure 4-20. Plots of the airflow rate and air temperature as it enters the chamber, respectively, is shown in Figure 4-21. The peak temperature is slightly higher, roughly 5°C, stabilizing near 52°C after a similar 16 cycles. These results show that cooled air is not as important likely as just having airflow to remove heat.

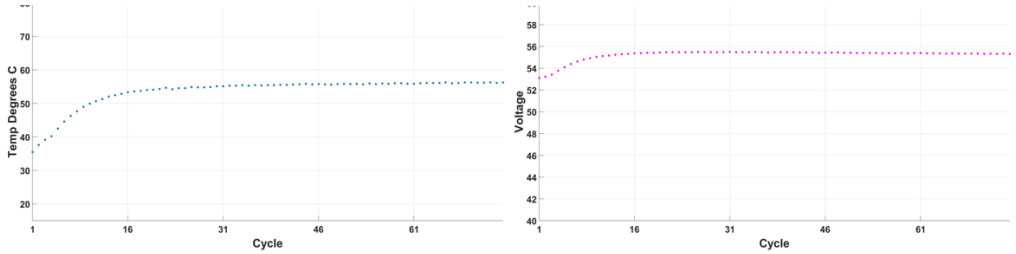

Figure 4-20. Peak temperature (left) and minimum conduction voltage (right) measured from each of the 10 VRLA modules during Test Series 3.

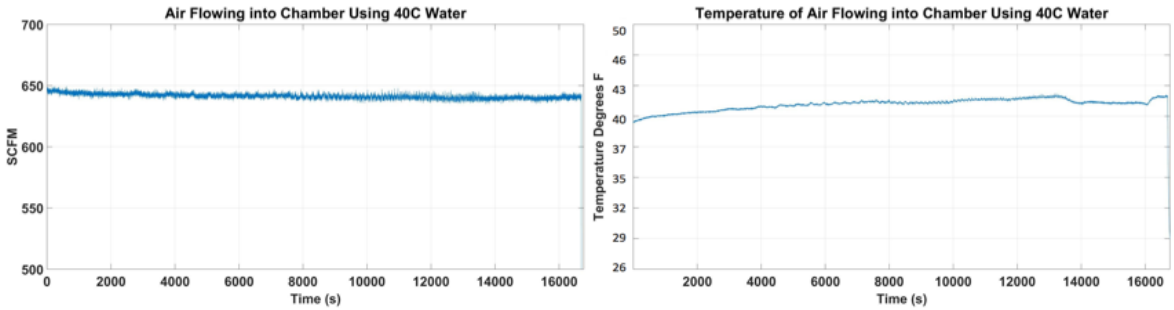

Figure 4-21. Plots of the air speed measured at the Venturi nozzle (left) and the air temperature through the Venturi nozzle (right).

After the completion of Test Series 5, 256 high rate cycles had been performed on the battery meaning that it was time to re-baseline select modules. As shown in

Table 7 and Figure 4-22, cells Q, P, M, M, I, H, and F were baselined and quite a variation in their usable 10 hr rate capacity was measured. The EIS measurements made after 256 high rate cycles are completed show remarkable consistency despite the variation in usable capacity. There is also not a significant increase in the real impedance or even the charge transfer impedance as was expected given the reduction in capacity.

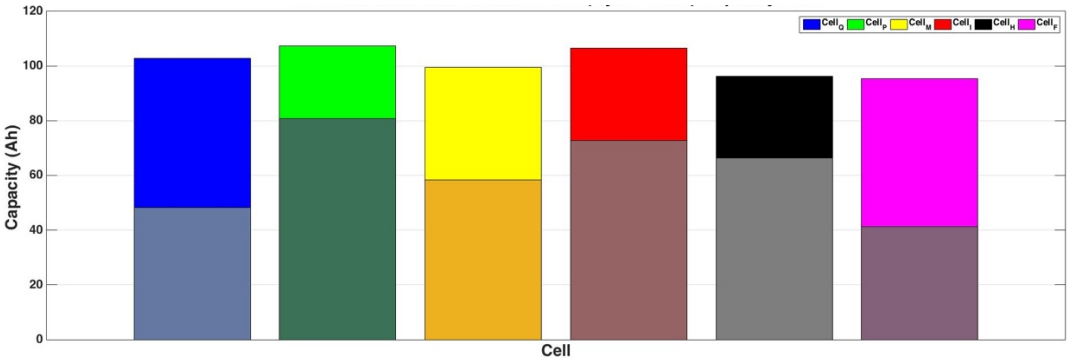

Figure 4-22. Capacity baseline measurements made on select VLRA modules after 256 high rate cycles. The light color bars represent measurements made of the capacity before testing while the darker color bars are the measured capacity after 256 cycles.

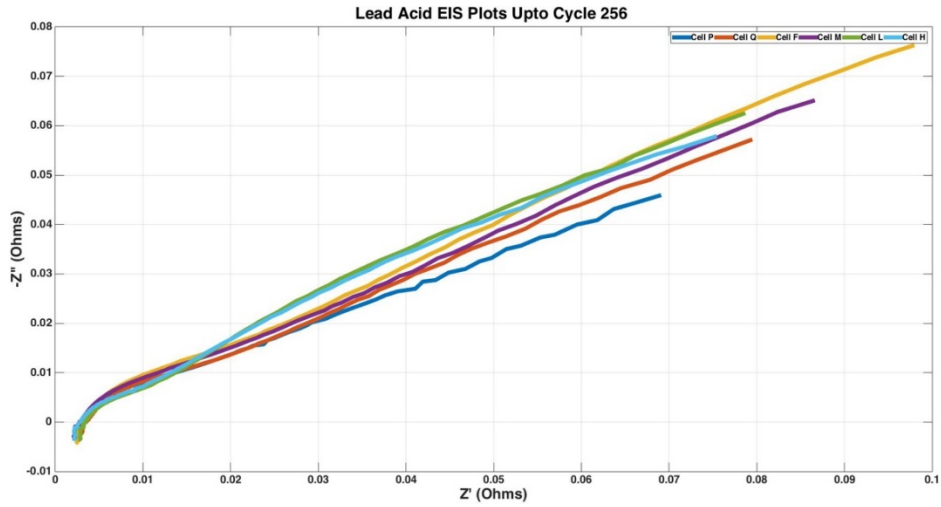

Figure 4-23. EIS measurements made from select VRLA modules after 256 cycles.

Figure 4-24 shows an overview of module placement within the battery. At the low end, a capacity of 41 Ah was measured from module F while on the high end 80 Ah was

measured from module P. Keep in mind that the initial capacity of all modules was above 90 Ah meaning that significant fade has occurred. This amount of fade and the variation is higher than was expected from the data measured on the single module presented earlier. It was after this baseline that equalization was performed, which entailed to over-charge the cells to 14.2 V until the current was under 100 mA using a CC-CV charge procedure.

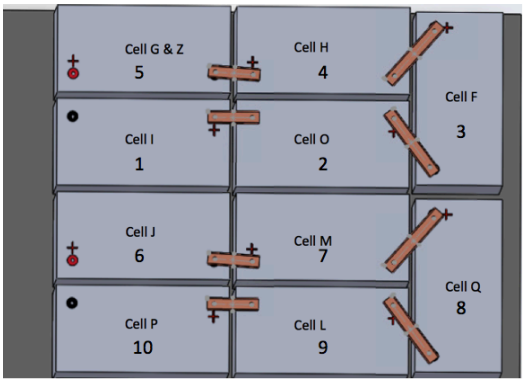

Figure 4-24. Graphical representation of module locations within the 5S/2P VRLA battery.

During the baseline measurements made after 256 cycles, something occurred with a programmable load that resulted in module ‘G’ being completely discharged. It is still unclear what happened, but at the time it was thought to have been some sort of fluke hardware problem. The data during this error was not a good reflection of the test and considered to be ‘trash’ data. As a result, module ‘G’ was replaced with a new module, being named module 'Z’. Since module ‘G’ was dead, its top was removed to observe the internal parts of it. The module uses casted bus bars to connect the six internal cells. The white pads between the ‘Z’ fold of the electrodes is fiberglass that acts as an absorber of the sulfuric acid electrolyte. Pressure caps above each of the six respective cells are used to accommodate the battery’s ‘recombinant’ nature. The valves ensure that the oxygen produced by the positive plate is contained within the cell’s region so that it can

be reabsorbed by the negative plate. This causes the production of hydrogen by the negative plate to cease, prolonging the life of the battery and keeping harmful gasses from escaping into the storage area. Further evaluation of the module found that one cell within the battery had been completely discharged. Since only one cell was discharged, it is unlikely that it could have been a hardware problem; but likely something that happened internally to the cell itself. It remains unclear what caused the cell to fail.

As discussed earlier, the manufacturer recommends that all modules be serviced often by equalizing them to 14.2 V. This forces the cells to overpressure slightly and balance electrochemically. It should be noted that no form of servicing occurred through the first 256 cycles. This is primarily because this type of procedure is something that would be extremely hard for the sponsor to implement in the field. Therefore, a worst case study was performed here after Test Series 5. As shown earlier, there is significant capacity fade on the modules after the small number of cycles performed. It is unclear to what extent frequent service may or may not have improved the level of capacity fade. Repeating these experiments with repeated servicing is something that should be studied in the future.

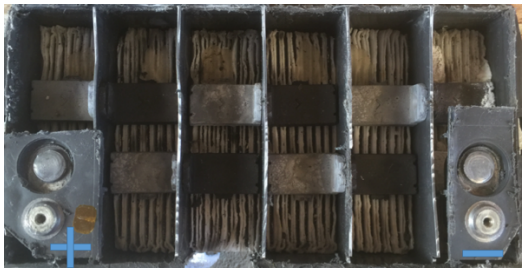

Figure 4-25. UPS400MR disassembled to show inner configuration of cells and bus work.

Once the module was replaced, the sixth and final test series was performed. This was done after equalizing the single modulus on a separate setup, which is the same setup used for the single cell testing. Even though the battery was able to complete discharge 256, it was not able to complete cycle 259. During the 259th cycle, Cells J and Q voltage

dropped below the minimum value, 10 Volts, before the 5-minute discharge had completed. Despite not completing the 259th cycle, approximately 60 more cycles were attempted with hope that the modules would become better balanced and continue to meet the load requirements. While the cells did improve slightly with each additional cycle, they were still not able to meet the loads requirements after 61 additional cycles had been performed. This is evident from Figure 4-26, Figure 4-27, and Figure 4-28 in which the last measured conduction voltage, maximum temperature, and supplied capacity from each of the 316 cycles performed. Of importance is to notice the somewhat downward linear trend in the end conduction voltage after steady state temperature has been reached in each prolonged test series. This downward trend indicates an increase in the DC impedance and increase in aging as the modules are cycled. It should be noticed that the extracted capacity in Figure 4-28 is relatively stable during all of the 43 kW CP discharge cycles up until Test Series 6. Because the CP discharge does not quite draw 800 A from the battery, the capacity supplied during the early 800 A CC discharge cycles is slightly higher. During Test Series 6, it is clear to see how the capacity sourced started out near nothing, but rose as the 61 cycles were performed. It is concluded after equalizing the modules did not perform as intended, the equalization process could have aged the cells and caused more damage than good.

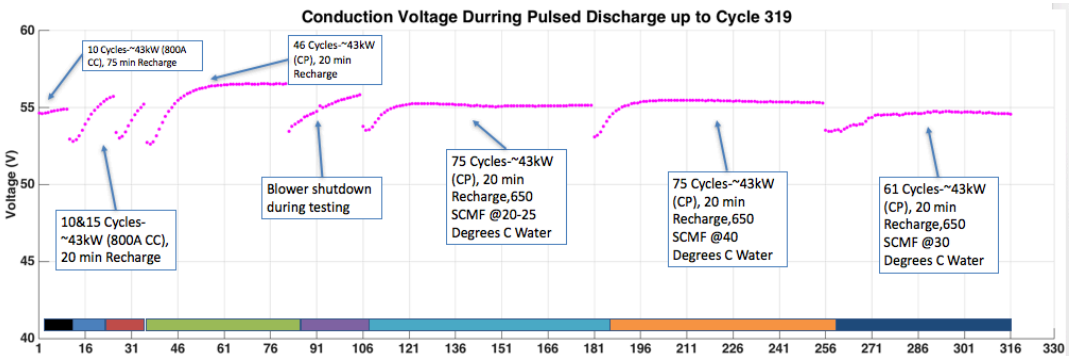

Figure 4-26. Plot of the last conduction voltage measured in each of the 316 cycles performed through Test Series 6.

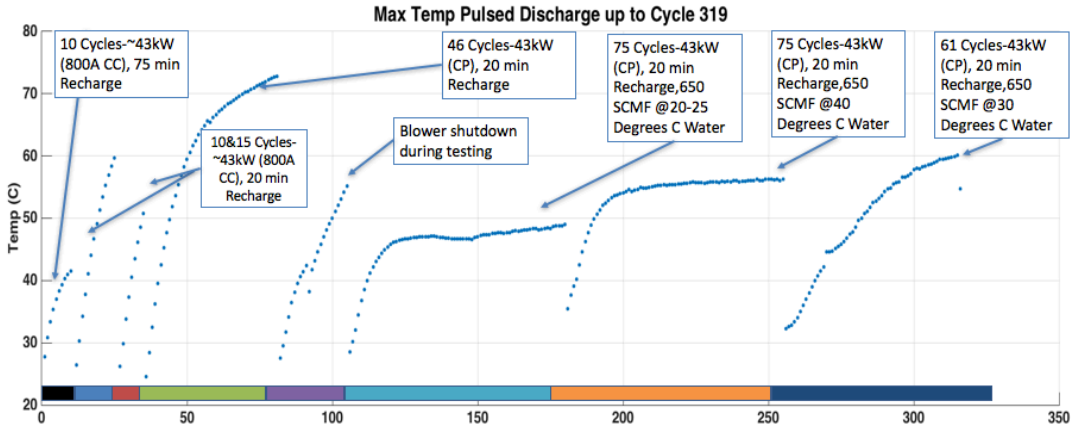

Figure 4-27. Plot of the Max Temperature measured in each of the 316 cycles performed through Test Series 6.

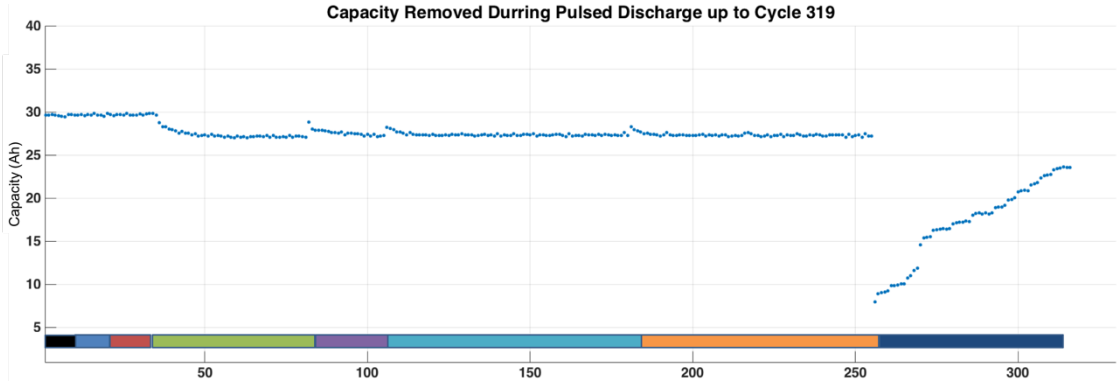

Figure 4-28. Plot of the removed capacity measured in each of the 316 cycles performed through Test Series 6.

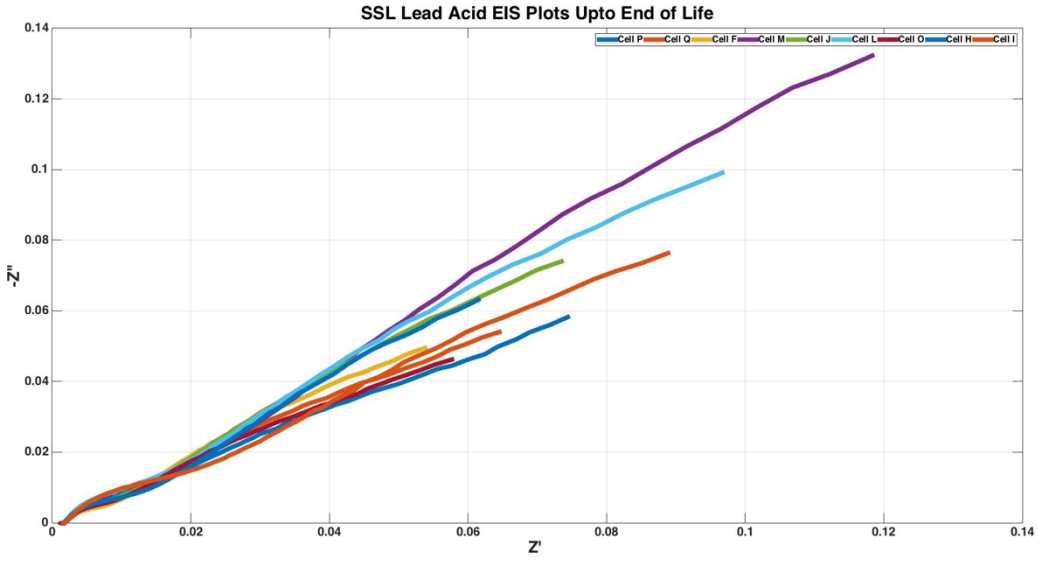

Figure 4-29. This plot shows the EIS data collected at the end of life for each battery cycled since the beginning of testing.

Once cycling was complete, EIS was performed one last time to understand how the parameters had changed. Two cells were selected to fully describe how the system has

aged. The first cell was considered to be the healthiest and the other cell to be considered to be the weakest. To define the health of the cell, the remaining capacity of the cell was used. For instance, the cell that had retained the most capacity after the cycling is considered the healthiest and the cell that has the least capacity is considered the weakest. Cell H was considered to be healthiest cell and Cell Q being the weakest.

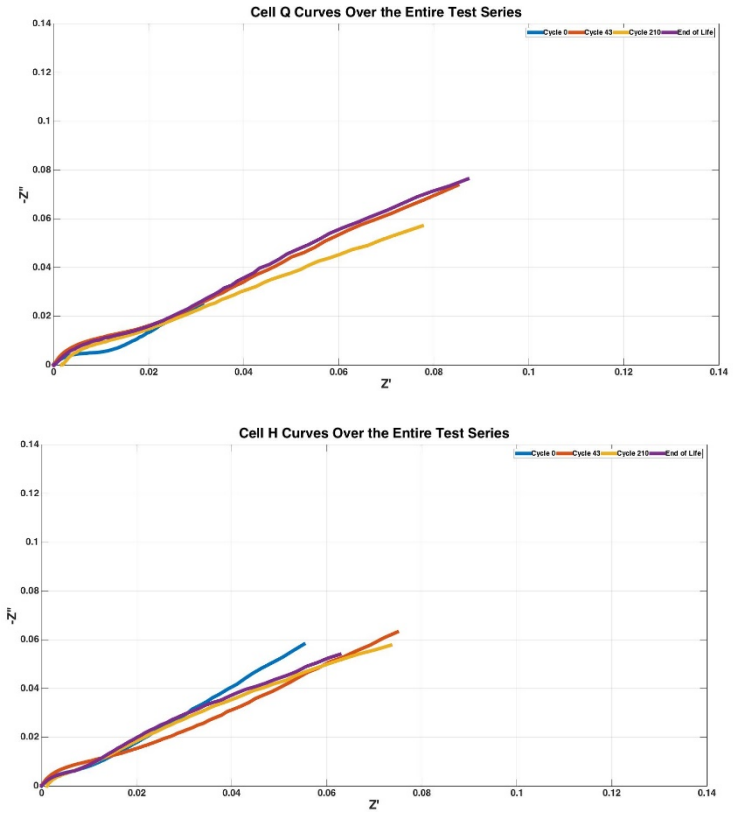

Figure 4-30. These plots show the EIS data collected over the lifespan of the experiment. While the data in plotted form does not denote what is happening internally to the the cell, the table above does indicate some changes happening in the cell.

Beyond this point it is suggested to read “Characterization of high-power lithium-ion batteries by electrochemical impedance spectroscopy. I. Experimental investigation” by D. Andrea, M. Meilera, K. Steinera, Ch. Wimmera, T. Soczka-Gutha, and D.U. Sauerb to

better understand Electrochemical Impedance Spectroscopy. (Andre, Meilera, Steinera, Wimmera, & Soczka-Gu, 2011)

To discover how the batteries have aged over time, EIS modeling was used to understand what was changing inside the cell. These measurements were taken after every single cell discharge at its 10hr rate. The circuit used to demonstrate how the internal of the cells are aging is shown in Figure 4-9. L1 of the circuit is used to represent the inductance in the system. Normally, this comes from the measurement leads but other factors in the battery, such as construction of the internal connections, causes inductance. R1 represents the resistance in the measurement leads and the ESR of the batteries. C1 is used to understand the capacitance between both of the anode and cathode. C2 is used to understand the growth and decay of the SEI layer. R2 is used in conjunction with C2 to understand how the SEI layer is changing.

Figure 4-30 shows the Electrochemical Impedance Spectroscopy, EIS, data collected over the lifetime of the Lead Acid test series. The data has been normalized where the initial spectrum crossed the real axis, also known as the Z prime axis, to the origin of the plot. The other measurements were shifted by the same degree with respect to the initial measurement. By examining the plots there are shifts in the real and imaginary axis from the first cycle to the last on both batteries. The mid and high frequency areas change significantly after the first 43 cycles of testing. This can constitute that the normal operation is allowing high frequency to pass through the batteries, which means charge is not being stored at high frequency. The battery is behaving as a high pass filter and not storing the energy due to the kinetics are slowed as the battery degrades. Although at the lower frequency's the charge is allowed to be stored. To help understand this, at higher currents the batteries charge cannot be transferred fast enough to support high rate recharges and discharges. Although these plots show that at lower frequencies, the

charge transfer can be more efficient. To help describe how the batteries are degrading over time, a circuit model was created to understand the impedance changes with respect to cycle life.

Table 8 gives the values used in the above circuit to achieve a matched curve for the EIS spectrum of two cells tested under the pulsed profile. After examining the results, we can conclude that major decay in electro capacity of the anode and cathode. Although only using two references for this test we cannot be clear on which electrode was degrading. It should be noted that the diffusion of the electrodes is becoming more resistive, which indicates that the charged cannot be stored fast enough, meaning that during high rate cycling there is not an efficient transfer in storage. The RC circuit values show a decrease in capacitance that indicates that the SEI layer is becoming more resistive than capacitive which increases the amount of energy loss during operation.

Table 8. Values used to achieve a matching EIS curve for two of the ten batteries used in the pulsed profile testing

Cell Q	Cycle 0	Test Series 2	Test Series 5	Test Series 6
Inductance (H)	2.07E-08	4.27E-08	3.65E-08	3.27E-08
Resistance 1 (Ohm)	0.0002021	0.0001248	0.0003269	0.0001257
Capacitance 1 (F)	52.36	38	15.57	3.90E-07
CPE ($s\text{-}sec^{n}$)	709.4	413.3	397.3	366.8
Frequency Power (n)	0.2144	0.5401	0.8	0.5169
Resistance 2 (Ohm)	0.003642	0.001083	0.0005926	0.0008137
Capacitance 2 (F)	7506	131	166.2	149.8
Chi-squared	0.004739	0.006094	0.001678	0.004328
Cell H				
Inductance (H)	3.98E-08	4.18E-08	5.73E-08	3.59E-08
Resistance 1 (Ohm)	0.0001547	0.0001184	0.0002469	0.000151
Capacitance 1 (F)	25.68	39.49	13.27	4.89E+00
CPE ($s\text{-}sec^{n}$)	448.9	438.2	409.1	468.3

Frequency Power (n)	0.3697	0.5115	0.488	0.5259
Resistance 2 (Ohm)	0.01712	0.0009516	0.0002012	0.0003281
Capacitance 2 (F)	5544	123.3	285.6	145
Chi-squared	0.01011	0.006191	0.002573	0.0007483

Once baselines were established, the UT Arlington Pulsed Power and Energy Laboratory has broken-down the results into multiple figures to help understand the aging of the VRLA cells. Figure 4-31 establishes the capacity over the lifetime of testing. Note that not all cells were tested at 260 Cycles due to time constraints. However, for the final evaluation, all cells were test with the same baseline procedure that was used in the beginning. This figure helps show how capacity has decreased over cycle and calendar life. The high rates used in the profile greatly affected the capacity of the cells after 260 Cycles, due to high heat generation and the effect of the pulsed profile. Figure 4-32 graphically shows the 60Hz impedance growth over the cycle life, but the EIS method does not show any significant advantage to detect a failing cell. However, the decrease in the conduction voltage shown in Figure 4-26 indicates that the DC ESR is increasing as the cycle life is increasing.

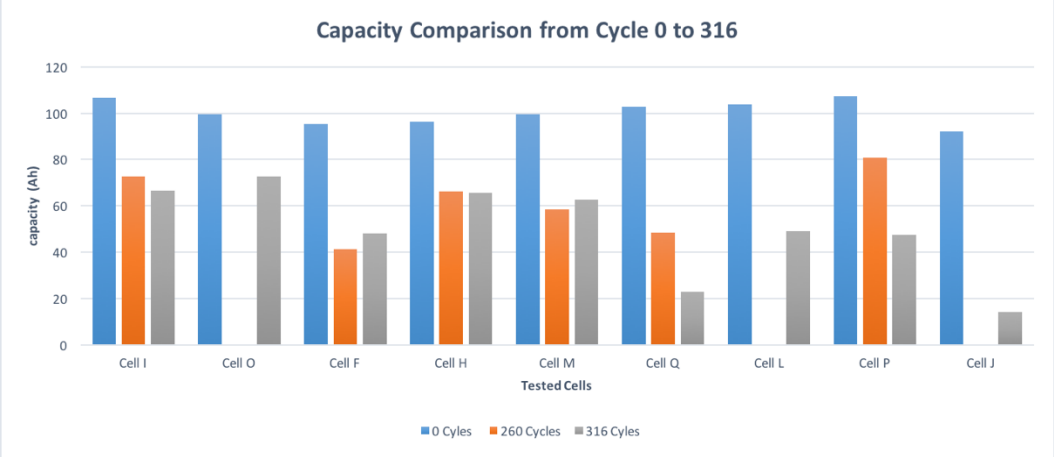

Figure 4-31. Tested capacity of each cell during the lifetime testing.

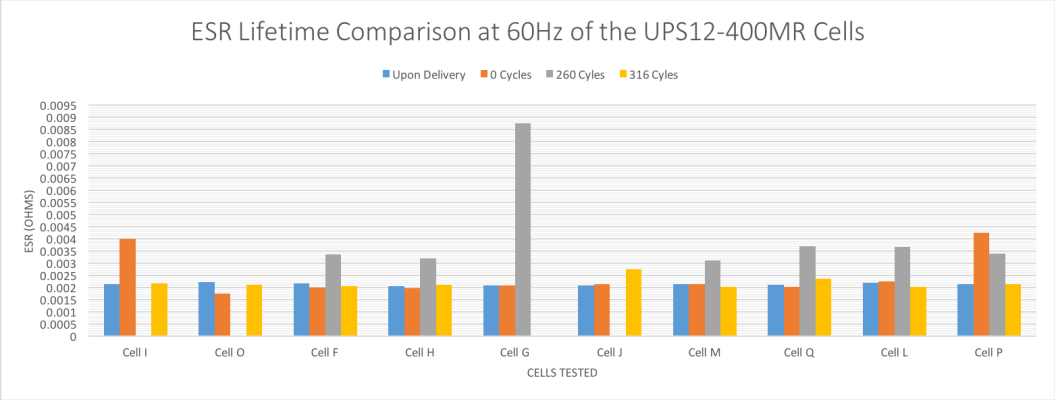

Figure 4-32. Tested 60Hz ESR of each cell during the lifetime testing, note that cell G was damaged during a single test. Cell G is to only show that the cell completely failed after the single test.

Table 9. Results from cells tested to gather a large sample space to establish the baseline standards for a new cell.

Cell Results From the Digital Automotive Analyzer to Establish a Baseline							
	Setting of CCA				Setting of CCA		
Cell	**1000A**	**1200A**	**Comments**	**Cell**	**1000A**	**1200A**	**Comments**
9C	12.59V	12.59V		8M	12.53V	12.51V	
	1.64 mOhm	1.52 mOhm			1.68 mOhm	1.6 mOhm	
	1615 CCA	1738 CCA			1577 CCA	1648 CCA	
9H	12.53V	12.53V		4C	12.57V	12.57V	
	1.59 mOhm	1.75 mOhm			1.63 mOhm	1.63 mOhm	
	1659 CCA	1512 CCA			1619 CCA	1621 CCA	
9M	12.57V	12.56 V		4H	12.57V	12.57V	
	1.67 mOhm	1.61 mOhm			1.62 mOhm	1.62 mOhm	
	1585 CCA	1639 CCA			1632 CCA	1631 CCA	
8C	12.54V	12.53V		4M	12.51V	12.51V	
	1.59 mOhm	1.59 mOhm			1.6 mOhm	1.6 mOhm	
	1658 CCA	1657 CCA			1649 CCA	1647 CCA	
8H	12.51V	12.51V		3C	12.46V	12.46V	
	1.6 mOhm	1.69 mOhm			1.52 mOhm	1.64 mOhm	
	1647 CCA	1562 CCA			1741 CCA	1609 CCA	
3M	12.35V	12.34 V		3H	12.33V	12.32 V	
	1.77 mOhm	1.65 mOhm			1.95 mOhm	1.79 mOhm	
	1494 CCA	1604 CCA			1358 CCA	1476 CCA	

Table 10. Results from Cen-Tech Digital automotive analyzer, these values were used to compare the cycled cells to the baselined in prior table.

CEN-Tech Digital Automotive Battery Analyzer (Model 66892) Test Results from 43kW Profile Cells							
Bank A Results				Bank B Results			
Setting of CCA				Setting of CCA			
Cell Letter	**1000A**	**1200A**	**Comments**	**Cell Letter**	**1000A**	**1200A**	**Comments**
Z	12.31V	12.30V	Replacement Cell for cell G	**J**	12.48V	12.48V	Cell could not support load after 260 Cycles
	1.73 mOhm	1.67 mOhm			1.77 mOhm	1.978 mOhm	
	1530 CCA	1585 CCA			1498 CCA	1344 CCA	
H	12.52V	12.51V		**M**	12.51V	12.59V	
	1.57 mOhm	1.61 mOhm			1.57 mOhm	1.65 mOhm	
	1685 CCA	1643 CCA			1687 CCA	1600 CCA	
F	12.57V	12.52V		**Q**	12.49V	12.48V	
	1.65 mOhm	1.74 mOhm			1.97 mOhm	1.65 mOhm	
	1632 CCA	1518 CCA			1338 CCA	1604 CCA	
O	12.56V	12.56V		**L**	12.56V	12.56V	
	1.50 mOhm	1.63 mOhm			1.62 mOhm	1.62 mOhm	
	1760 CCA	1620 CCA			1628 CCA	1627 CCA	
I	12.57V	12.56V		**P**	12.57V	12.56V	
	1.78 mOhm	1.62 mOhm			1.79 mOhm	1.61 mOhm	
	1488 CCA	1629 CCA			1518 CCA	1638 CCA	
				X	12.45V	12.44V	Replacement Cell for Cell J
					1.61 mOhm	1.61 mOhm	
					1637 CCA	1636 CCA	

Saft VL30AFe Lithium-ion

Prior to constructing the ~60 V Saft VL30AFe battery, a single VL30AFe cell was evaluated across a host of C rates to evaluate its usable capacity and temperature rise at each rate. This characterization was performed in an open-air environment without any form of cooling. Plots of the conduction voltage vs capacity at C rates ranging from ½C to 13C are presented in Figure 4-33. The plot in the top leftmost portion of Figure 4-33 presents data collected when continuous discharges were performed and the top rightmost figure presents data collected when 5s on/ 5s off pulsed discharges were performed respectively. The bottom plot shows the temperature of the cell during the continuous discharge of several rates.

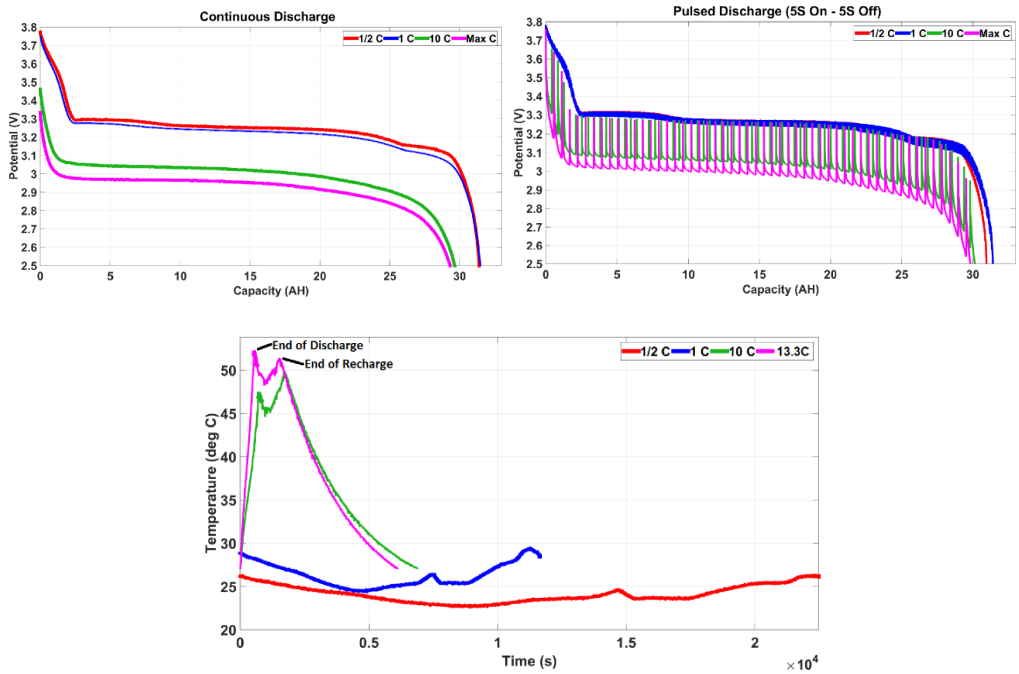

Figure 4-33. Baseline voltage vs. capacity measurements made across C-rates in continuous (left) and 5s on/ 5s off (right) profiles. The lower figure represents the temperature vs. time during a continuous discharge.

Due to the high usable capacities across all C rates evaluated, the full Saft LFP-LI battery was assembled. As seen in Tables 1 – 4 earlier, the Saft VL30AFe battery was constructed as a 20S/2P battery. Having twenty cells in series resulted in an OCP slightly higher than 60V, but the cold plates were already designed to support 10S/1P modules. Despite only using four modules for the tests, six total modules were assembled. Initially all sixty of the cells were assigned random ID numbers for assembly into six modules labeled A – F. Within a letter group, each cell was randomly numbered from 0 – 9. Two cells from each of the six modules were characterized at the ½C rate and EIS measurements were made at 100% SOC. Each of the twelve cells characterized at the ½C rate had were incredibly consistent with respect to their capacity. The capacities measured at the ½C rate are very similar to those presented in Figure 4-33, therefore an additional plot will not be shown here. The EIS measurements made from each pack are shown in Figure 4-37. Due to these cells having such a low internal impedance, there is some variation measured in the charge transfer impedance as well as the real impedance offset. The cell variations can be contributed to the impedance introduced through connection of the potentiostat to the cell under test, as well as the fact that the cells were new without a significant level of conditioning. The variation of more importance in the experiments performed here is the variation in the EIS shape as a function of cycle life that correspond to internal chemistry changes.

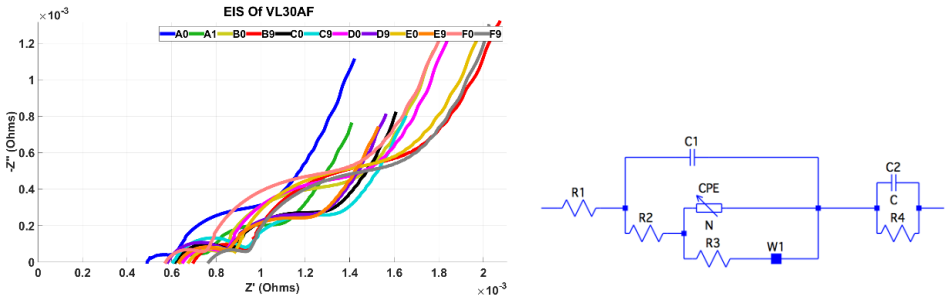

Figure 4-34. EIS measurements made on twelve random VL30AFe cells before cycling began. Along with the circuit model used to analyze the EIS data.

After the full experimental setup of the Saft battery, a few set of experiments were performed to characterize its electrical and thermal performance when it was housed in polyethylene blocks and cycled at 43 kW, with and without forced air-cooling. A summary of the experiments performed to date are presented in

Table 11. The table shows baseline along with profile characterization procedures. Further, in this section each set procedure will be explained.

Table 11. Summary of experiments performed to date on the Saft VL30AFe Lithium-Ion Battery (20S/2P).

Date	Test Performed	CP	CC	Pulsed Discharge	Baseline	Discharge Rate	Charge Rate	Chiller Temp	Air Speed	# of Cycles	Comments
7/7/15	EIS										First EIS of Cells
7/23/15	½C Baseline		X		Yes	30A	30A			1	Baseline
7/23/15	1C Baseline		X		Yes	60A	60A			1	Baseline
7/29/15	½C Baseline		X		Yes	30A	30A			1	Baseline
7/29/15	1C Baseline		X		Yes	60A	60A			1	Baseline
8/5/15	20Min 5on 5 off Air Cool Only	X		5On-5Off		43kW	20-min/90A			1	Commissioning
8/6/15	20Min 5on 5 off Air Cool Only	X		5On-5Off		43kW	20-min/90A			2	Test Series 1a
8/6/15	20Min 5on 5 off Air Cool Only	X		5On-5Off		43kW	20-min/90A			2	Test Series 1b
8/13/15	20Min 5on 5 off Air Cool Only	X		5On-5Off		43kW	20-min/90A	20C	~450 SCFM	25	Test Series 2
1/10/16	20Min 5on 5 off Air Cool Only	X		5On-5Off		43kW	20-min/90A	30C	~450 SCFM	10	Test Series 3
1/11/16	20Min 5on 5 off Water Cool Only	X		5On-5Off		43kW	20-min/90A	20C	N/A	10	Test Series 4
1/12/16	20Min 30on 5 off Water Cool Only	X		30On-5Off		43kW	20-min/90A	20C	N/A	10	Test Series 5
1/13/16	20Min 5on 5 off Water Cool Only	X		5On-5Off		43kW	20-min/90A	40C	N/A	10	Test Series 6
1/14/16	20Min 30on 5 off Water Cool Only	X		30On-5Off		43kW	20-min/90A	40C	N/A	10	Test Series 7
1/14/16	20Min 5on 5 off Water Cool Only	X		5On-5Off		43kW	20-min/90A	40C	N/A	450	(Life Time Testing) Test Series 8

In Test Series 1, the 20S/2P battery was cycled 4 times without air-cooling using a constant power profile with a 5 second on time and 5 second off time, similarly to the VRLA battery test earlier. Initially, in Test Series 1a was configured to run for as many cycles as it could before any cell's body temperature to reach 60^{o}C. This is the temperature suggested by many manufacturer's as the upper thermal limit to allow cell

bodies to heat up to. Because the Saft VL30AFe is of the LFP chemistry, one of the safer lithium-ion chemistries, operation at temperatures slightly higher than 60°C could be achieved safely. This risks affecting the longevity of the cell. During the second recharge of Test Series 1a, a cell's body reached 60°C, halting the experiment. The thermal results measured during Test Series 1a are shown in Figure 4-35. In order to confirm these measurements, a second identical test series was initiated, Test Series 1b, which confirmed that the results of Test Series 1a were correct. From there it was determined that it is not feasible to consider using the Saft VL30AFe modules in a 2P configuration at these rates repeatedly without some form of cooling. Though not significant in this series, the last conduction voltage measured is plotted in Figure 4-36.

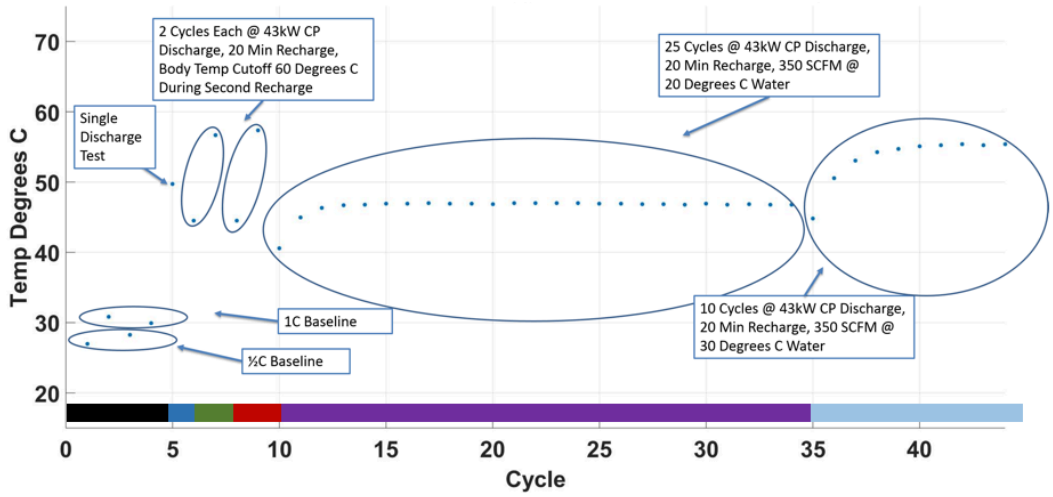

Figure 4-35. Plot of the peak temperature measured in each of the cycles performed through Test Series 3.

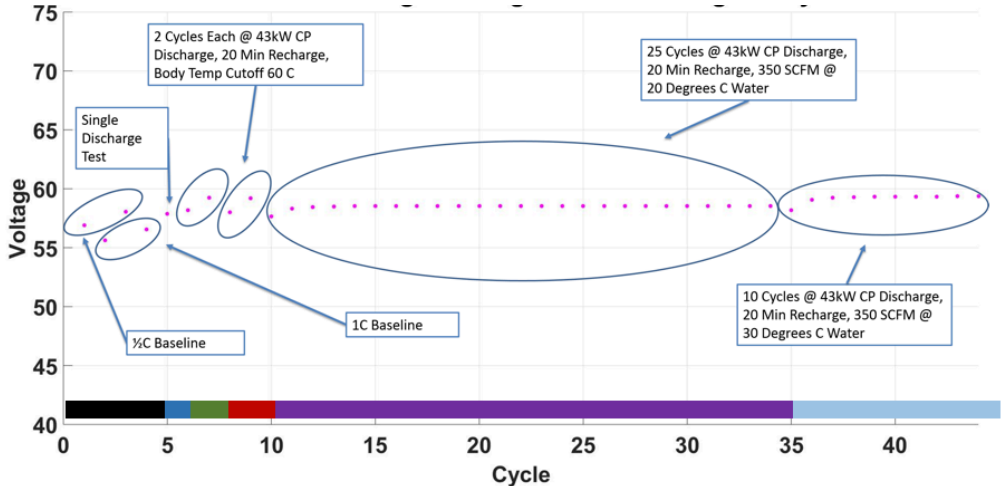

Figure 4-36. Plot of the last conduction voltage measured in each of the cycles performed through Test Series 3.

As seen in Figure 4-35, the next test series, Test Series 2, was carried out to evaluate how forced air-cooling would perform in cooling the cells during high rate operation. The water chillers were configured, shown in the experimental setup, to regulate the water temperature through the heat exchanger to 20°C. The goal was to evaluate how long it takes thermal equilibrium to be met with this style of cooling and measure what that stabilized temperature would become. The liquid flow rate through the heat exchanger was 30 gallons per minute and airflow into the chamber was roughly 450 SCFM. The 450 SCFM flow rate is lower than the 600 – 800 SCFM discussed earlier, however this was evaluated as a worst-case condition. As seen, the peak-stabilized temperature measured during the test series was roughly 47°C and that was reached during the 3rd cycle. This is of course a vast improvement over the results obtained with no cooling, and implies that forced air-cooling could be efficient in cooling a lithium-ion solution. Through the next test series, it will be dertermined if these cells could be cooled with warmer water to characterize the equalization temperature, in case a cooling system were to stop cooling at 20°C and increase to 30°C.

The next test series, Test Series 3, was performed while flowing 30°C water through the heat exchanger at 30 GPM and an air speed of 450 SCFM. Figure 4-35 shows that in this case a peak temperature of roughly 56ºC was reached during the third cycle. Only ten cycles were performed in this series since equilibrium was achieved so early and while a peak temperature of 56ºC is at the upper end of acceptable, it could be a borderline level of cooling. As seen in Figure 4-36, the end conduction voltages measured in Test Series 1 and Test Series 3, respectively, are slightly higher than it is in Test Series 2. This is expected since at higher temperatures, the ionic conductivity of the electrolyte is lower, decreasing the battery's equivalent series resistance (ESR) and therefore the voltage drop across the cell. The next test series will discuss the liquid cooling experimental results and compare both cooling methods later on in this section.

Upon completion of Test Series 3, it was decided that experimentation would characterize liquid cooling and determine the benefits. The air-cooled modules were disassembled and the impedance measurements of the 12 random cells were repeated since the cells had now had been more heavily conditioned. The results of those experiments are shown in Figure 4-37. Comparison of this data to that shown earlier in Figure 4-34, shows that the impedance spectra of all the cells to be much more consistent with each other, which is expected after conditioning has occurred.

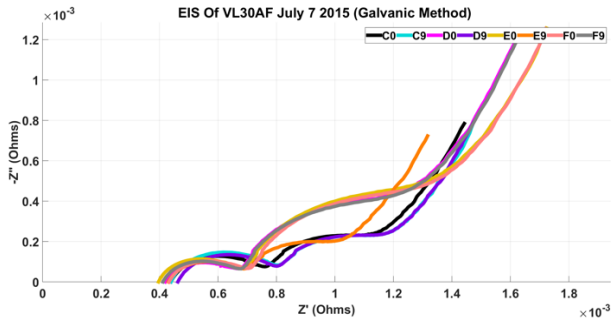

Figure 4-37. EIS measurements made on the same twelve VL30AFe cells after Test Series 3.

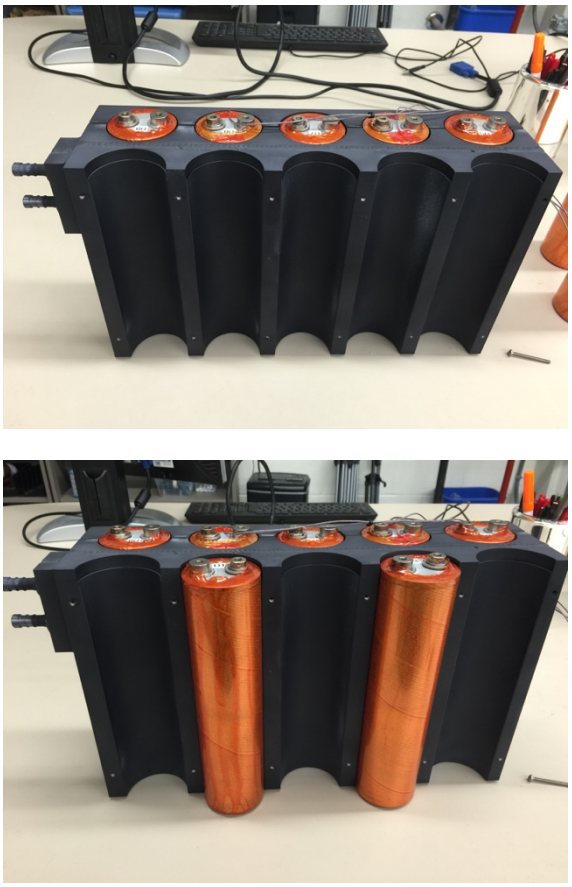

Figure 4-38. Photograph taken during assembly of one of the 10S/1P Saft VL30AFe modules. Shown is the cold plate and cells wrapped in orange Mylar wrapping.

Originally, the cold blocks were painted with a boron nitride as a dielectric hold off coating. However, it was found that the coating was not effective due to its brittleness. That coating was removed to evaluate how anodization would perform. From hi-pot testing, it turns out that anodization is not much better. Hi-pot testing is used to ensure dielectric hold off. The anodization only held off ten volts in select areas, which is considered all but un-usable in a future high voltage battery. Also of note from the figure is that the Saft cells are wrapped in an orange Mylar heat shrink to act as a secondary, more robust form of dielectric isolation from the aluminum cold-block. Mylar's high

dielectric strength, 6 kV/mill (DuPont Teijin Films, 2003), will make it an effective insulator in high voltage batteries.

Testing of the cooling blocks include Test series 4 through 7. Test series 4 shown in Figure 4-41 is shown as cycles 1 through 10. This series demonstrates the cooling efficiency of the aluminum blocks vs. the air cooling tests. Allowing each cooling block to receive roughly 5 LPM allowed the max temperature to drop by 16^{o}C, which is a massive improvement that should be expected with contact cooling. The aluminum shell that wraps around the cells allows the maximum heat transfer to the flowing water. Unlike air cooling where there has to be direct air movement around the cell in order to achieve a high efficiency of heat transfer. Remembering that heat is the enemy when it comes to preserving the lifetime of a battery and at high rates there is always an abundant amount of heat being generated. The heat being generated in a lithium cell considerably low due to their low DC ESR but maximizing the heat transfer out of a lithium cell will greatly increases their lifetime.

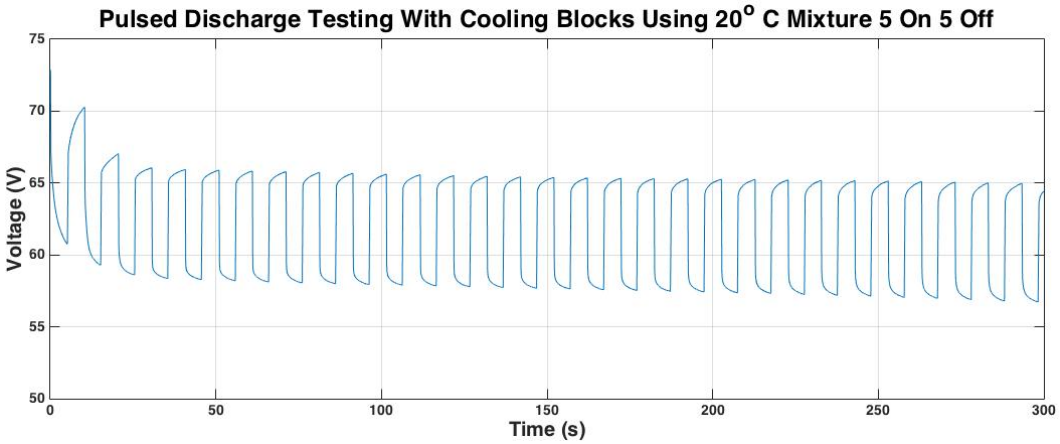

Figure 4-39. Conduction voltage during a discharge test utilizing the 5 on 5 off profile.

End conduction voltage is lower than the 40^{o}C water test with the same profile.

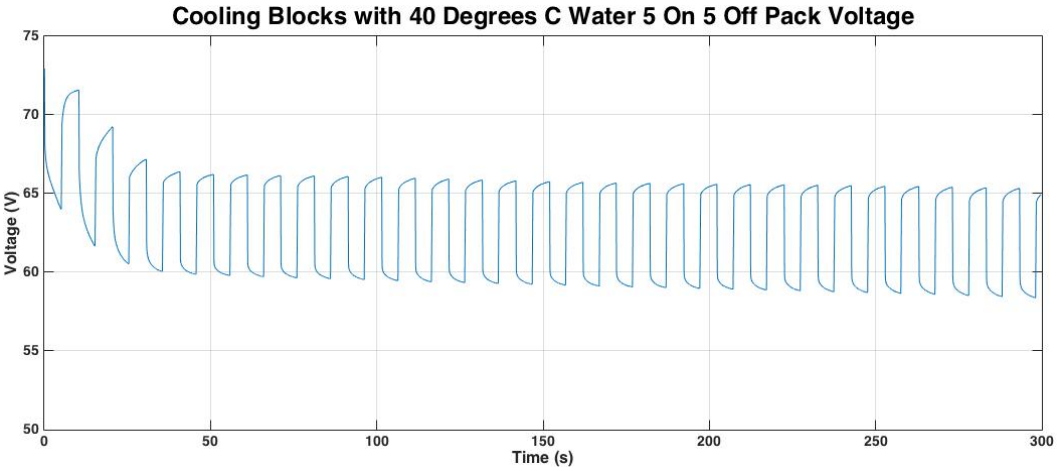

Figure 4-40. Conduction voltage during a discharge test utilizing the 5 on 5 off profile. End conduction voltage is high than the 20°C water test with the same profile.

During this set of Test series 4 through 7, a new profile was added, at request of the program sponsor, to understand a new pulsed application. This profile entailed the battery modules to be stressed under the same power level, but conducting for 30 seconds instead of 5 seconds. This added more complexity to discover how well the aluminum housings are performing. Five times the amount of energy was being generated into heat in the cell during this discharge profile. The test profile is shown in Figure 4-43. The new profile raised the max temperature by roughly 15°C, but remained in the operation condition that no cell body could go over 60°C. These tests show that liquid cooling the batteries is not only very efficient, but should be attractive when these cells are used in high rates. This type of efficient cooling should also increase lifetime at these high rates. (Yuksel & Michalek, 2006) By evaluating two different profiles on this chemistry, we can further understand the performance of the Lithium chemistry.

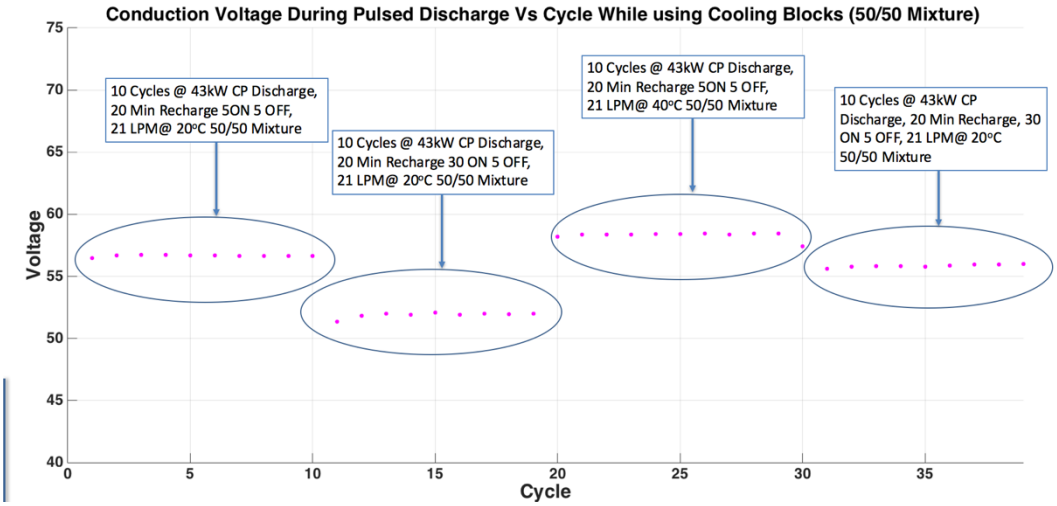

Figure 4-41. Conduction voltage performace of the cooling blocks with both profiles used at a 43kW discharge and a 20 minute recharge. Test Series 4 through 7

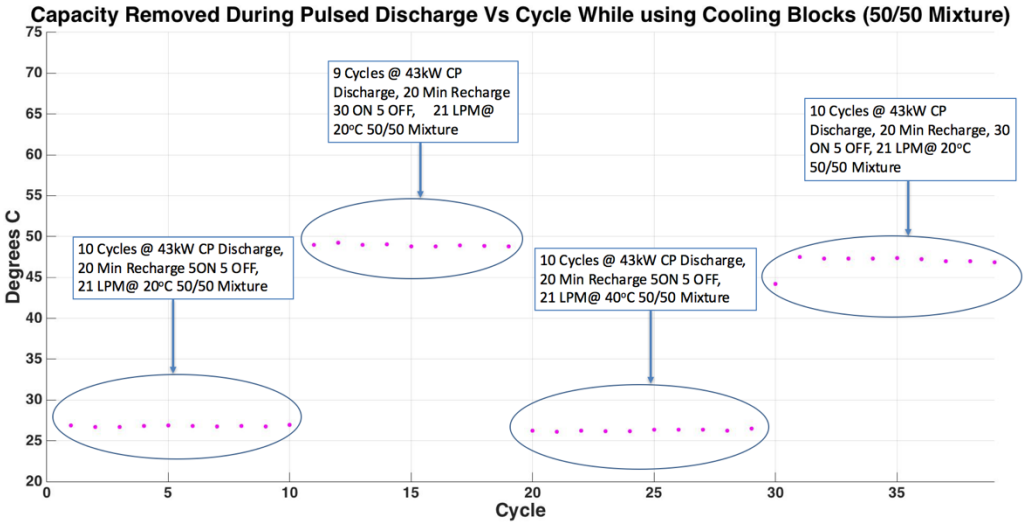

Figure 4-42. Max temperature recorded on the body of the cells during both sets of profiles and chiller settings. Test Series 4 through 7

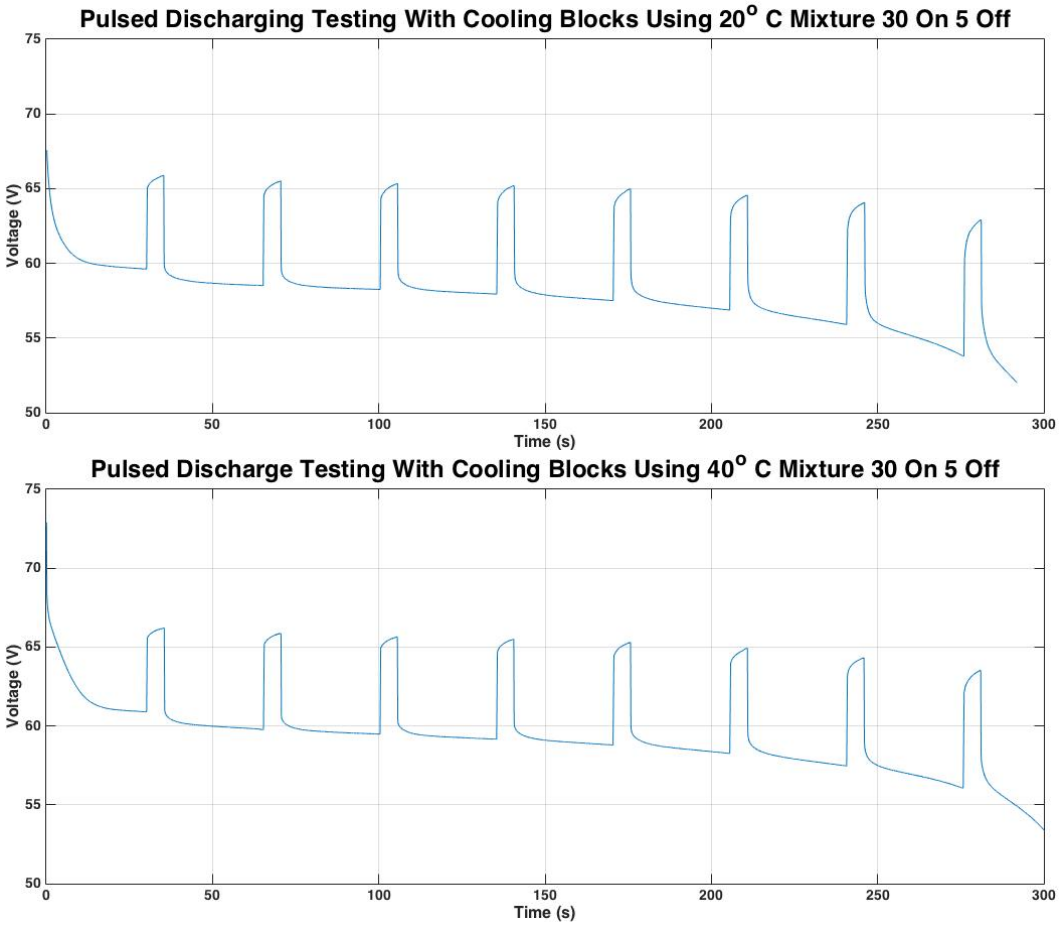

Figure 4-43. The top plot shows a 30 ON 5 OFF pulsed profile at 43kW. The temperature difference in cooling shows how conduction voltages is directly related to the cooling temperature.

After analyzing both pulsed profiles for the Lithium-ion battery, it becomes apparent that cooling temperature is directly related to conduction voltage. This is because of the ionic conduction. (Parka, Zhanga, & Chunga, 2010) Ionic conduction is the movement of ions through a crystal structure. By allowing these batteries to get hotter than normal operation, the ionic conduction increases therefore decreasing the internal resistance of the cell. With a lower ESR, the cell's conduction voltage raises and has a higher power

output. Although this heat does lead to accelerated aging, which could matter during the long-term characterization of the chemistry (Pesaran, 2001).

After examining the performance of these cells with different profiles and cooling methods lifetime cycling was performed, known as Test Series 8. The cells remained in the liquid cooling setup and cycled at 43kW constant power and the chiller set to 40°C. 450 cycles were performed during lifetime cycling and below are the results from this Test Series.

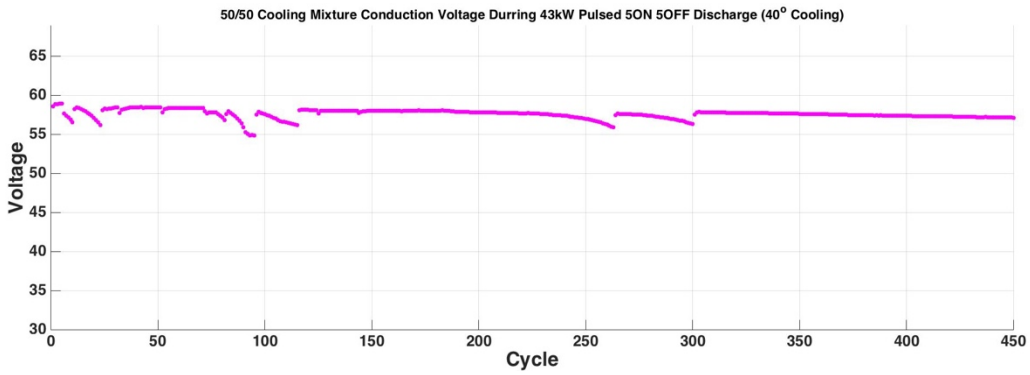

Figure 4-44. Lifetime performance of the Lithium-ion technologies conduction voltage up to 450 Cycles completed from Test Series 8.

The conduction voltage remains consistent during the entire experiment test series. As the experiment continued, the recharge current has to be adjusted to match the 20-minute recharge condition. This is due to an increased ESR. As the ESR increases, more energy is dissipated as heat and not stored in the cell. There is a slightly downward trend with the end conduction voltage due to the ESR of the cells increasing. This typically is not as apparent in low rates but when cycling at high rates the aging process accelerates. From this, we can conclude that the internal structure of the cell is being

altered due to these high rates that causes an ESR increase. The EIS section later will show this.

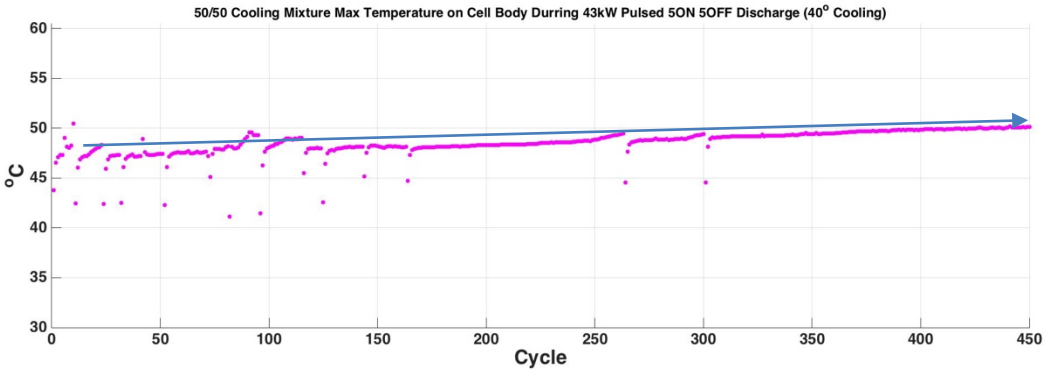

Figure 4-45. Lifetime performance of the Lithium-ion technologies conduction maximum cell temperature up to 450 Cycles completed in Test Series 8.

The maximum cell temperature is rising during the lifetime testing, which indicates that during a discharge the more heat is being dissipated throughout the cycle life during Test Series 8. This indicates that ESR is increasing and the cooling blocks are maintaining their cooling efficiency. This is one reason why Lithium-ion chemistries are desirable for high rate applications that require a consistent lifetime. The slow rise in ESR with pulsed profiles allows these to be a great candidate for pulsed loads.

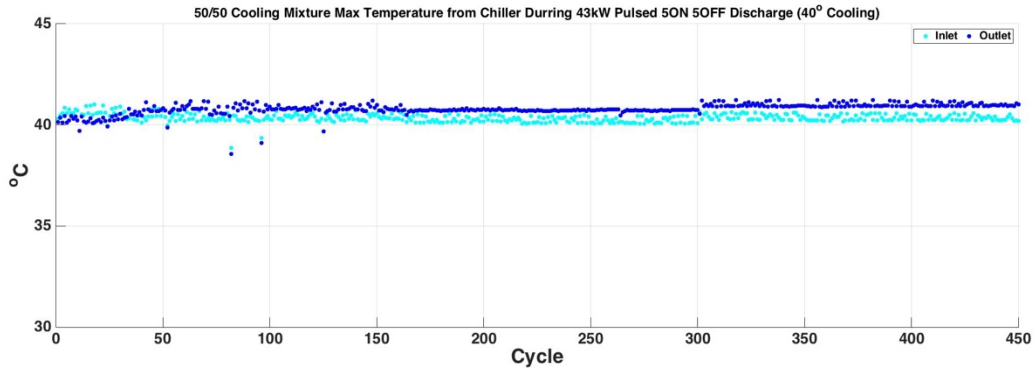

Figure 4-46. Cooling block inlet and outlet mixture temperature up to 450 cycles. The chiller inlet and outlet remain the same temperature during the entire test period.

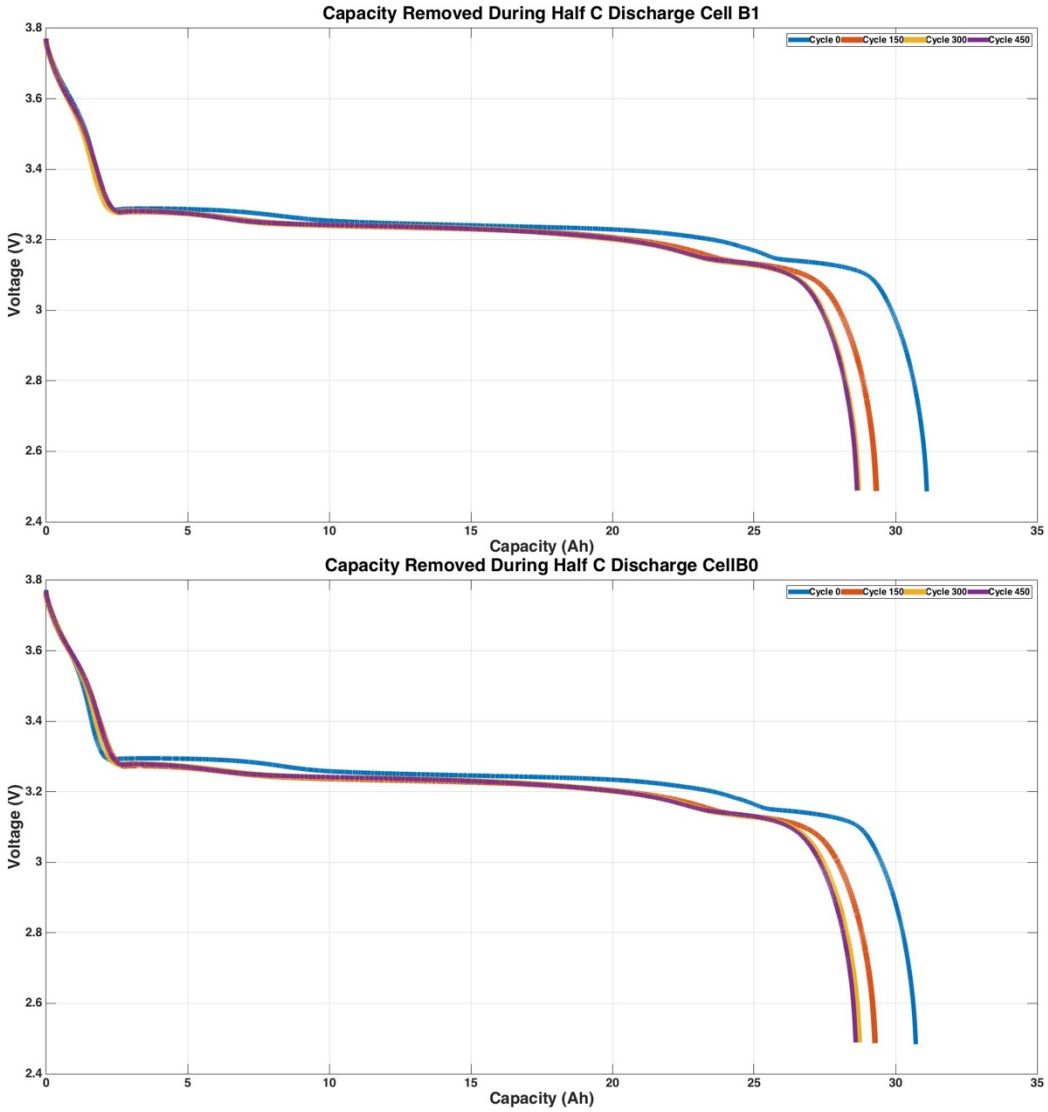

Figure 4-47. Both plots show the ½ C Discharge Capacity vs. Voltage. This extends from first cycle to last of the lifetime cycle done in Test Series 8.

During Test Series 8, the capacity of multiple cells were tested by discharging each cell at its ½ C rate until the lower voltage limit was reached; then an EIS scan was performed. Figure 4-47 shows the capacity loss during increments of 150 cycles. The initial loss is due to the different profile testing with air and liquid cooling. After the cooling tests were

performed, the capacity was roughly 28 Ah. This is a significant loss, but not detrimental. Compared to the VRLA setup the capacity fade is drastically different, still making the Lithium-ion a strong contender in the high rate testing. After 450 cycles, the capacity fade slowed down drastically, maintaining a capacity of ~27Ah. Through this data, we can infer minimal capacity will be lost during the cycle life of the cells and the system is now fully conditioned.

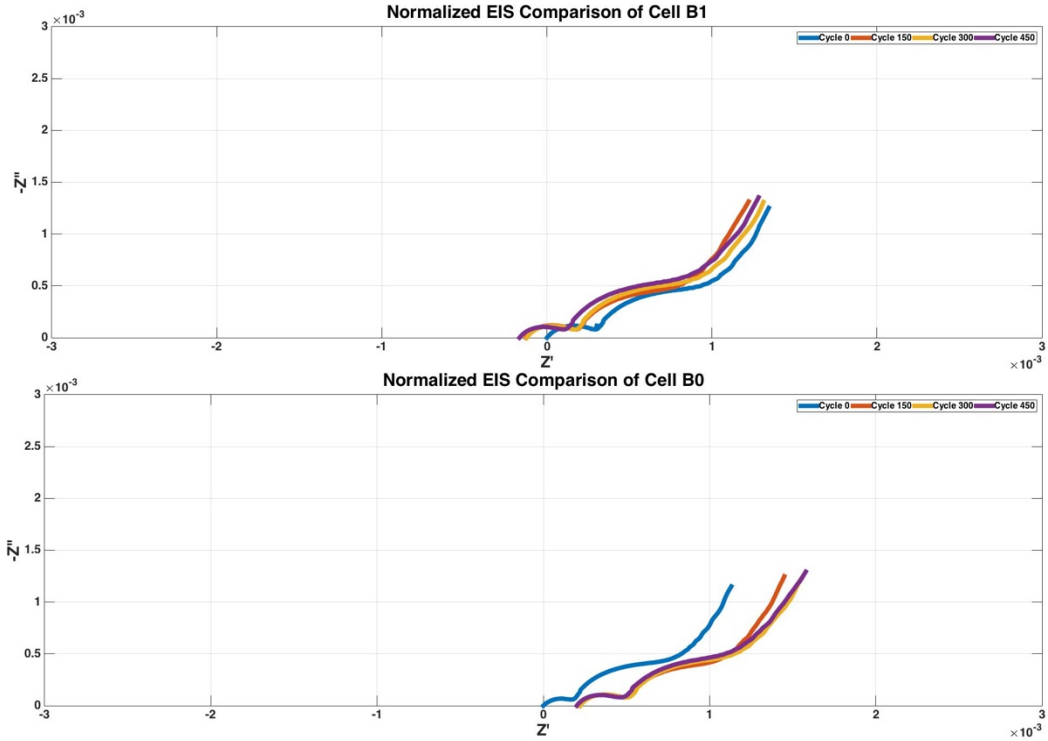

Figure 4-48. The upper and lower plots show the normalized EIS plots over the cycle life of the battery. The shifts in the plots indicated the internal ageing of the cell.

The EIS normalized curves help show the impedance growth in the cell over cycle life. Figure 4-48 demonstrates how the impedance growth is occurring during increased cycle life. Cell B0's ESR has increased but stabilized during the consistent cycling. However, Cell B1's ESR has decreased, this is typical for the first hundred or so cycles, where the SCI layers resistance is decaying and the cell is still considered to be in a "break in

period”. This is dramatically different then VRLA’s, mainly because the Lithium-ion have already out performed the Lead Acid chemistry in cycle life but because the ESR has shifted less than a quarter of a milli-ohm. The tail end of each EIS curve indicates the Warburg impedance changing; meaning the diffusion of the lithium is being altered due to cycle life. Through these normalized curves, we have shown how little impedance growth has occurred during the cycle life and how the Lithium-ion technology does not have the same accelerated growth that the VRLA batteries experienced. In Fig 5-49, R1 is known as the ESR of the cell, C1 is the electrode material capacity, and C2 & R4 is known as the SCI growth and decay. The Warburg impedance is known to be the diffusion of the Lithium-ion cell. With all of these impedance components modeled, the aging during the cycle life of the battery can be discovered and related back to specific components inside the cell.

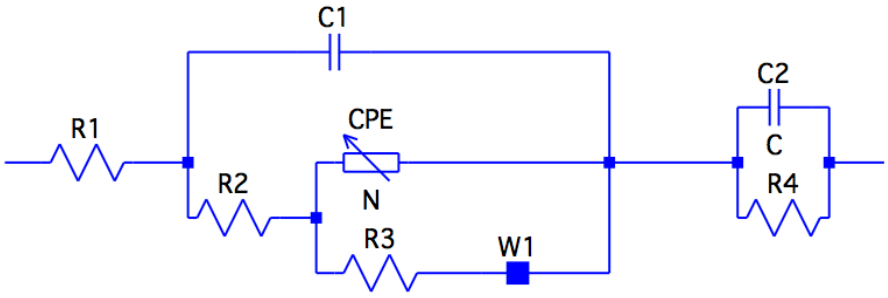

Figure 4-49. Aging Model of the Lithium-ion cells during the pulsed discharge cycling.

Table 12. Impedance values of the circuit model that change during its cycle life.

Cell B0 Circuit Values

	Cycle 0	Cycle 150	Cycle 300	Cycle 450
Resistance 1 (Ohm)	0.0006737	0.0008662	0.0008926	0.0007846
Capacitor 1 (F)	38.57	14.39	16.75	21.9
Resistance 2 (Ohm)	1.48E-04	0.0002556	0.0002352	0.0002286
Constant Phase Element (S-Sec^n)	5395	3903	3547	3730
Frequency Power (N)	0.6917	0.6046	0.5729	0.6229
Resistance 3 (Ohm)	0.01366	3.67E+13	1.06E+10	2.30E+05
Warburg (S-Sec^.5)	2.77E-06	1.27E-08	6.91E-10	4.93E-11
Capacitor 2 (F)	1739	2000	2166	2023
Resistance 4 (Ohm)	0.0004564	0.0003435	0.0003763	0.000489
Chi-squared	0.0002573	0.000725	0.000215	0.003118

Cell B1 Circuit Values

	Cycle 0	Cycle 150	Cycle 300	Cycle 450
Resistance 1 (Ohm)	0.0009559	0.0008041	0.0008238	0.0008702
Capacitor 1 (F)	22.52	15.39	16.37	18.09
Resistance 2 (Ohm)	0.000262	0.0002703	0.0002598	0.0002245
Constant Phase Element (S-Sec^n)	1236	1350	1324	1237
Frequency Power (N)	0.9154	0.8435	0.8492	0.8602
Resistance 3 (Ohm)	0.0007518	8.58E-04	9.67E-04	2.13E-07
Warburg (S-Sec^.5)	1.20E+04	4.57E+06	1.29E+11	6.81E+15
Capacitor 2 (F)	1.55E+04	1.17E+04	1.23E+04	2317
Resistance 4 (Ohm)	0.005548	2.47E-04	3.40E-04	0.0003593
Chi-squared	0.0003039	2.44E-04	2.56E-04	0.0003778

The experiments result for the Lithium-ion chemistry shows how cycle life has increased impedance during lifetime, but not drastically. Meaning, at high rates pulsed profiles these cells performed increasingly better than their counter VRLA batteries.

Making this chemistry an ideal source when lifetime is of concern in a design. With both chemistries fully characterized, we can conclude the hypothesis at the beginning of the paper.

Chapter 5

Conclusion

Two batteries were constructed to characterize two chemistry's performance during high rate pulsed discharge testing. The experimental set up utilized two types of cooling techniques along with the ability to test different pulsed profiles. The evaluation of Lead Acid and Lithium-ion batteries at high rates has shown significant evidence to validate that Lithium-ion archived not only a higher cycle life, but also be the preferable chemistry for high rate pulsed loads.

The characterization of ~60V Lead Acid and Lithium-ion batteries at high rates has shown significant evidence to validate that Lithium-ion is favorable in these pulsed tests. The lithium ion battery outlasts the VRLA setup with forced air and liquid cooling. It was hypothesized that the lead acid chemistry would age rapidly due to high rates, which did occur as shown in the VRLA results section where two batteries capacity's fall below their usability. It was also hypothesized that the lithium ion chemistry would have minimal capacity losses and age uniformly throughout cycle life. The results from the lithium ion test section show that capacity fade was not drastic during its set of test series and EIS curves did not show any advanced aging. Thus, our hypothesis was correct in making LFP the best choice for this pulsed profile.

Moving forward from this evaluation of the two chemistries, it would be of interest to see different profiles that were not just square. Different power levels would be interesting to analyze with aging effects. Mainly higher power levels for shorter periods. Ideally, the VLRA technology should have individual cells exposed for better cooling for future work, instead of having a VRLA that contains six single Lead Acid cells. Allowing single cells would also produce better EIS data and build a better model to understand how the impedance of the batteries is changing over cycle life. Switching to galvanostatic on the

Lead Acid chemistry would also increases the resolution of the EIS model. By exploring these new parameters into future work, there can be a new study to understand different methods of ageing at high rates with obscure pulsed profiles.

Appendix A

How to run the Experimental setup, a manual crated by Christopher Williams & Matt Martin

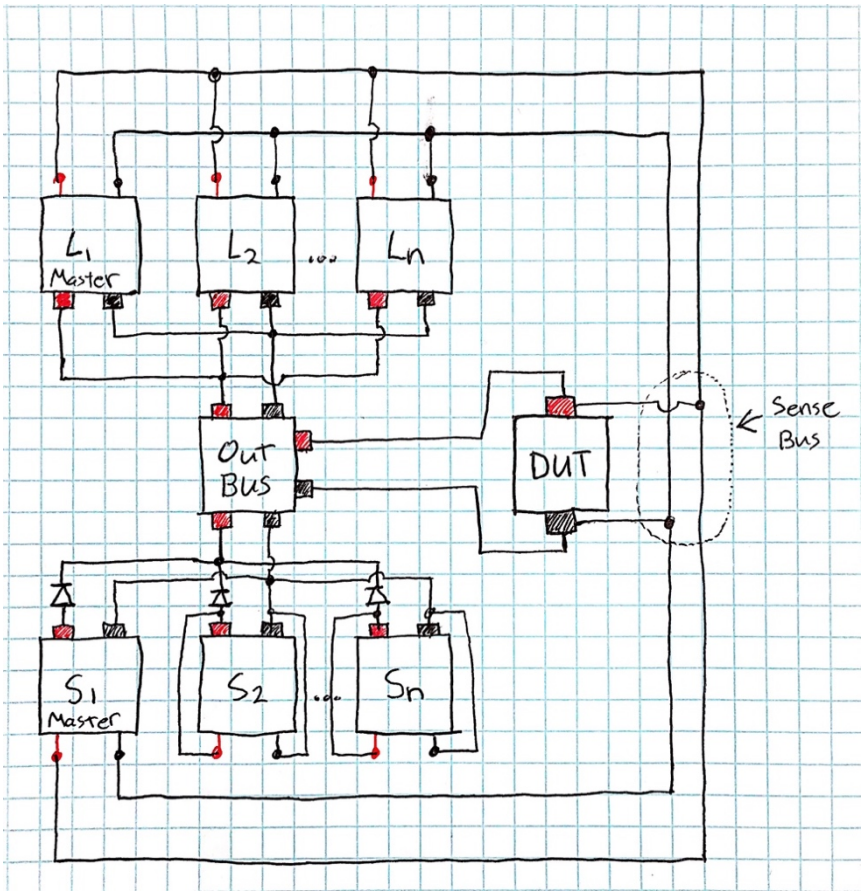

Figure 0-1. Example layout of experiment with paralleled sources and lode, notice the diodes on the source

Preparing the hardware

1. Disconnect everything before starting, unless you are 100% sure of the existing connections. In particular, make sure the device under test (DUT) is not connected to the bus, and that the bus is at 0V.
2. Identify how many loads and supplies you need in parallel and gather the corresponding power leads.
3. Connect the required power leads to the output bus. Keep this clean. NO RATS NEST!

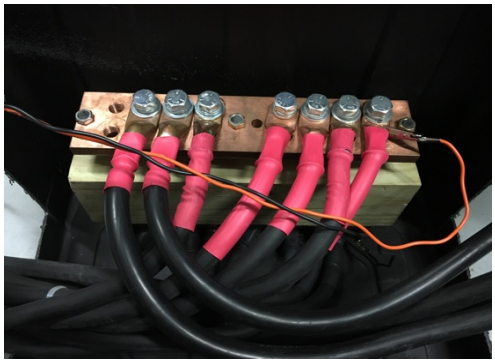

Figure 0-2

4. Connect the sense leads from all of the loads being used in parallel to the sense bus (as shown in Figure 1).
5. Connect the sense leads from the master supply to the sense bus (as shown in Figure 1).
6. Connect the sense leads from all slave supplies directly to their own respective output, before the diode (as shown in Figure 1).
7. Verify all connections using a multi-meter. Check for continuity from each load and supply to the output bus, and then make sure there is no continuity between the positive and negative rails of the output bus.

Configuring the load and supply

1. On the load, set the range according to the device you are testing. Low range is all tests from 0 to 16V and High range is all tests from 0 to 80V.

Figure 0-3

2. On the master load, set the hard limit for the lower voltage. On the front panel of the master load, choose “Conf./Local”, navigate to “Von Protection”, and set the lower voltage point limit to 75% of your expected lowest test voltage. Press enter to save your setting.

Figure 0-4

3. If you have more than one load in parallel, verify that the master/slave cable is daisy chained from the master to each of the subsequent slaves.

Figure 0-5

4. If you have more than one load in parallel, you have to assign addresses to the slaves.
    a. On each slave, choose “Sys”, then navigate to “GPIB Address” and set the address number in accordance with the daisy chain. Slaves start with GPIB 1 and move up to GPIB N

Figure 0-6

    b. On each slave, choose “Sys”, then navigate to and set “Parallel = Slave”.

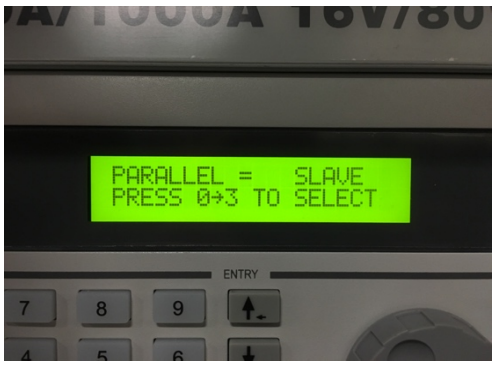

Figure 0-7

c. On the master load, navigate to and set “Parallel = Master”, then press enter. For each subsequent slave address that will be used, set the slave mode to “63209”.

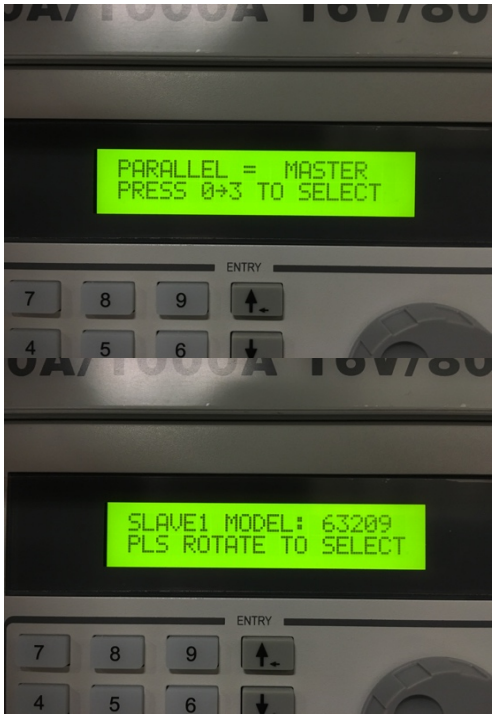

Figure 0-8

5. If you are only using one single load, set the master to single load mode. Choose “Sys” then navigate to and set “Parallel = None”.

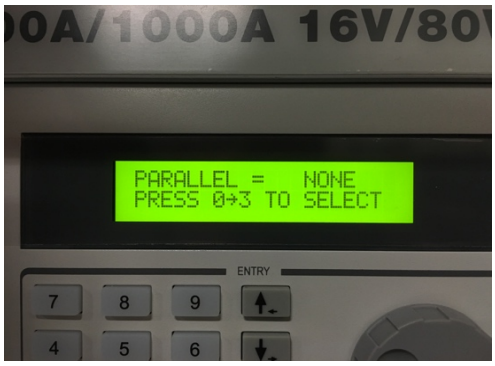

Figure 0-9

Connecting the DUT

1. Connect a spare Anderson SB350 to ring terminal pigtail to the DUT using the ring terminals.

Figure 0-10

2. Connect a sense cable to the DUT by clipping alligator clips directly to the terminals.

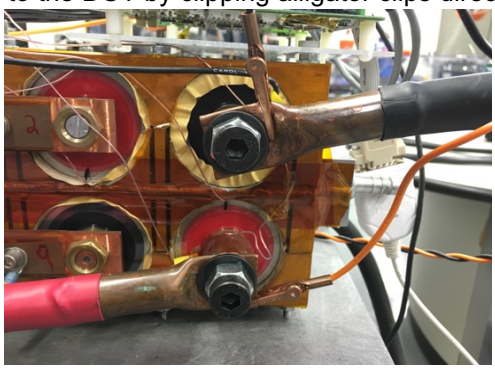

Figure 0-11

3. Connect a pre-charge cable to the output bus by clipping the alligator clips directly to the bus (same as above). These cables will be labeled, and can be found hanging on the end of the rack, near the SB350 to ring terminal pigtails.

Figure 0-12

4. Connect the orange and black connector on the sense cable to the orange and black connector on the pre-charge cable. The pre-charge cable has a resistor in series that will slowly charge the output bus to the DUT voltage. High DV/Dt on the bus can cause transient spikes that can damage the equipment.
5. Once the front panel of the load/supply reads the voltage of the DUT, directly connect the power leads from the bus to the power leads you attached to the DUT. Keep the pre-charge cable in place during this process.
6. Once the bus is directly connected to the DUT, remove and store the pre-charge cable. You are done with it.
7. Connect the sense leads from the DUT (that were attached to the pre-charge cable) to the sense bus (as shown in first figure) so that the loads and supplies can directly sense voltage at the battery, which accounts for the voltage drop across the cables, connectors, and bus.
8. YOU ARE NOW READY TO START YOUR TEST.

Checklist for experiment:

☐	**OUTPUT BUS IS FREE OF CONNECTIONS TO OTHER/PAST EXPERIMENTS.**
☐	Number of parallel loads needed: _____
☐	Number of parallel supplies needed: _____
☐	All load and supply power leads connected to bus.
☐	All load sense leads are connected in parallel to the sense bus.
☐	Master power supply sense leads are connected to sense bus.
☐	Slave power supply sense leads connected to respective outputs before diode.
☐	Output bus verified using a multi-meter.
☐	Load voltage range set properly for experiment.
☐	Load lower voltage limit is set appropriately at _____ V.
	If using multiple loads
☐	Master/slave cable(s) are appropriately in place for the loads.
☐	Slave loads appropriately assigned GPIB addresses.
☐	Slave loads set to “Parallel = Slave” mode.
☐	Master load set to “Parallel = Master” and slaves set to “63209”.
	If using a single load
☐	Master load set to “Parallel = None”.
☐	SB350 pigtail connected to DUT.

- [ ] Sense lead pigtail attached to DUT.
- [ ] Pre-charge cable attached to output bus.
- [ ] Pre-charge cable attached to sense lead on DUT and bus voltage = DUT voltage.
- [ ] SB350 from DUT connected to SB350 on output bus (with correct polarity).
- [ ] Pre-charge cable removed and DUT sense lead connected to sense bus.

How to use the Labview Software

How to set up equipment to the VI

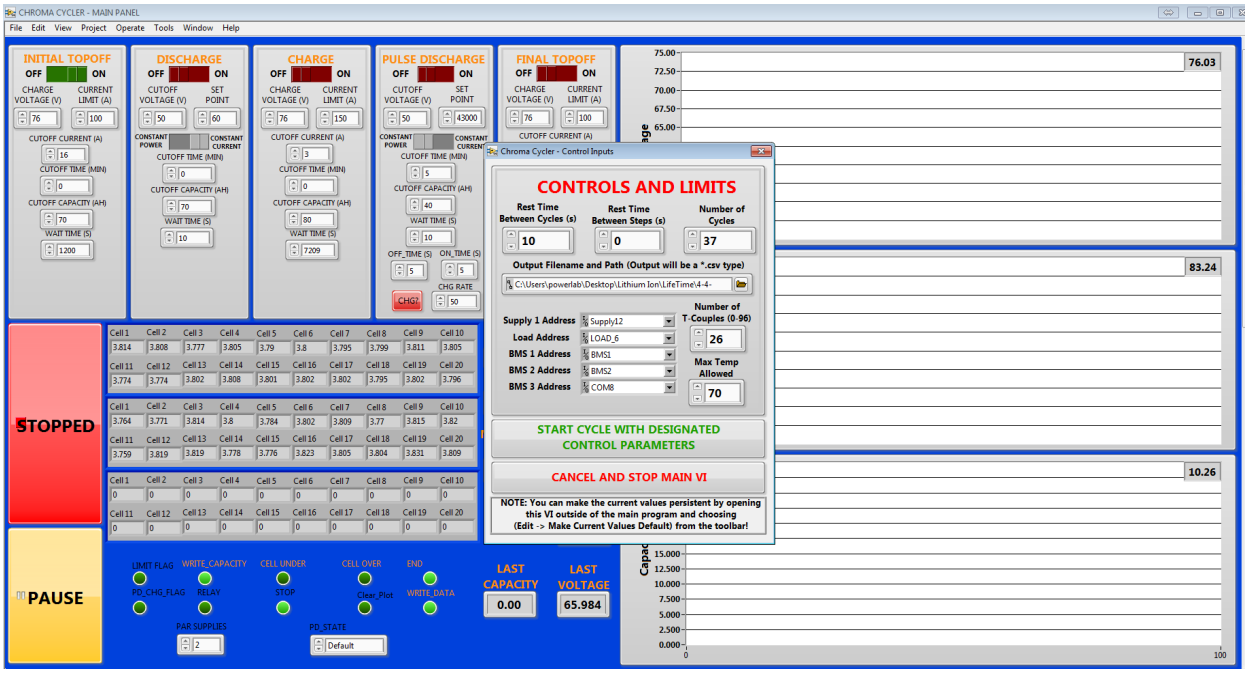

How to prepare the VI to run a set profile

After starting the VI, by using the arrow in the upper right hand corner the controls and limit VI with appear.

Step 1: Set Rest time between cycles, steps and number of cycles to a desired amount needed for the profile. 10 seconds is normal a good setting for both rest times.

Step 2: Choose an output file location and name

Step 3: Choose the supply, electronic load, and BSM. This has to be set up in NI max, refer to NI.com for using of NI max.

Step 4: Choose the number of thermocouples in the system that are needed. These selected thermocouples will be watched for over temp which is set right below. Regardless of how many you choose all NI 9213's connected to the system will be recorded in the end file, which contains all of the results from the test.

Step 5: Click start to begin testing

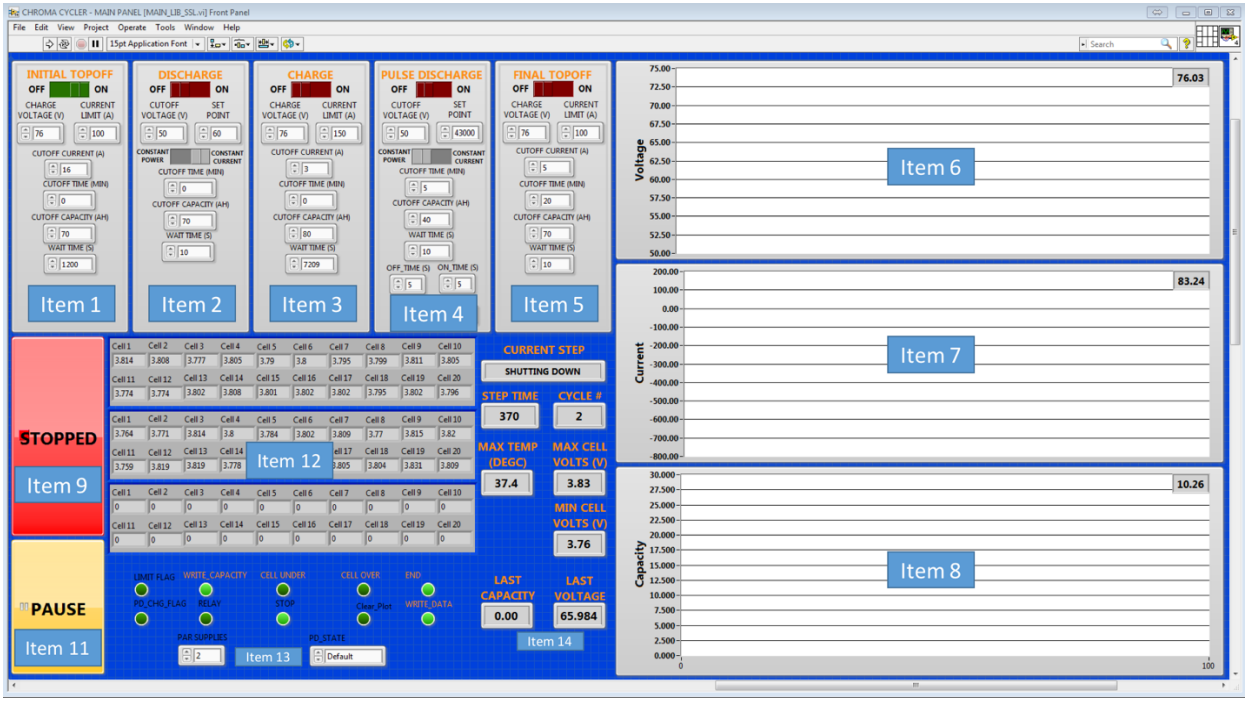

List of items in program VI

Item 1- Initial Topoff charging profile settings

Item 2- Discharge profile settings

Item 3- Charge profile settings

Item 4- Pulsed discharge profile settings

Item 5- Final Topoff charging profile settings

Item 6- Voltage graph for length of test, notice the current voltage in the right hand corner of the graph

Item 7- Current graph for length of tests, notice the current amperage in the right hand corner of the graph

Item 8- Current capacity graph of tests, notice the current capacity in the right hand corner of the graph

Item 9- Stop button to end the program for any reason

Item 10- The current setup shown right below the Item 5

Item 11- The pause button to pause the program after the current step is complete

Item 12- The current measurements of each cell in the system

Item 13- The multiplying factor for how many power supplies are connected to the system

Item 14- Indicators to show the last capacity and voltage from the previous step performed

This example will show how to set up a normal profile to test the capacity of battery that has a lower voltage of 50 Volts, charge voltage of 70 Volts and a capacity of 60 Amp hours.

Step 1:

To first understand the state of the battery, a Topoff cycle must be completed. Slide the OFF/ON bar to ON, this is located in Item 1. Set the voltage to the charge voltage of the battery, this case it would be 70 Volts. Then set the max current to charge the battery at. Let's

choose 100 Amps. After a cut off capacity can be chosen the cut off current can be chosen, normally this is C/10. Final setting should be the cut off time, normally this is set to a few hours.

Step 2:

Setting up a consent current discharge, Item 2 should be turn on by sliding the OFF/ON bar. After the Constant power/ Constant current bar should be slid to to constant current. Then the lower voltage point should be set, for the example 50 Volts. The discharge current should be the 1C rate, so 60 Amps. After cut of time and capacity can be set.

Step 3:

The Charge step should be setup the same as the Topoff in step 1. Values can change depending on the type of profile needed.

Step 4:

The pulsed discharge setup in item 4 should be set up exactly like the discharge step in item 2. The user can only produce square pulses with this program. No other shaped pulse can be produced. The pulse times can be changed with two parameters, on time and off time. This sets the duty cycle of the pulses.

Step 5:

The final set up is to perform a final top off, shown as Item 5. Go back to Step 1 to change the settings for the final Topoff. Theses items are exactly the same.

Appendix B

Title of Appendix Here

Appendix B content goes on this page

References

DuPont Teijin Films. (2003, June 1). *Mylar.* Retrieved March 22, 2016, from http://usa.dupontteijinfilms.com/informationcenter/downloads/Electrical_Properties.pdf

A123. (2015). *Nanophosphate® Lithium Iron Phosphate Battery Technology*. (A123) Retrieved April 16, 2016

Andre, D., Meilera, M., Steinera, K., Wimmera, C., & Soczka-Gu, T. (2011, June). Characterization of high-power lithium-ion batteries by electrochemical impedance spectroscopy. I. Experimental investigation. *Journal of Power Sources, 292*(12), 5334–5341.

Bazant, M., & Pinson, M. (2010, January 1). *Theory of SEI Formation in Rechargeable Batteries: Capacity Fade, Accelerated Aging and Lifetime Prediction.* Retrieved April 11, 2016, from http://arxiv.org/pdf/1210.3672.pdf

Brodd, R. J. (2009, January 1). *Comments on the History of Lithium-Ion Batteries.* Retrieved March 22, 2016, from https://www.electrochem.org/dl/ma/201/pdfs/0259.pdf

Cohen, I., Westenhover, C., Wetz, D., Heinzel, J., & Dong, Q. (2015, June 4). Evaluation of an actively contolled battery-capacitor hybrid energy storage module (HESM) for use in driving pulsed power applications. *Pulsed Power Conference (PPC), 2015* , 1-5.

D. Andrea, M. M.-G. (2011). Characterization of high-power lithium-ion batteries by electrochemical impedance spectroscopy. I. Experimental investigation. *Journal of Power Sources, 196*(12), 5334–5341.

East Penn Manufacturing. (2015, March 15). *Guied to VRLA Batteries.* Retrieved March 20, 2016, from http://www.eastpennmanufacturing.com/wp-content/uploads/Guide-to-VRLA-Batteries-1927.pdf

Georga Sate University . (2000, August 1). *Lead-Acid Battery*. (Georga Sate University) Retrieved March 12, 2016, from http://hyperphysics.phy-astr.gsu.edu/hbase/electric/leadacid.html#c1

Gilson Engineering. (2012, January 1). *Flower Meters.* Retrieved April 1, 2016, from http://www.gilsoneng.com/reference/flowmeter.pdf

Huibin, S., & Wei-Jen, L. (2011). An AMI Based Measurement and Control System in Smart Distribution Grid . *Industrial and Commercial Power Systems Technical Conference (I&CPS), 2011, 2011*(1), 1-5.

K2 Energy Solutions. (2015). *K2 Energy 26650 LFP Datasheet.* Retrieved March 5, 2016, from http://www.k2battery.com/

lafdacs. (2014, January 1). *DEEP CYCLE BATTERY FREQUENTLY ASKED QUESTIONS.* Retrieved March 22, 2016, from

http://www.lafdacs.org/pdf_files/DEEP%20CYCLE%20BATTERY%20FREQUENTLY%20ASKED%20QUESTIONS.pdf

Li, E. M. (2001). Studies on the Cycle Life of Commercial Lithium Ion Batteries During Rapid Charge-Discharge Cycling. *Journal of Power Sources*(102), 294-301.

Lithium Battery Saftey and Handling Guildline. (2006, April 11). Retrieved March 22, 2016, from http://www.whoi.edu/cms/files/LithiumBatterySafetyGuideSG10_26006.pdf

M. Dubarry, B. L.-S.-S.-C.-T.-H. (2010). Identifying battery Ageing mechanisms in large format Li ion cells. *Journal of Power Sources*.

Magnet Academy. (2010, December 10). *Planté Battery – 1859*. (Magnet Academy) Retrieved March 20, 2016, from https://nationalmaglab.org/education/magnet-academy/history-of-electricity-magnetism/museum/plante-battery

Nagaura , T., & Tozawa, K. (1998). *Lithium Ion Batteries: Fundamentals and Performance.* Tokyo: Wiley.

North Western University . (2015, June 22). *Power System*. (Notrth Western Univerity) Retrieved Febuary 14, 2016, from http://www.qrg.northwestern.edu/projects/vss/docs/power/1-what-are-batteries.html

Parka, M., Zhanga, X., & Chunga, M. (2010). A review of conduction phenomena in Li-ion batteries. *Journal of Power Sources, 195*(24), 7904–7929.

Pesaran, A. A. (2001, Febuary 5). *Battery Thermal Management in EVs and HEVs: Issues and Solutions.* Retrieved March 22, 2016, from http://www.nrel.gov/transportation/energystorage/pdfs/aabc_presentation.pdf

Sigma Aldrich. (2008, December 2). *U.S. Department of Energy's Materials Research for Advanced Lithium Ion Batteries - See more at: http://www.sigmaaldrich.com/technical-documents/articles/material-matters/u-s-department-of0.html#sthash.AsTuUpMq.dpuf*. (Sigma Aldrich) Retrieved Febuary 22, 2016, from http://www.sigmaaldrich.com/technical-documents/articles/material-matters/u-s-department-of0.html

Sudhakaran, S. (2014, February 14). *The Complete Guide to Camera Batteries (Part One)*. (Wolfcrow) Retrieved March 29, 2016, from http://wolfcrow.com/blog/the-complete-guide-to-camera-batteries-part-one/

TU Delft OpenCourseWare. (2013, March 26). *Sustainable Hydrogen and Electrical Energy Storage*. (TU Delft) Retrieved Febuary 22, 2016, from https://ocw.tudelft.nl/course-lectures/supercapacitors/

Turner, G., Kelly, J., Storm, C., Wetz, D., & Wei-Jen, L. (2015, January). Design and Active Control of a Microgrid Testbed. *TRANSACTIONS ON SMART GRID, 6*(1), 73-81.

Wang, Y. Z.-Y. (2009). Cycle-Life Characterization of Automotive Lithium-Ion Batteries with LiNiO2 Cathode. *Journal of the Electrochemical Society, 156* (7), A527-A535.

Wetz, D. A. (2011). *Investigation of Aging Phenomena in Electrochemical Storage Devices when Cycled at Elevated Rates.* Arlington: University of Texas at Arlington.

Wetz, D., Shrestha, B., & Novak, P. (2013, January 25). Back to Results Elevated Rate Cycling of High-Power Electrochemical Energy Storage Devices for Use as the Prime Power Source of an EM Launcher. *IEEE Transactions on Plasma Science, 41*(5), 1319 - 1325.

Wetz, D., Shrestha, B., Novak, P., & Donahue, S. (2014, July). Capacity fade of a high power battery when evaluated for use within a prime power supply. *Electromagnetic Launch Technology (EML), 2014 17th International Symposium, 1*(1), 1-7.

Wilhelm, A., Surgenor, B., & Pharoah, J. (2006). Design and evaluation of a micro-fuel-cell-based power system for a mobile robot. *IEEE/ASME Transactions on Mechatronics, 11*(4), 471 - 476.

Williams, C., Martin, M., Wetz, D., & Gnegy-Davidson, C. (2015). Study of the Impedance Growth and Capacity Fade of High Power Lithium-Iron Phosphate, Valve Regulated Lead Acid, and Nickel Metal Hydride Batteries When Cycled in High Rated Pulsed Profiles. *Energy Storage Modules.*

Wong, J., Taufik, T., Anwari, M., & Ldris, N. (2011). A parallel energy-sharing control for fuel cell-battery-ultracapacitor hybrid vehicle. *IEEE Energy Conversion Congress and Exposition*, 2923 - 2929.

Yuksel, T., & Michalek, J. (2006, January 1). *Evaluation of the Effects of Thermal Management on Battery Life in Plug-in Hybrid Electric Vehicles.* Retrieved March 25, 2016, from http://www.cmu.edu/me/ddl/publications/2012-Battery-Congress-Yuksel-Michalek-Thermal-Mgmt.pdf

Biographical Information

Christopher Williams is currently in a research program aimed at characterizing and understanding how electrochemical energy storage devices will be utilized in the future Naval fleet to drive both conventional applications as well as advanced electrical weaponry. Christopher started out as an undergraduate researcher during the past summer and fall 2014 semesters and was instrumental in setting up a new research effort we just started in which we are evaluating lead acid, lithium-ion, and nickel metal hydride batteries for the Navy under very high pulsed current rates. Christopher graduated with his BSEE in December 2014 and now finished a Masters in Electrical Engineering at the University of Texas at Arlington. Christopher Williams hopes to get into the distribution industry and provide new ideas on improving the Texas power gird with renewable recourses and battery storage systems.